UNIVERSITI TEKNOLOGI MARA

# EVALUATION OF THE CORROSION INHIBITION BEHAVIOR OF MILD STEEL USING HARUMANIS MANGO PEEL EXTRACT AS A GREEN INHIBITOR IN HYDROCHLORIC AND SODIUM CHLORIDE MEDIA

NUR AINA BINTI RADIN SUKIMI

MSc

March 2026

# UNIVERSITI TEKNOLOGI MARA

# EVALUATION OF THE CORROSION INHIBITION BEHAVIOR OF MILD STEEL USING HARUMANIS MANGO PEEL EXTRACT AS A GREEN INHIBITOR IN HYDROCHLORIC AND SODIUM CHLORIDE MEDIA

**NUR AINA BINTI RADIN SUKIMI**

Thesis submitted in fulfilment
of the requirements for the degree of
**Master of Sciences**
**(Chemistry)**

**Faculty of Applied Sciences**

**March 2026**

# CONFIRMATION BY PANEL OF EXAMINERS

I certify that a Panel of Examiners has met on 13 January 2026 to conduct the final examination of Nur Aina Binti Radin Sukimi on her Masters of Science thesis entitled "Evaluation of the Corrosion Inhibition Behaviour of Mild Steel Using Harumanis Mango Peel Extract as a Green Inhibitor in Hydrochloric and Sodium Chloride Media" in accordance with Universiti Teknologi MARA Act 1976 (Akta 173). The Panel of Examiner recommends that the student be awarded the relevant degree. The Panel of Examiners was as follows:

Raja Razuan Raja Deris, PhD
Associate Professor
Faculty of Applied Sciences
Universiti Teknologi MARA
(Chairman)

Sheikh Ahmad Izaddin Sheikh Mohd Ghazali, PhD
Associate Professor
Faculty of Applied Sciences
Universiti Teknologi MARA
(Internal Examiner)

Siti Hawa Mohamed Salleh, PhD
Senior Lecturer
Faculty of Chemical Engineering & Technology
Universiti Malaysia Perlis
(External Examiner)

**PROFESSOR DR HJH ZURAEDA IBRAHIM**
Dean
Institute of Postgraduates Studies
Universiti Teknologi MARA

Date: 25 March 2026

# AUTHOR'S DECLARATION

I declare that the work in this thesis was carried out in accordance with the regulations of Universiti Teknologi MARA. It is original and is the results of my own work, unless otherwise indicated or acknowledged as referenced work. This thesis has not been submitted to any other academic institution or non-academic institution for any degree or qualification.

I, hereby, acknowledge that I have been supplied with the Academic Rules and Regulations for Post Graduate, Universiti Teknologi MARA, regulating the conduct of my study and research.

| | | |
|---|---|---|
| Name of Student | : | Nur Aina binti Radin Sukimi |
| Student ID. No. | : | 2022217708 |
| Programme | : | Master of Science (Chemistry) – AS756 |
| Faculty | : | Applied Sciences |
| Thesis Title | : | Evaluation of the Corrosion Inhibition Behaviour of Mild Steel using Harumanis Mango Peel Extract as a Green Inhibitor in Hydrochloric and Sodium Chloride Media |
| Signature of Student | : | …….. |
| Date | : | March 2025 |

# ABSTRACT

Organic plant extracts are increasingly used as green corrosion inhibitors. However, their practical application is limited by factors such as corrosion dependence, sensitivity to temperature variations, competition with aggressive ions, and the instability of the protective inhibitor film. Thus, this study aims to explore the potential of a local mango peel as a green corrosion inhibitor for mild steel. The Harumanis mango peel extract (HMPE) was obtained through solvent extraction with 60:40 (ethanol-water) system. The chemical characterization has shown that the appearance of vital functional groups such as aromatic rings, hydroxyl groups, and carbonyl groups proves that HPME is a good corrosion inhibitor. The effectiveness of HMPE corrosion inhibitors in different concentrations investigated in mitigating mild steel corrosion in acidic (0.5 M HCl) and near-neutral (0.6 M NaCl) media. The corrosion inhibition performance was evaluated using several corrosion tests, such as weight loss, potentiodynamic polarization, and electrochemical impedance spectroscopy (EIS). The surface of the mild steel also was analyzed using optical microscopy (OM), scanning electron microscopy (SEM), and x-ray photoelectron microscopy (XPS). Mild steel samples were immersed in both acidic and near-neutral media in the presence of different concentrations of HMPE ranging from 0 to 350 ppm. The immersion tests found the highest inhibition efficiency at 350 and 250 ppm in acidic and near-neutral media, respectively. The polarization studies demonstrated a decrease in corrosion current density ($i_{corr}$) after the addition of HMPE, thus confirming the inhibitor effect for both mediums. The lowest $i_{corr}$ obtained were 35.99 μA $cm^{-2}$ at 350 ppm and 1.76 μA $cm^{-2}$ at 250 ppm in both 0.5 M HCl and 0.6 M NaCl, respectively. Furthermore, the Tafel analysis also identified the HMPE corrosion inhibitor as a mixed-type inhibitor in both 0.5 M HCl and 0.6 M NaCl solutions but predominantly anodic in 0.6 M NaCl. The EIS result indicated increased in charge transfer resistance ($R_{ct}$) as the HMPE inhibitor was added, which signified higher inhibition efficiency with the highest at 76% and 90% in 0.5 M HCl and 0.6 M NaCl, respectively. The OM observations revealed that the mild steel samples treated with HMPE exhibited smoother surfaces compared to the sample in blank, indicating reduced in corrosion damage. SEM analysis also supported these findings by showing significant improvements on the surface with HMPE in both 0.5 M HCl and 0.6 M NaCl. In addition, XPS analysis confirmed the adsorption of HMPE components on the mild steel surface, forming protective film rich in carbon, oxygen, and nitrogen-containing species. Peaks corresponding to C–C, C=O, $Fe_2O_3$, and FeOOH indicated the formation of a stable organic–inorganic layer that reduced further metal dissolution. Moreover, adsorption studies also show that the inhibition mechanism followed the Langmuir adsorption isotherm. Hence, these findings highlight the potential of Harumanis mango peel extract as a green corrosion inhibitor for mild steel in acidic and near-neutral media.

# ACKNOWLEDGEMENT

Firstly, I wish to express my deepest gratitude to God for His abundant blessings, guidance, and strength throughout the journey of my master's degree. I would like to extend my sincere appreciation to my supervisor, Dr Solhan Yahya for her invaluable support and insightful guidance.

I also want to express my heartfelt thanks to my co-supervisors, Dr Nurul Zawani and Dr Shaiful Rizam for their constructive feedback, guidance, and support throughout this project. A special thanks to my dear friends, Intan, Huda, Aina, Syiba, Wani and Memey who stood by me through the ups and downs of this journey.

Finally, to my beloved parents, Radin Sukimi and [redacted], thank you for your unconditional love, prayers, and sacrifices. Your constant support and belief in me have been my strongest source of motivation. Alhamdulilah.

# TABLE OF CONTENTS

# LIST OF TABLES

# LIST OF FIGURES

# LIST OF SYMBOLS

**Symbols**

| | |
|---|---|
| A | Amps |
| $\beta_a$ | Anodic Slopes |
| $\beta_c$ | Cathodic Slopes |
| b | Number of Blocks (b=1,2,3.....,K) |
| CPE | Constant Phase Elements |
| $E_{corr}$ | Corrosion Potential |
| $i_{corr}$ | Current Density |
| $K_{ads}$ | Adsorption Equilibrium Constant |
| $R^2$ | Correlation Coefficient |
| $R_{ct}$ | Charge Transfer Resistance |
| $R_s$ | Solution Resistance |
| V | Volts |
| $\Delta G_{ads}$ | Gibbs Free Energy |
| Ω | Ohms |

# LIST OF ABBREVIATIONS

**Abbreviations**

| | |
|---|---|
| AFM | Atomic Force Microscopy |
| CE | Counter Electrode |
| EIS | Electrochemical Impedance Spectroscopy |
| FTIR | Fourier Transform Infrared Spectroscopy |
| GC-MS | Gas Chromatography–Mass Spectrometry |
| HPLC | High-Performance Liquid Chromatography |
| OM | Optical Microscopy |
| PP | Potentiodynamic Polarization |
| RE | Reference Electrode |
| SEM | Scanning Electron Microscopy |
| SEM-EDS | Scanning Electron Microscopy-Energy Dispersive Spectroscopy |
| UV-Vis | Ultraviolet–Visible Spectroscopy |
| WE | Working Electrode |
| WL | Weight Loss |
| XPS | X-Ray Photoelectron Spectroscopy |

# CHAPTER 1
# INTRODUCTION

## 1.1 Research Background

Corrosion is the deterioration of materials, primarily metals, due to chemical or electrochemical interactions with their environment. Compared to other industrial materials like plastics, ceramics, and composites, metals are much more vulnerable to corrosion. The most common example of corrosion is rust, which is the degradation of iron and alloy. Globally, corrosion-related expenses are estimated to cost hundreds of billions of dollars annually (Berradja, 2019; Harsimran et al., 2021). This is because repairing and replacing the equipment caused by corrosion is expensive. Corrosion also can affect the environment due to the failures of a structure or components in oil and gas pipelines which can cause leakage.

For instance, mild steel which is a low-carbon steel is often used for building construction (Umeozokwere et al., 2016), machinery elements, pipelines, metal fabrication, and body ships. This is because mild steel has excellent mechanical qualities, low-cost, and is readily available (Rao & Nayak, 2019). According to Umeozokwere et al. (2016), mild steel has exceptional ductility and tensile strength, as well as excellent machinability and weldability. However, the issue with mild steel is its poor corrosion resistance when exposed to corrosive environments (Umeozokwere et al., 2016; Chigondo & Chigondo, 2016; Rao & Nayak, 2019). Thus, corrosion prevention and control are needed to delay or prevent corrosion from happening.

There are various types of corrosion preventions and controls, such as material selection, environmental modification, electrochemical protection, coating, and corrosion inhibitor. Corrosion inhibitors are commonly used in the industry to reduce the corrosion rate of metals and alloys. However, the use of inorganic corrosion inhibitors can be toxic to humans and the environment due to carcinogenic chemicals such as chromates and their non-biodegradable features (Wei et al., 2020). Thus, research has focused extensively on developing and implementing novel environmentally friendly corrosion inhibitors in recent years.

Numerous studies have been done on green corrosion inhibitors derived from plant extracts because of their characteristics in inhibiting corrosion. According to

Salleh et al. (2021), plant extracts were reported to contain naturally synthesized chemical compounds that have been applied as corrosion inhibitors to various industrial systems. Verma et al. (2018) also stated that organic compounds in plant extracts containing heteroatoms such as sulfur, nitrogen, oxygen, and phosphorus could effectively adsorb on metal surfaces and function as corrosion inhibitors. The corrosion inhibitor from plant extracts also reveals high inhibition efficiency through corrosion tests (Alrefaee et al., 2020). Despite the high inhibitor efficiency, green corrosion inhibitors are also lower in cost, environmentally friendly, and safe for humans.

Accordingly, green corrosion inhibitors from plant extracts are important to be studied to replace the toxic inorganic corrosion inhibitor. Besides that, using plant extracts such as fruit peels as corrosion inhibitors can add value to the waste. Hence, the use of local Harumanis mango peel as raw materials for corrosion inhibitors motivates the research interest.

## 1.2 Problem Statements

Metals are extensively used in many industries, such as oil and gas, construction, marine, and agriculture. However, metals are susceptible to corrosion, which raises safety risks and can cause economic loss. According to Verma et al. (2021), the most recent estimate by the NACE (National Association of Corrosion Engineers) places the global cost of corrosion at around $2.5 trillion, or 3.5% of the world's gross domestic product. Therefore, strategies for implementing, controlling, and monitoring corrosion are necessary. Among these, corrosion inhibitors have become one of the most practical and widely researched methods, providing a cost-effective way to extend the lifespan of metal structures and equipment.

However, despite their effectiveness, conventional corrosion inhibitors have raised environmental and health concerns, suggesting the need to a safer alternative. Recently, scientists have been more directed to develop an eco-friendly and low-cost corrosion inhibitors to replace the toxic and harmful corrosion inhibitors. The use of inorganic corrosion inhibitor is becoming a major concern due to the presence of heavy metals such as chromate and phosphate, which is toxic to environments and humans. Accordingly, plant-based green organic corrosion inhibitors are produced to overcome this problem. Nevertheless, in current research, the use of plant extracts as corrosion inhibitors in the near-neutral medium is limited. Hence, this study used a local plant

extract, Harumanis mango peel extracts as organic and green corrosion inhibitors in both acidic and near-neutral media.

Although Harumanis mango peel extract has the potential as a green corrosion inhibitor, there is also a limited study on its chemical characterization. Most of the existing studies on mango peel were focus on other applications, such as food products, cosmetics, and pharmaceuticals (Kucuk *et al*., 2024). In studies investigating mango peel extract as a corrosion inhibitor, the focus frequently is on its performance rather than identifying the functional groups and active compounds that contribute to the inhibition effect. It is challenging to explain the inhibition mechanism and improve the extract's effectiveness without the chemical properties' information. Thus, the chemical analysis of the Harumanis mango peel would improve the formulation strategies and enhance the potential of Harumanis mango peel extract as a green corrosion inhibitor.

Some studies have been done using mango waste as a corrosion inhibitor in the past, but there is limited research on a near-neutral medium compared to an acidic medium. This is due to the wide finding of corrosion inhibitor studies showing that plant extract is more effective in acidic environments (Hossain *et al.,* 2020; Miralrio & Espinoza Vázquez, 2020). Besides that, prolonged experimental duration has likewise contributed to the limited reporting of studies in near-neutral medium. However, chloride media in general present challenges that hinder the abilities of plant extracts to inhibit corrosion effectively. In acidic chloride medium (HCl), the low pH and chloride ions accelerate the metal dissolution, and also degrade the extract molecules. In a near-neutral medium (NaCl), the chloride ions may destabilize the protective film on the metal surface; thus, the extract molecules may precipitate, reducing stability. Therefore, the corrosion inhibition efficiency of Harumanis mango peel extract was evaluated in both acidic and near-neutral media to identify the optimal concentration range that offers effective and stable protection for mild steel.

However, the difficulty in determining the plant extract's anticorrosive properties as its presence in neutral makes it difficult to describe the occurrence of inhibitory phenomena (Karattu Veedu *et al.,* 2019), yet, this constraint could be overcome by improving the formulation or synthesis of the inhibitor and corrosion test parameters. Thus, a study on mango waste as a corrosion inhibitor in both acidic and near-neutral media was conducted to understand more about the inhibitory properties of the inhibitor. The study starts with an extraction of the local Harumanis mango peel

followed by corrosion tests. The adsorption study performed was used to determine the types of corrosion mechanisms.

As a result, in this study, Harumanis mango peel extract was used as a green corrosion inhibitor for mild steel in HCl and NaCl to fulfil the leaving gap in sustainable corrosion prevention strategies.

## 1.3 Hypothesis

i) The chemical compound of the Harumanis mango peel will consists of phenolic compounds such as hydroxyl and carbonyl groups.
ii) The higher the concentration of Harumanis mango peel extract corrosion inhibitor, the greater the inhibition efficiency, and lower the corrosion rates.
iii) The higher the temperature and concentration of the Harumanis mango peel extract, the higher the adsorption of Harumanis mango peel molecules onto the mild steel surface.

## 1.4 Research Objectives

To make this research, the objectives of the study are:

a) To identify the chemical functional groups and compounds of Harumanis mango peel extract using Fourier-transform infrared spectroscopy (FTIR), Ultraviolet-visible spectroscopy (UV-Vis), High-performance liquid chromatography (HPLC), and Gas chromatography-mass spectrum (GC-MS).
b) To evaluate the performance inhibition efficiency of Harumanis mango peel extract as a corrosion inhibitor for mild steel in acidic (0.5 M HCl) and near-neutral (0.6 M NaCl) environments by weight loss and electrochemical analysis.
c) To investigate the adsorption behaviour and surface interactions of the Harumanis mango peel extract on mild steel in order to determine the mechanism of corrosion inhibition.

## 1.5 Research Question

i) Why the chemical compounds found in Harumanis mango peel extract can inhibit corrosion?
ii) How does Harumanis mango peel extracts perform as corrosion inhibitor in acidic and near-neutral solutions for mild steel?
iii) How does the Harumanis mango peel corrosion inhibitor adsorbs on the metal surface?

## 1.6 Scopes and Limitations of Study

In this research study, Harumanis mango peel is the raw material that will be used for formulating a green organic corrosion inhibitor. The Harumanis mango peel will be collected from Harumanis Farm UiTM Arau Plantation, Perlis, Malaysia. The crude Harumanis mango peel extract was used as a corrosion inhibitor without isolating specific compounds. The metal that was used in this study is mild steel. The mild steel was immersed in two corrosive mediums: 0.5 molar hydrochloric acid (0.5M HCl) and 0.6 molar sodium chloride (0.6 M NaCl). The 0.6 M NaCl is chosen as a neutral corrosive medium since the concentration is similar to the salinity of seawater.

The chemical functional groups and compounds in Harumanis mango peel extract such as hydroxyl and carbonyl groups that may shows as corrosion inhibitory properties were analyzed. The analysis of the functional groups and chemical structure of the Harumanis mango peel was done using Fourier-transform infrared spectroscopy (FTIR), Ultraviolet-visible spectroscopy (UV-Vis), High-performance liquid chromatography (HPLC), and Gas chromatography-mass spectrum (GC-MS).

The corrosion test was performed in two methods: weight loss test and electrochemical method (potentiodynamic polarization and electrochemical impedance spectroscopy). In the weight loss method, the mild steel was immersed in an acidic medium (0.5 M HCl) and neutral medium (0.6 M NaCl) and in the presence of Harumanis mango peel corrosion inhibitor for 1, 3, 5, 7, and 10 days. The concentration of the Harumanis mango peel varied from 50 to 350 ppm for both tests.

Furthermore, the adsorption behaviour was evaluated using adsorption isotherm models (Langmuir and Temkin) based on the data obtained from the weight loss test. In addition, the surface study of the metal in the corrosive mediums and in the presence of

Harumanis mango peel extract inhibitor was analyzed using an optical microscope (OM), scanning electron microscope (SEM), and x-ray photoelectron spectroscopy (XPS).

A limitation of this research is that studying the near-neutral medium requires a longer time to produce results compared to the acidic medium, where mild steel reacts more readily. In addition, the research was also done under static laboratory conditions; therefore, the effects of flow and real industrial conditions were absent. Another limitation of this study is that the Harumanis mango peel extract, derived from a single plant source, was used as a corrosion inhibitor. The extract was used as a whole, without fractionation and isolation of its active inhibitory compound.

# CHAPTER 2
# LITERATURE REVIEW

## 2.1 Corrosion

Corrosion is a process of degradation of metal due to an electrochemical reaction with its surroundings (Tait, 2018, Harsimran *et al*., 2021, Ibrahimi *et al*., 2021). Corrosion occurs in metals and alloys when they come into contact with specific corrosive medium, such as aqueous solutions containing salts, acidic or alkaline environments, gases like oxygen or sulphur dioxide, or in conditions with high humidity. A simple example of a corrosion process is the deterioration of iron and its alloy, which will form rust as a corrosion product. Figure 2.1 show the mechanism of corrosion.

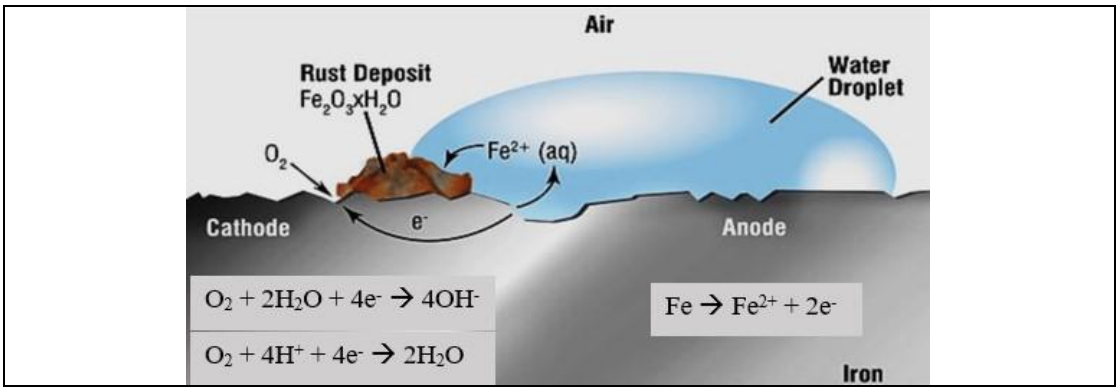


Figure 2.1 Mechanism of Corrosion (Aljamali et al., 2019)

In general, there are four conditions must be met for metals and alloys to undergo corrosion. First, an anodic reaction occurs where metal atoms lose electrons, leading to the formation of metal ions. Second, a correspond cathodic reaction takes place, typically involving the reduction of hydrogen ions or oxygen. Third, the presence of an electrolyte is essential to facilitate the flow of ions between anodic and cathodic sites. Finally, a metallic path is required to allow the flow of electrons between anode and cathode, completing the electrochemical circuit. These conditions collectively drive the corrosion process.

In the corrosion process, anodic and cathodic reactions occur simultaneously to maintain electrical neutrality. At the anodic site, the metal atoms lose electrons and form

ions, while at the cathodic site, these electrons are consumed in reduction reactions. This interplay drives the electrochemical process and leads to the degradation of the metal surface. The following equations illustrate the specific reaction occurring at the anode and cathode during corrosion. Oxidation occurs at anode, where the following reaction takes place in 2.1):

$$Fe \rightarrow Fe^{2+} + 2e^{-} \qquad 2.1)$$

In the electrochemical process, electrons are emitted by the formation of metallic ions at the anode flow via the current-carrying pathway to the cathodic regions. Both anodic and cathodic reactions restore the system's electrical balance (Kamachi Mudali *et al*., 2019).

For reduction reaction at cathodic, the most common is reduction of $H^+$ or $O_2$ as shown in Equation 2.2), 2.3), and 2.4) below:

$$2H^+ + 2e^- \rightarrow H_2 \qquad \text{(acidic)} \qquad 2.2)$$

$$O_2 + 4H^+ + 4e^- \rightarrow 2H_2O \qquad \text{(acidic)} \qquad 2.3)$$

$$O_2 + 2H_2O + 4e^- \rightarrow 4OH^- \qquad \text{(alkaline or neutral)} \qquad 2.4)$$

As shown in Figure 2.1, the corrosion product deposited (rust) is a hydrated ferric oxide ($Fe_2O_3.xH_2O$) which can be seen in the colour of reddish brown. The $OH^-$ ions react with $Fe^{2+}$ ions produced at the anode to form ferrous hydroxide ($Fe(OH)_2$), as shown by Equation (2.5).

$$Fe^{2+} + 2OH^- \rightarrow Fe(OH)_2 \qquad 2.5)$$

Equation 2.6 shows $Fe(OH)_2$ is then oxidized to $Fe(OH)_3$ due to the oxygen in the air.

$$4Fe(OH)_2 + O_2 + 2H_2O \rightarrow 4Fe(OH)_3 \qquad 2.6)$$

Then, $Fe(OH)_3$ is converted to $Fe_2O_3.xH_2O$ or rust, as depicted in equation 2.7.

$$2Fe(OH)_3 \rightarrow Fe_2O_3.xH_2O + (3-x)H_2O \quad 2.7)$$

## 2.2 Types of Corrrosion

Corrosion is classified into several types depending on its characteristics and underlying mechanism.

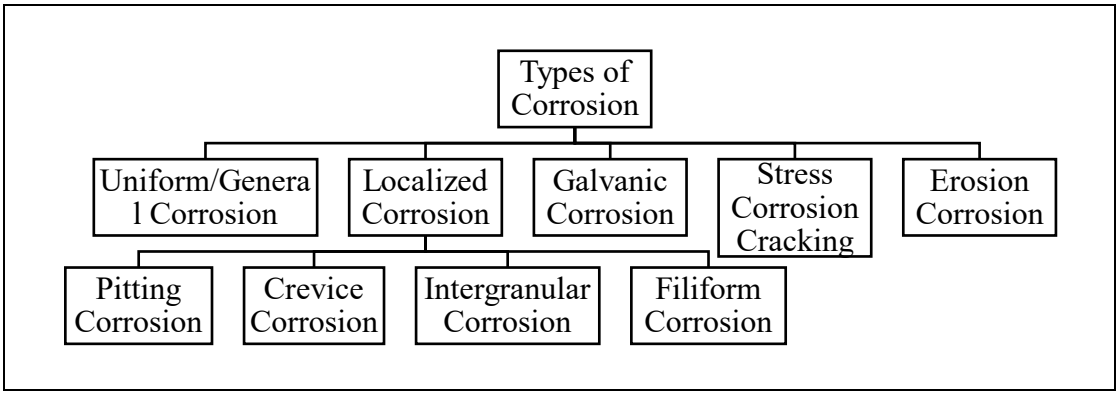


Figure 2.2 Types of Corrosion (McCafferty, 2011 & Ibrahimi *et al*., 2021)

The most common type of corrosion is uniform corrosion or general corrosion. This type of corrosion will deteriorate uniformly. There are four different types of localized corrosion: pitting corrosion, crevice corrosion, intergranular corrosion, and filiform corrosion. These corrosions usually cause damage in concentrated places and are often more severe than uniform corrosion. Galvanic corrosion occurs under certain conditions when two dissimilar metals come into electrical contact in a corrosive environment. These phenomena cause the more anodic metal to corrode more quickly due to electrochemical potential different (Verma, 2022; Osman & Abdel-Salam, 2020). Next, stress corrosion cracking (SCC) is the formation of cracks in a corrosive environment, aggravated by tensile stress from the manufacturing process. This type of corrosion is especially dangerous as it can cause failure to the materials without causing major deformation (Evangeline *et al.,* 2023; Khasanova, 2022). Lastly, erosion is a combined process in which mechanical erosion and electrochemical corrosion interact, resulting in material loss. This is common in systems that transport fluids, such as pipelines (Zadeh, 2023).

## 2.3 Corrosion Prevention and Control

The severe damage that corrosion causes have a negative impact on human life in many ways. However, it is something that can be prevented or controlled. Thus, Figure 2.3 depicts corrosion control to prevent properties from deteriorating.

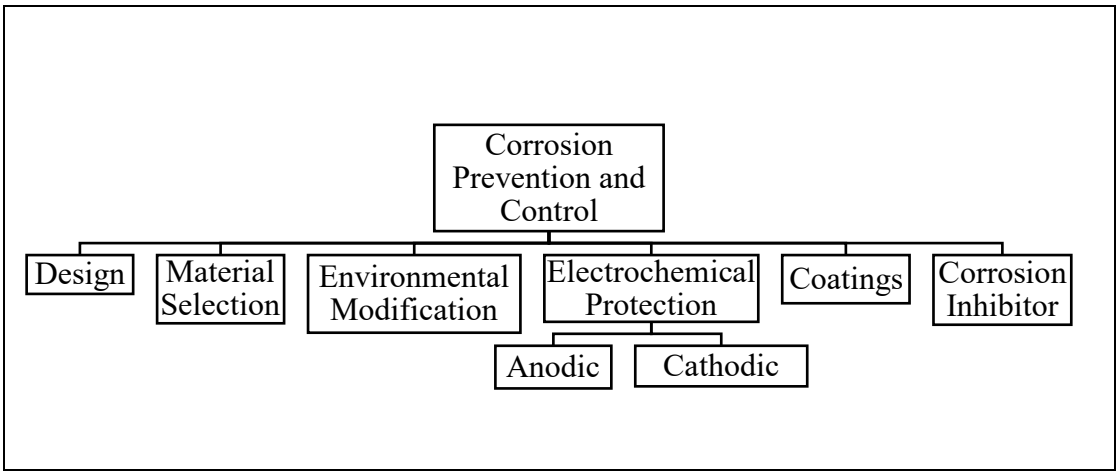


Figure 2.3 Types of Corrosion Prevention and Control (McCafferty, 2011 & Wei *et al*., 2020)

Corrosion prevention and control include a variety of solutions for reducing or eliminating the damaging effects of corrosion. The methods include proper design and material selection to increase durability, environmental modification to reduce corrosive conditions, and electrochemical protection using anodic and cathodic systems. Other options are applying coatings to protect the material's surface and using corrosion inhibitors to slow down the corrosion rate. Among these methods, this study will focus on the use of corrosion inhibitors on metal surfaces and investigate their efficiency in reducing corrosion.

## 2.4 Corrosion Inhibitor

A corrosion inhibitor is a chemical substance that, when introduced to a corrosive environment, can significantly reduce the rate of metal corrosion or, in some cases, delay its onset (Wei *et al.,* 2020). According to Taghavikish *et al.* (2017), adding a minimal amount of corrosion inhibitor to an interfacial layer can slow the rate of metal corrosion significantly and in some cases, prevent its occurrence. Monticelli (2018) & Reza *et al.* (2021) stated there are three classifications for corrosion inhibitors: i)

cathodic corrosion inhibitor, ii) anodic corrosion inhibitor, and iii) mixed-types corrosion inhibitor. Cathodic inhibitors work by reducing the cathodic reaction rate either by slowing down the reduction of oxygen or hydrogen evolution or by precipitating insoluble compounds on the cathodic sites, blocking electron transfer. For example, the use of 3-methylsalicylate (3-MeSA) as a corrosion inhibitor on magnesium alloys, where it binds to Fe ions, preventing their re-deposition onto the surface and thus, reducing the cathodic reaction (Yang *et al.,* 2024). Next, anodic inhibitors slow down the anodic reaction rate by forming a passive oxide layer on the metal surface to inhibit further oxidation and limit the dissolution of metal ions into the electrolyte. A study by Wang *et al.* (2024) found that benzotriazole was an anodic inhibitor in the study of nitrogen-containing organic compounds for corrosion prevention on copper, significantly reducing the anodic dissolution of copper in an alkaline slurry. Finally, the mixed-type inhibitors affect both anodic and cathodic reaction rates by creating protective films on the metal surface, effectively reducing the overall corrosion rate without favouring any reaction.

Many types of inhibitors would produce a film at the metal/solution interface, though some may act through other mechanisms such as altering the electrochemical environment. These are three different types of the film formed:

- Passivating film: This type of inhibitors can provide effective corrosion protection by forming a thick oxide film.
- Precipitation film: This type of inhibitor forms impermeable protective films by reacting with soluble substances in the environment.
- Adsorption film: This type of inhibitor adsorbed the inhibitor molecules to prevent oxygen and water from diffusing to the metal surface.

### 2.4.1 Classification of Corrosion Inhibitor

Corrosion inhibitors are typically classified into categories such as organic and inorganic. The classification of the inhibitors can be seen in Figure 2.4. These corrosion inhibitors play critical roles in preventing the metal surfaces from degradation. Organic corrosion inhibitors are known for their ability to adsorb on metal surfaces and form a protective film to prevent metal degradation. This adsorption might be either physical, chemical, or film-forming, depending on the nature of the inhibitor and metal surface (Garg *et al.,* 2024; Zhao *et al.,* 2023). Next, inorganic corrosion inhibitors were divided

into two types: anodic and cathodic. Anodic inhibitors function by forming a protective oxide film on the metal surface, whereas cathodic inhibitors function by slowing the cathodic reaction (Alvarez *et al*., 2023).

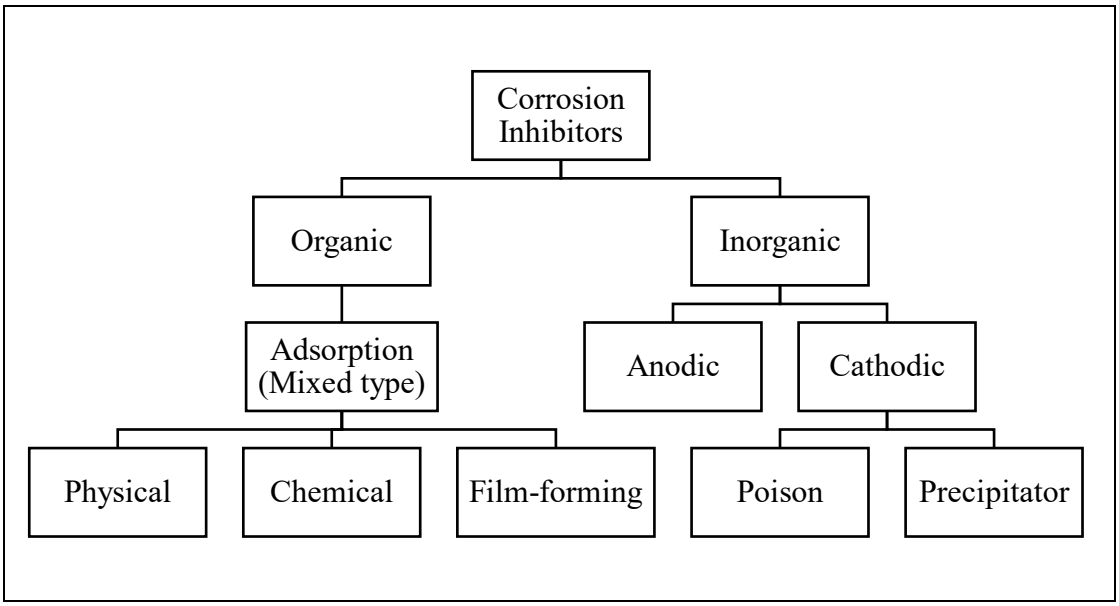


Figure 2.4 Classification of Corrosion Inhibitors (McCafferty, 2011; Dariva & Galio, 2014; Alrefaee *et al*., 2021)

The disadvantages of some conventional inorganic corrosion inhibitor are that it can be inherently harmful and hazardous to the environment and humans due to their chemical composition. Inorganic corrosion inhibitors such as chromates are known to be carcinogens and can cause severe health issues with prolonged exposure. Other substances like nitrates and benzoate may pose health or environmental risks depending on their concentration and usage (Omotosho *et al*., 2016 & Reza *et al*., 2021). Many conventional inorganic corrosion inhibitors are non-biodegradable, which can result in long-term environmental harm (Fidrusli *et al.,* 2018, Verma *et al*. 2018, Alrefaee *et al*., 2021). Some of inorganic corrosion inhibitors can also be costly to produce and apply, especially in large-scale or specific industrial contexts (Alrefaee *et al*., 2021). The drawbacks of traditional corrosion inhibitors illustrate why green corrosion inhibitors should be used instead. Due to the environmental and health concerns associated with conventional inhibitors, researchers are exploring organic green inhibitors as safer and more sustainable alternatives.

## 2.5 Plant Extracts as Corrosion Inhibitor

Nowadays, many sources can be used as natural green corrosion inhibitors, including biopolymers (chitosan), amino acids, and plant extracts (Miralrio & Espinoza Vázquez, 2020 & Salleh *et al.,* 2021). However, researchers are keen to study the characteristics and effectiveness of plant extracts as corrosion inhibitors due to their availability, cost-effectiveness, and compatibility with the environment.

Plant extracts have been widely studied as natural organic corrosion inhibitors because their phytochemical compounds, such as flavonoids and alkaloids, possess antioxidant properties, which can neutralize reactive species involved in corrosion. Vorobyova *et al.,* (2019) also claimed it has been discovered that plant components such as biopolymers, protein, flavonoids, and alkaloids demonstrate efficient inhibitory activity, primarily due to their ability to adsorb onto metal surfaces and reduce oxidative reaction.

### 2.5.1 Plant Extracts as Corrosion Inhibitors in Different Corrosive Mediums

Studies have shown that plant extracts as corrosion inhibitors often exhibit higher efficiency in acidic mediums compared to neutral or alkaline solutions, likely due to the increased reactivity of the acidic environment. While extensive research has demonstrated the effectiveness of plant extracts in acidic mediums, studies exploring their potential in neutral environments remain relatively limited. In this study, the potential and effectiveness of Harumanis mango peel extract as a corrosion inhibitor was investigated in both acidic and near-neutral media.

#### *2.5.1.1 Corrosion Inhibition in Acidic Mediums*

A lot of studies have been done on plant extracts as corrosion inhibitors in acidic mediums. Table 2.1 depicts the current research that has been done using plant extracts in acidic medium.

Table 2.1
Studies on Plant Extracts as Corrosion Inhibitors in Acidic Medium.

| **Plant and Part Extract** | **Extracting Solvent** | **Corrosive Medium** | **Corrosion Test Methods** | **References** |
|---|---|---|---|---|
| *Cyptocarya Nigra* bark | Hexane, Dichloromethane, Methanol | 1 M HCl | PP, EIS, SEM-EDS, FTIR, UV-Vis | Faiz *et al.* (2020) |
| *Luffa cylindrical* leaves | Ethanol | 1 M HCl | WL, PP, EIS, FTIR | Ogunleye *et al.* (2020) |
| *Ziziphora* leaves | Water | 0.5 M $H_2SO_4$ | FTIR, UV-Vis, EIS | Dehghani *et al.* (2020) |
| *Cannabis Sativa* leaves | Methanol | 0.5 M $H_2SO_4$ | WL, PP, EIS, SEM, AFM | Haldhar *et al.* (2021) |
| *Garcinia indica* fruits | Water | 1 M HCl | WL, PP, EIS | Thomas *et al.* (2020) |
| *Punica Granatum L* barks | Methanol | 1 M HCl | WL, PP, EIS | Marsoul *et al.* (2020) |
| Rhoeo discolor plant leaves | Ethanol | 0.5 M HCl | PP, EIS | Gayakwad *et al.* (2022) |

WL, weight loss; PP, potentiodynamic polarization; EIS, electrochemical impedance spectroscopy; FTIR, fourier-transform infrared spectroscopy; UV-Vis, ultraviolet-visible spectroscopy; SEM-EDS, scanning electron microscopy-energy dispersive spectroscopy; AFM, atomic force microscopy.

According to Ogunleye *et al*. (2020), a study has been done on Luffa cylindrica Leaf Extract (LLCE) as a corrosion inhibitor in 0.5 M HCl for mild steel. The highest inhibition efficiency was obtained at 87.89% at the concentration of the inhibitor 1.0 g/L LLCE in 12 h immersion time. The high inhibition efficiency of the inhibitor is attributed to the presence of the hydroxy aromatic compounds, such as phenolic derivatives, which promote adsorption on the metal surface. The adsorption of LCLE on mild steel surfaces at all studied temperatures and duration was found to be followed the Langmuir isotherm model.

A study on Ziziphora leaves extract as a corrosion inhibitor in 1 M HCl for mild steel was evaluated by Deghani *et al.* (2020). The maximum inhibition efficiency of 93% was obtained at 800 ppm after 2.5 h through electrochemical impedance spectroscopy (EIS) study. The polarization curves reveal that the corrosion inhibitor exhibits mixed-typed behavior. The adsorption of the Ziziphora leaves corrosion inhibitor on the metal surfaces obey Langmuir isotherm model.

The evaluation of the methanolic extract of *Punica Granatum* L. bark as a corrosion inhibitor for mild steel in 1 M HCl was studied by Marsoul *et al.* (2020). The results obtained from EIS showed that the optimum inhibition efficiency is 88% at a concentration of 1 g/L. The corrosion inhibitor is mixed-type according to the polarization curves. The corrosion inhibitor adsorption also followed the Langmuir isotherm model.

### *2.5.1.2 Corrosion Inhibition in Near-Neutral Medium*

Many plant extract corrosion inhibitors have been done in acidic rather than neutral mediums. This is likely because plant extracts corrosion inhibitors often demonstrate higher adsorption and reactivity in acidic solutions, leading to better inhibition efficiency. However, several studies on plant extracts as corrosion inhibitors in neutral solutions exhibited excellent results, as shown in Table 2.2.

Table 2.2
Studies on Plant Extracts as Corrosion Inhibitors in Near-Neutral Medium.

| Plant Extracts | Findings | References |
|---|---|---|
| *Allium Sativum* or garlic extract | The garlic extract corrosion inhibitor prepared in concentration (2mL – 10mL) was studied by PP and EIS for mild steel in 3.5% NaCl. The highest inhibition efficiency obtained is 95% at concentration of 10 mL. The complex compounds in the garlic extract, such as S-allylcysteine and S-allymercapto-L-cysteine, which are rich in sulphur content was contributed to the inhibition effect. The polarization study showed the inhibitor is mixed-type and protective film formed on the metal surface. | Devikala *et al*., (2019) |
| *Elettaria cardamomum* extract | The ethanol extract of *Elettaria cardamomum* (E. cardamomum) was used as a corrosion inhibitor for mild steel in 3.5% NaCl. The inhibitory of the extract was studied using weight loss test, PP, and EIS. The maximum inhibition efficiency obtained was 73.5% for 1 day at 250 ppm. The PP test revealed that the inhibitor primarily exhibited cathodic protection behaviour. The adsorption process of the inhibitor was physisorption and obeyed the Langmuir isotherm model. | Shyamvarnan *et al*., (2020) |
| *Vicia Faba* peel extract | The *Vicia Faba* (VF) peels were extracted using two different solvents (hexane and acetone). The inhibitory effects of both extracts for mild steel in 3.5% NaCl were studied using PP and EIS. The results show the highest inhibition efficiency for both extracts were at 200 ppm with 97.84% for hexane and 88.67% for acetone. The presence of benzene rings likely enhances adsorption on the metal surface, thereby increasing the inhibitor's efficiency. Both extracts function as mixed-type inhibitors. | Abdelshafeek *et al*., (2022) |

### 2.5.2 Harumanis Mango

Harumanis mango, or its scientific name *Mangifera indica L.*, is a very popular mango commercially cultivated in the North Peninsular State of Malaysia, Perlis (Sani *et al*., 2018). The Harumanis mango is a once-a-year seasonal fruit with a current market price of up to 10 USD, which is quite expensive compared to other mango varieties (Uda *et al.,* 2020). Even though it is expensive, the mango is still the most popular among Malaysians and has become well-known and iconic in Perlis. With the high amount of Harumanis mango produced every year, there is a lot of mango waste, such as mango kernel and peel abundance. Thus, many researchers have transformed this waste to produce useful green by-product since mango peels and seeds are known to have many advantages.

Harumanis mango contains a number of compounds that have been shown to have antioxidant activity, for example, mangiferin (Ifmaily, 2019). Mangiferin is a polyphenolic compound found in mangoes. It is a yellow-orange crystalline solid that is soluble in water and ethanol. The biological activities of mangiferin include antioxidant, anti-inflammatory, anti-diabetic, and anticancer properties. Peel of the mango fruit contains the highest concentration of mangiferin. The flesh of the mango fruit contains mangiferin, though in a lesser concentration. Figure 2.5 depicts the mangiferin compound. Hence, the Harumanis mango peel compound will be studied in this research.

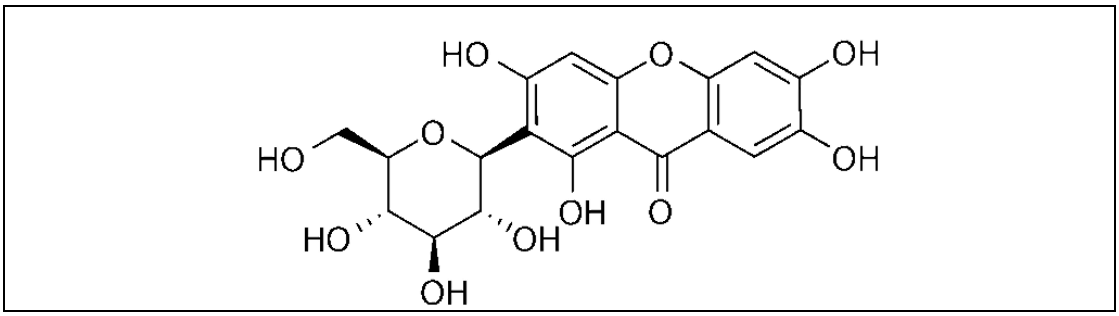

Figure 2.5 Mangiferin

Ali et al. (2012) found that mango peel has a high concentration of phytochemicals, such as polyphenols and flavonoids, that have potent antioxidant activity. According to Rocha et al. (2014), using mango peel as a corrosion inhibitor in 1M HCl with carbon steel depicts high inhibition efficiency using both gravimetric and

electrochemical methods. The highest efficiency obtained in the weight loss, potentiodynamic polarization, and electrochemical impedance methods were 97, 96, and 94%, respectively.

Nonetheless, there are limited studies on the mango peel's inhibition behaviour in a near-neutral solution. Therefore, in this research, the chemical compounds, the performance, and the adsorption of the Harumanis mango peel as a corrosion inhibitor for mild steel was studied more in both acidic and neutral mediums.

## 2.6 Corrosion Monitoring

Corrosion monitoring is a crucial process for monitoring metal degradation in various environments. The methods involved in this monitoring are weight loss analysis, electrochemical study (potentiodynamic polarization and electrochemical impedance spectroscopy), and surface study. This monitoring is important for industries to avoid structural failures, extend the lifespan of equipment, and optimize maintenance strategies.

### 2.6.1 Weight Loss Measurement

The weight loss via immersion is a conventional or gravimetric method used to determine corrosion rate. The corrosion rate is calculated using Equation 2.8, which measures the weight loss of a known surface area during a given immersion period in a corrosive solution (Ibrahimi *et al.,* 2021).

$$\text{Corrosion rate (mm/y)} = \frac{K \times W}{D \times A \times T} \qquad 2.8)$$

Where,

K = Constant ($8.76 \times 10^4$)

W = Weight Loss (g)

D = Density of metal ($g/cm^3$)

A = Area of metal ($cm^2$)

T = Time of exposure (hours)

The inhibition efficiency of the corrosion inhibitor can be calculated using Equation 2.9.

$$\text{Corrosion rate (mm/y)} = \frac{K \times W}{D \times A \times T} \quad 2.9)$$

Where,

$CR_o$ = corrosion rate of uninhibited metal (g)

$CR_f$ = corrosion rate of inhibited metal (g).

The inhibition efficiency of the corrosion inhibitor can also be calculated using weight loss data by applying Equation 2.10.

$$\text{Inhibition efficiency, IE\%} = \frac{WL_o - WL_f}{WL_o} \times 100 \quad 2.10)$$

Where,

$WL_o$ = weight loss of uninhibited metal (g)

$WL_f$ = weight loss of inhibited metal (g).

For example, figure 2.6 shows graph for corrosion rate and inhibition efficiency versus inhibitor concentration for a study using banana peel as corrosion inhibitor for mild steel in 1 M HCl (Rosli *et al.,* 2019). According to the graph, the corrosion rate decrease and inhibition efficiency increase as the concentration of the inhibitor increase. This is because the adsorption coverage on the mild steel surface increased as the concentration increased, thereby blocking the reaction sites. The highest inhibition efficiency which is 88.99% was also obtained at 500 ppm.

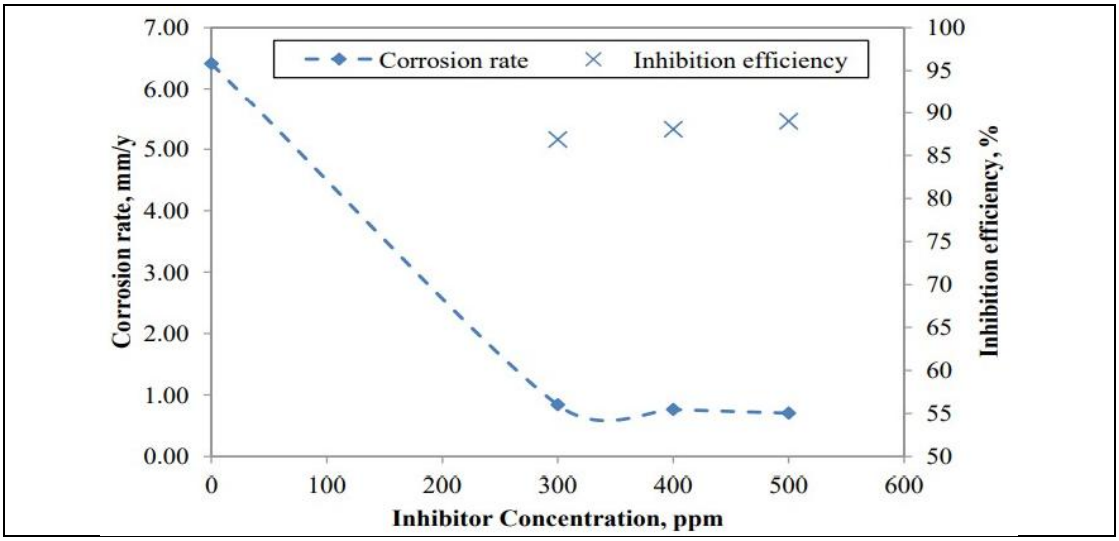

Figure 2.6 Corrosion Rate and Inhibition Efficiency versus Concentration of Banana Peel Inhibitor Graph (Rosli *et al*., 2019)

Numerous studies have used this method, which is relatively simple, easy, and inexpensive, to obtain corrosion rate (Thangarasu & Anand, 2019). However, more than this technique is required for accurate analysis.

### 2.6.2 Electrocchemical Study

#### *2.6.2.1 Potentiodynamic Polarization*

The potentiodynamic polarization test is the most commonly recognized electrochemical technique for measuring metal corrosion (Keshavamurthy et al., 2021). This method provides information on some important electrochemical corrosion parameters, including corrosion current density (icorr) and corrosion potential (Ecorr), as well as cathodic and anodic Tafel slopes (Ibrahimi et al., 2021). The measurements are conducted in standard; a three-electrode cell consisting of the reference electrode (RE), auxiliary or counter electrode (CE), and the working electrode (WE) (Brycki et al., 2018). The WE is the sample metal where the reaction occurs. CE receives voltage, which supplies sufficient current to compensate for redox reactions occurring at WE, while RE measures the WE potential (Dryden & Wheeler, 2015). Commonly used RE are saturated calomel electrodes (SCE) and Ag/AgCl, and for CE are platinum, graphite, and gold.

The information from the intersection of the Tafel slopes on the polarization curves obtained, such as $E_{corr}$ and $i_{corr}$, can be used to calculate corrosion rate and

inhibition efficiency (Salleh et al., 2021). Equations 2.11 and 2.12 show the calculation of the corrosion rate and inhibition efficiency, respectively.

$$\text{Corrosion rate (mm/y)} = \frac{i_{corr} \times \kappa \times EW}{\rho \times A} \quad 2.11)$$

$$\text{Inhibition efficiency (IE\%)} = \frac{(i_{corr})_a - (i_{corr})_p}{(i_{corr})_a} \times 100 \quad 2.12)$$

Where $i_{corr}$ is current density ($Am^{-2}$), κ is conversion factor, EW is equivalent weight (g), ρ is density of the metal ($g/cm^3$), A is sample area ($cm^2$), and $(i_{corr})_a$ and $(i_{corr})_p$ is current density in the absence and presence of the inhibitor, respectively.

A study by Kumar & Yadav (2020) using Musa Acuminata or banana peels as corrosion inhibitors for mild steel in 5 M HCl classified the inhibitor as mixed-type. According to the study, the current densities ($i_{corr}$) decrease for both cathodic and anodic branches in the presence of Musa Acuminata peel inhibitor. The cathodic and anodic polarization was retarded to the same degree, and corrosion inhibition also increased as the concentration of the inhibitor increased. Figure 2.7 depicts the example of potentiodynamic polarization plots for the corrosion of mild steel with and without inhibitor in 5 M HCl solution.

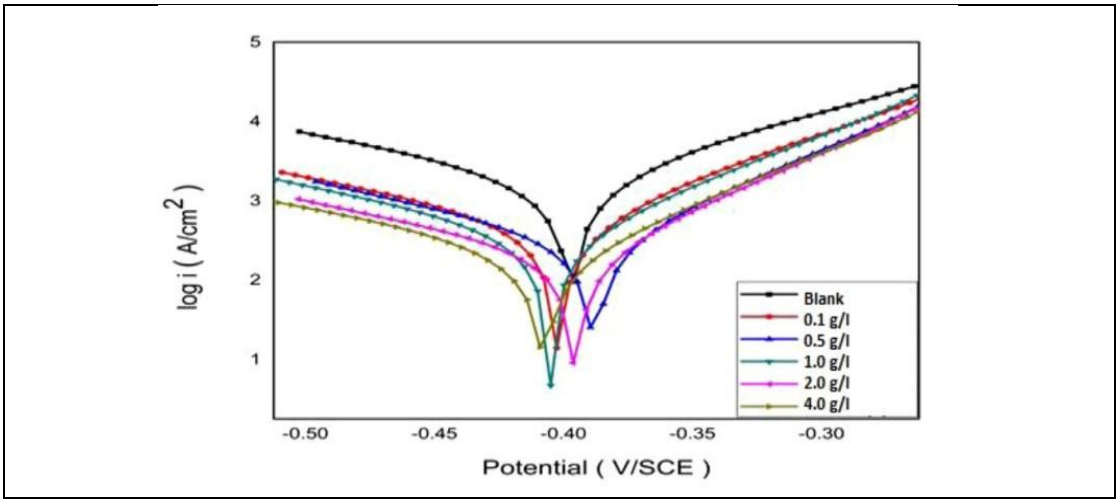


Figure 2.7 Potentiodynamic Polarization Plots for Musa Acuminata as Corrosion Inhibitor for Mild Steel in 5 M HCl (Kumar & Yadav, 2020)

### *2.6.2.2 Electrochemical Impedance Spectroscopy*

Electrochemical Impedance Spectroscopy (EIS) is one of the most effective methods for monitoring metal corrosion. EIS is often measured by delivering alternating current (AC) potential to an electrochemical cell; it depicts the circuit's response to an alternating current or voltage as a function of frequency (Hernández *et al.,* 2020). The polarization resistance, $R_p$, is the basic measurement parameter in direct current (DC) methods such as potentiodynamic polarization. In DC theory (where the frequency is equal to 0 Hz), resistance is described by Ohm's Law, as shown in Equation 2.13.

$$E = IR \tag{2.13}$$

where, E is defined as potential in volts (V), I is equal to current in amps (A), and R is resistance in ohms (Ω).

Resistance and impedance both refer to opposition to the flow of electrons or electrical current. Thus, according to AC theory, when the frequency is non-zero, the related Equation 2.14 is as below:

$$E = IZ \tag{2.14}$$

where everything is the same as the previous equation 2.13 except Z which is impedance also measure in ohms (Ω).

In corrosion studies, impedance measurements of the corrosion system can determine the effectiveness of a corrosion inhibitor. The level of corrosion protection can be measured by comparing the impedance obtained in the presence and absence of inhibitors in the corrosive environment. The charge transfer resistance values obtained from the Nyquist plots in the impedance measurements can be used to calculate the inhibition efficiency (IE*%).* Equation 2.15 shows the calculation for the inhibition efficiency.

$$\text{IE\%} = \frac{R_{ct(inh)} - R_{ct}}{R_{ct(inh)}} \times 100 \tag{2.15}$$

Where,

$R_{ct(inh)}$ = charge transfer resistance with inhibitor.

$R_{ct}$ = charge transfer resistance without inhibitor.

For example, a study by Stango and Vijayalakshmi (2018) using orange peel waste as corrosion inhibitor for mild steel in 1 M HCl depicts Nyquist plots in Figure Figure 2.8. The Nyquist plots show increasing the concentration of the inhibitor, increase the diameter of the capacitive loop. The study also states the charge transfer resistance increase and capacitance decrease as the concentration of the inhibitor increase which confirms the formation of the protective layer on the metal surface at the electrolyte interface.

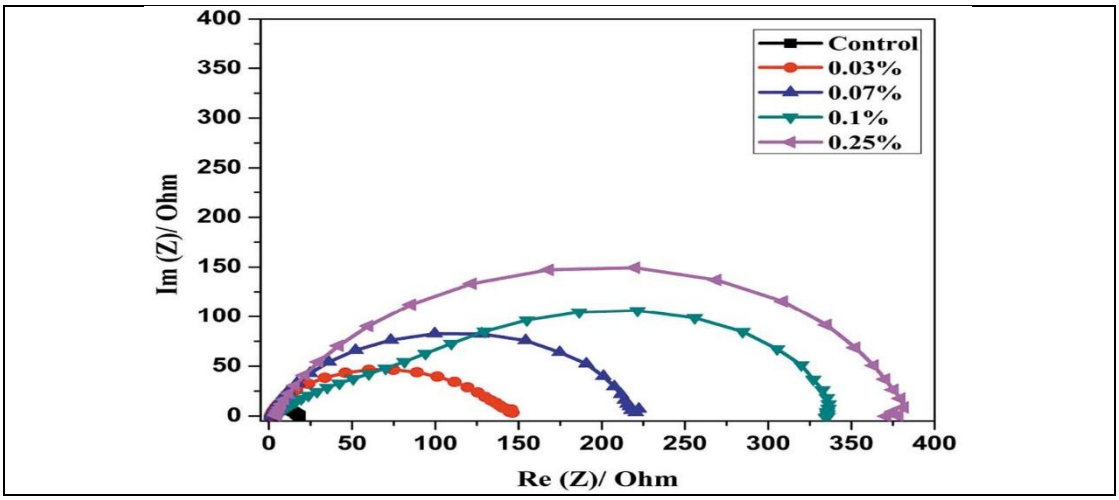


Figure 2.8 Nyquist Plots for Mild Steel in 1 M HCl and in the Presence of Orange Peel Waste as Corrosion Inhibitor (Stango & Vijayalakshmi, 2018)

## 2.7 Corrosion Surface Study

Besides the corrosion test using weight loss measurement and electrochemical methods, the effect of corrosion on the metal surface is also studied by using optical microscopy, scanning electron microscopy, and chemical surface study using x-ray photoelectron spectroscopy.

### 2.7.1 Optical Microscopy Study

The optical microscope, also known as the "light optical microscope," is the oldest type of microscope that magnifies images of small materials using visible light

and a set of lenses (Di Gianfrancesco, 2017). In this corrosion study, the optical microscope can be used to observe the morphology of corrosive surface metal with or without an inhibitor.

A research by Loto (2018) studied the surface coverage of low-carbon steel in HCl with Rosmarinus officinalis and zinc oxide (RSZ) as corrosion inhibitors using an optical microscope. The result obtained can be seen in Figure 2.9. It can be seen from Figure 2.9 that the inhibited steel shows better morphology than the uninhibited steel. The surface of the deteriorated steel from the HCl solution (Figure 2.9a) displays a severely degraded appearance with macro and micro pits compared with the inhibited RSZ. This is because the adsorption of RSZ cations on steel limits the diffusion and electrolytic transport of $Cl^-$ ions.

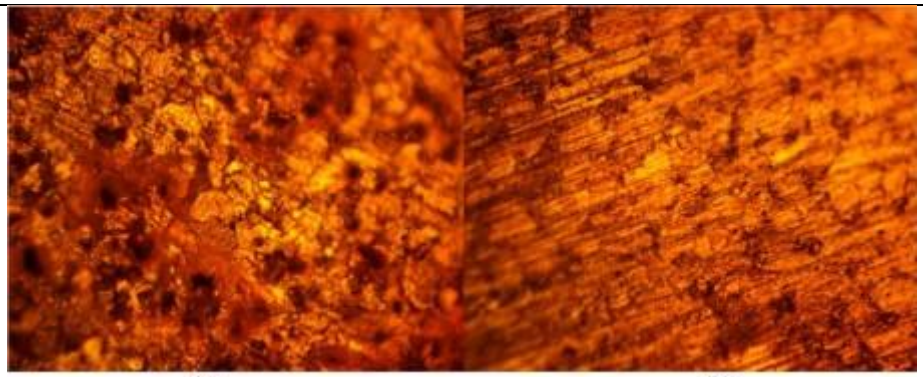


Figure 2.9 (a) Optical Micrographs Low-Carbon Steel Surface in HCl (b) Optical Micrographs Low-Carbon Steel Surface in HCl with RSZ Corrosion Inhibitor (Loto, 2018)

### 2.7.2 Scanning Electron Microscopy Study

Scanning Electron Microscope (SEM) is a technique that generates a picture of a sample by scanning an electron beam across its surface. The sample electrons will react with various atoms on the sample surface and produce a range of signals that provide information about the sample surface's shape and composition (Pinto *et al.,* 2018). SEM has a lot higher resolution, allowing for much greater magnification of closely spaced specimens than an optical microscope which allows a better image of metal corrosion surface study.

### 2.7.3 Chemical Surface Study (XPS)

X-ray photoelectron spectroscopy is a quantitative technique to measure surface chemical characterization by providing information on the surface properties, elemental compositions, and binding states of the elements in the materials (Daniel, 2023). Electrons within a sample absorb photons with a particular energy level before erupting from the solid. The analysis of the kinetic energy of electrons emitted from a surface delivers information about the electronic states of elements in the surface region (Engelhard *et al.,* 2017). In corrosion studies, XPS will reveal the binding energy required to support the inhibitor and metal surface interaction.

## 2.8 Thermodynamic Study

### 2.8.1 Adsorption

In corrosion inhibition studies, thermodynamic study is very important to study the energy changes involves with the corrosion reaction. Adsorption is an interaction which involves the attachment of substances in atoms, molecules, or ions on a surface. The surface where the adsorption occurs is known as adsorbent, whereas the molecular substance adsorbed on the surface is called as adsorbate (Ituen *et al.*, 2017). According to Monticelli (2018), adsorption is an essential step in inhibition, not only for adsorption-type inhibitors but also for many other organic inhibitors. There are three types of corrosion inhibitor adsorption: physisorption, chemisorption, and mixed type.

Physisorption types of inhibitors attract the negative charge of the inhibitor with the positive charge of the metal surface. The type of electronic interaction of physisorption is electrostatic forces (Popoola, 2018) or Van der Waals. The adsorption of physisorption is reversible and fast because the activation energies temperature is low (Monticelli, 2018). Physisorption also is characterized by low adsorption energy (20kJ/mol).

The chemisorption types of inhibitors are in contrast with physisorption. Chemisorption involves the sharing of free electron pairs or the transfer of charge to generate strong chemical bonds between the inhibitors and the metal surface (Popoola, 2018). The adsorption is also slower than physisorption due to the high activation

energies (Monticelli, 2018). Chemisorption is also irreversible with higher heat of adsorption (40kJ/mol).

Mixed-types corrosion inhibitors are the combination of the physisorption and chemisorption. This form of corrosion inhibitor offers the highest level of protection because it inhibits both cathodic and anodic reactions (Brycki *et al*., 2018 & Salleh *et al.,* 2021).

### 2.8.2 Adsorption Isotherm

Adsorption isotherms models are essential for explaining the interaction between corrosion inhibitors and metal surfaces. There are a lot of adsorption isotherm models, but not all models are suitable for corrosion inhibitors. The models usually used for corrosion inhibitors are Langmuir, Temkin, Freundlich, Frumkin, Flory-Huggins, and thermodynamic/kinetic (El-Awady *et al*.) isotherms (Ituen *et al*., 2017). However, only Langmuir and Temkin isotherms will be studied in this research.

#### *2.8.2.1 Langmuir Isotherm*

Langmuir isotherm adsorption model is the most used model to study the adsorption of corrosion inhibitors. In 1916, Irving Langmuir created this model to explain the relationship between the surface coverage of an adsorbed gas and its pressure over its adsorbent at constant pressure (Ituen *et al.*, 2017). In this model, there are a few assumptions made by Langmuir:

- A monolayer adsorption of the adsorbate on the adsorption sites.
- There is no interaction between the molecules on different sites.
- The adsorption is homogenous means each molecule on site possesses constant sorption activation energy and enthalpy (Al-Ghouti & Da'ana, 2020).
- The adsorption is chemisorption in which the adsorption is strong.

The Langmuir adsorption isotherm is shown in Equation 2.16.

$$\frac{C}{\theta} = \frac{1}{K_{ads}} + C \qquad 2.16)$$

where C is the concentration of the inhibitor, θ is the surface coverage, and $K_{ads}$ is the adsorption equilibrium constant.

### *2.8.2.2 Temkin Isotherm*

The Temkin adsorption isotherm model is also usually used to explain the corrosion inhibitors' adsorption. The assumptions made by Temkin is:

- The adsorption of the adsorbate on the sites is multilayer (Kalam *et al.,* 2021).
- There is interaction or repulsive force between the molecules in the adsorbed layer (Ituen *et al.,* 2017).
- The adsorption on the sites is heterogenous.
- The adsorption is physisorption means the interaction between the adsorbate and the sites is Van de Waals forces.

The equation 2.17 present the Temkin adsorption isotherm.

$$\frac{C}{\theta} = \frac{1}{K_{ads}} + C \qquad 2.17)$$

Where θ is surface coverage, *f* is inhibitor interaction parameter, $K_{ads}$ is the adsorption equilibrium constant and C is concentration.

# CHAPTER 3
# RESEARCH METHODOLOGY

## 3.1 Material

Harumanis mango peel was collected from Harumanis Farm UiTM Arau Plantation, Perlis, Malaysia. Mild steel coupon used was obtained from Custom Steel Enterprise, Perlis, the hardware shop and a supplier for a few ranges of steel types.

## 3.2 Extraction of Harumanis Mango Peel

Mango waste extracts from Harumanis mango peel were prepared using solvent extraction. First, the mango peels were washed and dried in the sun. Then, the peels were crushed and ground into powder. The powdered peels (60 g) were extracted with 60% ethanol for three hours at 40ºC under a stirring hot plate. Then, the solvent was removed using a rotary evaporator. After that, the crude mango peel products were oven-dried, and the obtained powder was weighed and prepared for the inhibitor.

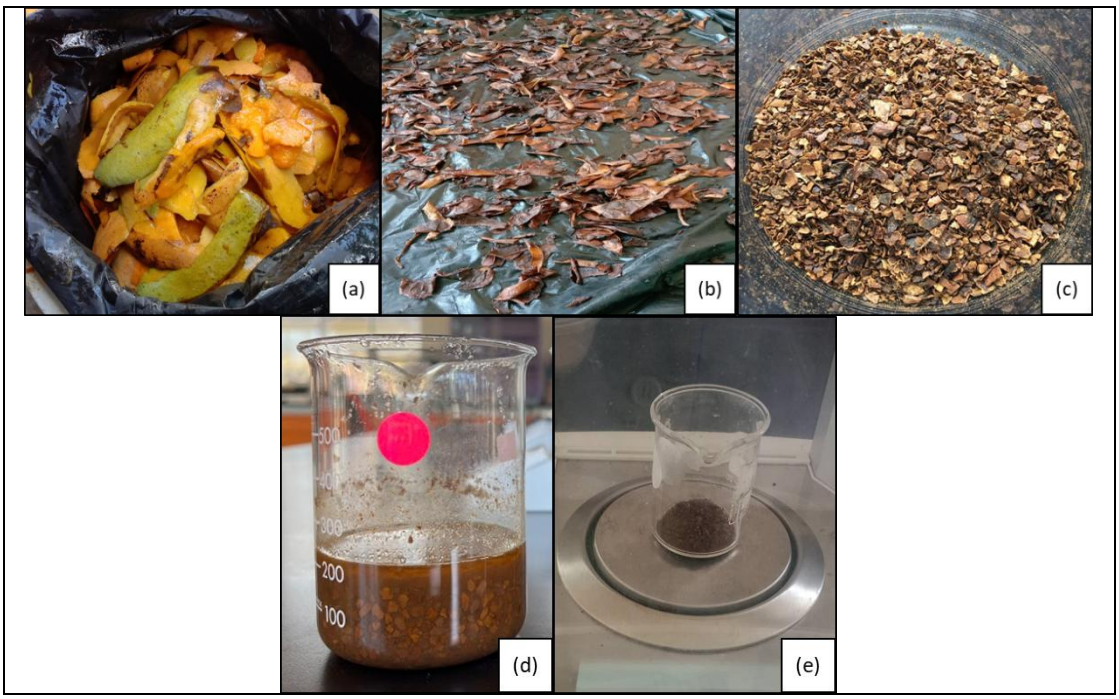


Figure 3.1 (a) Harumanis Peel Leftover (b) Harumanis Peel in Drying Process (c) the Dried Harumanis Peel was Crushed and Ground (d) the Crude Harumanis Peel Extract After Solvent Extraction (e) the Harumanis Peel Extract Powder Obtained After Rotary Evaporator and Drying (Radin Sukimi *et al.,* 2023)

### 3.2.1 Characterization of Harumanis Mango Peel Extract (HMPE)

Harumanis mango peel extract samples (HMPE) were characterized by Fourier-transform Infrared Spectroscopy (FTIR), Ultraviolet-visible Spectroscopy (UV-Vis), High-performance Liquid Chromatography (HPLC), and Gas Chromatography-Mass Spectroscopy (GC-MS).

#### *3.2.1.1 Fourier-transform Infrared Spectroscopy*

Fourier-transform Infrared Spectroscopy (FTIR) was utilized to determine the chemical compound of the HMPE. The use of FTIR is important as it can give information on the functional groups present in HMPE that can act as a corrosion inhibitor.

#### *3.2.1.2 Ultraviolet-visible Spectroscopy*

Ultraviolet-visible Spectroscopy (UV-Vis) was used to screen the phytochemicals from Harumanis mango peel. According to Patle *et al.* (2020), UV–Vis spectrophotometry was used to evaluate the presence of chromophoric groups and aromatic rings in plant extract samples by measuring the electronic transition of π-bonds, σ- bonds, and lone pairs of electrons. The UV-Vis spectrometer scans the Harumanis mango peel absorption spectra with a wavelength between 200 and 400 nm.

#### *3.2.1.3 High-performance Liquid Chromatography*

According to Shalavadi *et al.* (2019), High-performance Liquid Chromatography (HPLC) has been widely used to identify and quantify phenolics and flavonoids in plant extracts. Hence, the primary compound present in HMPE was identified using HPLC. The extract was injected at 20 µL at a flow rate of 1.0 mL min-1, with a detector wavelength of 254 nm. The mobile phase used was acetonitrile:water, 70:30.

#### *3.2.1.4 Gas Chromatography-Mass Spectrometry*

Gas chromatography-mass spectrum also was used to obtain the phytochemical analysis of the HMPE. The analysis was performed with helium as carrier gas (1 mL $min^{-1}$) with injection volume 1 µL; split (10:1); injector temperature 250°C.

## 3.3 Preparation of Sample

In this research, several types of sample preparation were involved. First, the metal specimen was grinded, polished, cleaned, and rinsed with acetone and distilled water. Next, two different corrosive mediums (0.5 M HCl and 0.6 M NaCl) were prepared. Then, HMPE was prepared in different concentrations from 50 to 350 ppm.

### 3.3.1 Preparation of Metal Specimen

The metal sample used was mild steel. The mild steel coupon was cut into pieces of 2 cm x 2 cm x 0.3 cm. Then, the coupon was grinded and polished with 600, 800, and 1000 grit sandpaper. After that, the metal specimen was cleaned, rinsed, and dried with acetone and distilled water prior to the immersion test.

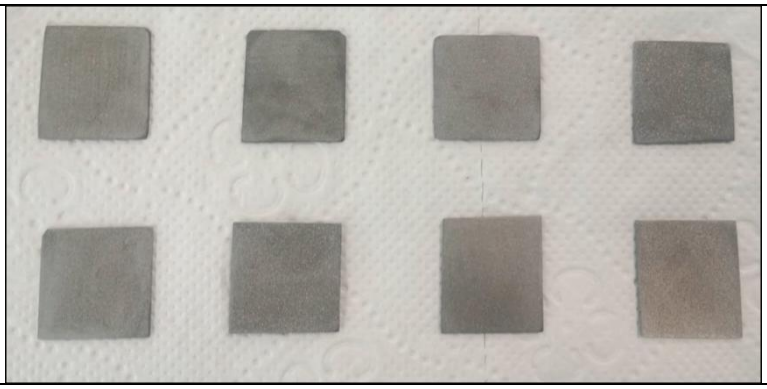

Figure 3.2 Mild Steel Coupon 2 cm x 2 cm x 0.3 cm

### 3.3.2 Preparation of Corrosive Mediums

In this experiment, 0.5 M HCl solution and 0.6 M NaCl solution was prepared as corrosive media for acidic and neutral environments by diluting 37% concentrated HCl and NaCl with distilled water, respectively. Both solutions were utilized in the absence and presence of an inhibitor.

### 3.3.3 Preparation of Harumanis Mango Peel Corrosion Inhibitor

The corrosion inhibitor was prepared with the concentration from 50, 100, 150, 200, 250, 300, and 350 ppm. A nominal 1000 ppm HMPE stock solution was prepared by adding 1 g of HMPE powder to 1 L of the corrosive medium and stirred. Since the HMPE is only partially soluble, the suspension was filtered and the filter with retained solids was dried to constant weight to determine the mass of undissolved material. The dissolved mass was calculated by subtracting the undissolved mass from the initial 1 g, and the actual stock concentration ($mg \cdot L^{-1}$ = ppm) was obtained by dividing the dissolved mass by the stock volume. The HMPE inhibitor (50–350 ppm) were prepared by volumetric dilution of the measured stock. All work involving acids and organic solvents were done according to the standard laboratory safety procedures. The acids and organic solvents should be handled in a fume hood to avoid inhalation of harmful vapours. The pH and conductivity of the HCl and NaCl media were monitored using calibrated meters before and after the HMPE added to ensure the stability of the experiment during the corrosion tests.

## 3.4 Corrosion Test

The corrosion test consists of two methods: the standard approach (weight loss test or immersion test) and the electrochemical test. The tests were done according to the American Society for Testing and Materials (ASTM) standard. ASTM G31-72, ASTM G59-97, and ASTM G3-14 were for the weight loss test, potentiodynamic polarization test, and electrochemical impedance test, respectively. Table 3.1 shows the variables and parameters proposed in this study.

Table 3.1
Parameters for corrosion test.

| Corrosion Medium | Corrosion Inhibitor Concentration (ppm) | Temperature (°C) | PP Setup | EIS Setup |
|---|---|---|---|---|
| 0.5 M HCl<br>0.6 M NaCl | 50, 100, 150, 200, 250, 300, 350 | 30, 40, 50, 60 (Immersion Test) | Scanning range from -800 and 200 mV with scan rate 1 mV s-1 | Frequency range 100 kHz – 10 mHz, AC voltage 10 mV |

### 3.4.1 Immersion Test (Weight Loss)

In this test, the prepared metal sample was weighed before immersion. The sample was immersed in acidic and near-neutral corrosive media and Harumanis mango peel inhibitors for 4, 24, 72, 120, 168, and 240 h at 30, 40, 50, and 60ºC using water bath and exposed to the atmosphere. After immersion, the metal was cleaned and weighed to determine its final mass. The procedure for this immersion corrosion test was carried out in accordance with ASTM G31-72. The test was replicated three times for the accuracy of the results. The corrosion rate and inhibition efficiency (IE%) was calculated using the following equation:

$$\text{Corrosion rate (mm/y)} = \frac{K \times W}{D \times A \times T} \quad 3.1$$

where K (constant) = $8.76 \times 10^4$, ΔW = weight loss (g), T = exposure time (h) D = density of the metal sample (g $cm^{-3}$), and A = area of metal exposure ($cm^2$)

$$\text{Inhibition efficiency, IE\%} = \frac{CR_o - CR_f}{CR_o} \times 100 \quad 3.2$$

where $CR_o$ = corrosion rate of uninhibited metal (g) and $CR_f$ = corrosion rate of inhibited metal (g).

Figure 3.3 Immersion test or weight loss method

### 3.4.2 Potentiodynamic Polarization (PP)

The potentiodynamic polarization test was utilized to monitor the reaction rate of the electrode interface and provide data on the inhibitor behavior by Tafel curves. A three-electrode cell, consisting of mild steel with a surface area of 2 cm X 2 cm as a working electrode (WE), platinum as a counter electrode (CE), and Ag/AgCl as a reference electrode (RE), were set up. The polarization curves were generated using the Gamry potentiostat-galvanostat and Gamry analysis software. The potentiodynamic polarization was performed with a scan rate of 1 mV $s^{-1}$ with the scanning range from -800 and 200 mV relative to the open circuit potential (OCP).

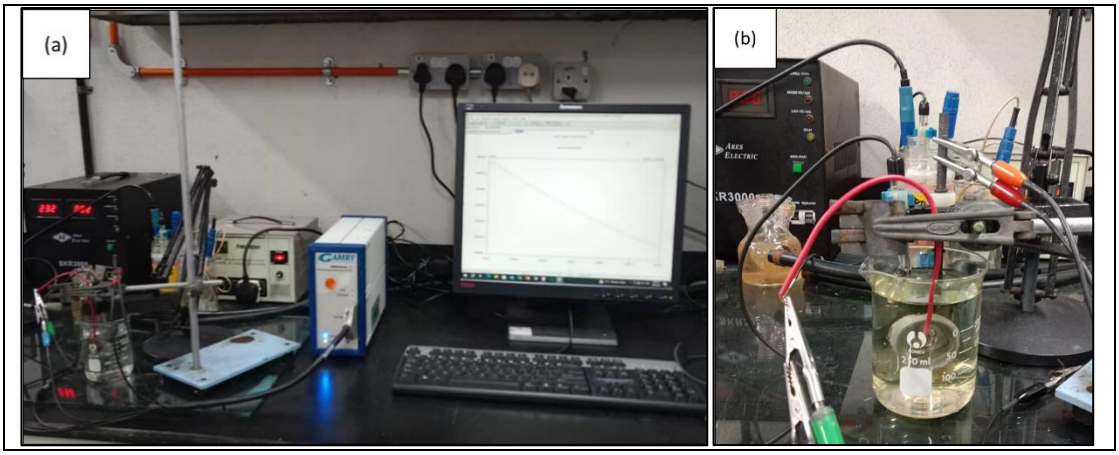


Figure 3.4 (a) Potentiostat used for potentiodynamic polarization and EIS (b) Potentiodynamic polarization and EIS setup

### 3.4.3 Electrochemical Impedance Spectroscopy (EIS)

EIS data was analysed to evaluate Harumanis mango peel corrosion inhibitor inhibition behaviour. The sample preparation was the same as the PP test. The EIS test was conducted at the initial frequency 100 kHz to the final frequency 10 mHz, with the AC voltage at 10 mV RMS. The Gamry potentiostat-galvanostat and Gamry analysis software generate the Bode and Nyquist plots.

## 3.5 Corrosion Surface Study

The surface morphology of the metal before and after immersion with and without inhibitor was observed using optical microscopy (OM), scanning electron microscopy (SEM), and x-ray photoelectron microscopy (XPS).

### 3.5.1 Optical Microscopy (OM)

The optical microscope namely Olympus CX22 LED with a 4x/0.1 lens magnification was used to observe the morphology of the metal surface. The micrographs of the metal sample were compared among the inhibited and uninhibited samples.

### 3.5.2 Scanning Electron Microscopy (SEM)

Surface morphology was performed through high-resolution microscopic techniques, scanning electron microscope, JEOL JSM-6010LV. The image of metal sample before and after inhibited was examined to observe the inhibition progression.

### 3.5.3 X-Ray Photoelectron Spectroscopy (XPS)

The XPS was measured using a VG ESCALAB 220 XL spectrometer. The study reveals the binding energy that may confirm the interaction within the inhibitor and metal surface.

### 3.6 Thermodynamic Study

The adsorption of the HMPE extract on the mild steel surface in both corrosive mediums were studied using the adsorption isotherm. The weight loss test data was fitted into Langmuir and Temkin adsorption isotherm model.

### 3.7 Summary

Table 3.2
Purpose and significant of the method.

| Method | Purpose | Significant |
|---|---|---|
| Solvent extraction | To extract the chemical compounds obtained in the Harumanis mango peel. | The chemical compounds obtained in the Harumanis mango peel can be analysed and identified as anti-corrosion agent as corrosion inhibitor. |
| Weight loss method (ASTM G31-72) | To determine the weight loss of mild steel before and after immersion with the corrosive medium with the absence and presence of the corrosion inhibitor. | The change in weight loss can be compared easily. The data can be used to measure corrosion rate and inhibition efficiency. |
| Potentiodynamic polarization test (ASTM G59-91) | To identify the types of corrosion inhibitor. | The Tafel slopes obtained can be used to identify the corrosion inhibitor types, either it is anodic, cathodic, or mixed-type inhibitor. |
| Electrochemical impedance spectroscopy test (ASTM G3-14) | To investigate the quantity of current flow and resistance value on the metal surface with and without the inhibitor. | The charge transfer resistance obtained from the Nyquist plot can be used to calculate inhibition efficiency. |
| Surface study | To view the corrosion surface study on the mild steel in the presence and absence of inhibitor in the corrosive medium. | The morphology of the corrosion between the inhibited and uninhibited on the metal surface can be observed and compared. |
| Thermodynamic Study | To measure the adsorption behaviour of the corrosion inhibitors on the metal surface. | The interaction between corrosion inhibitors and metal surfaces can be explain by using adsorption isotherms. |

**Flow Chart**

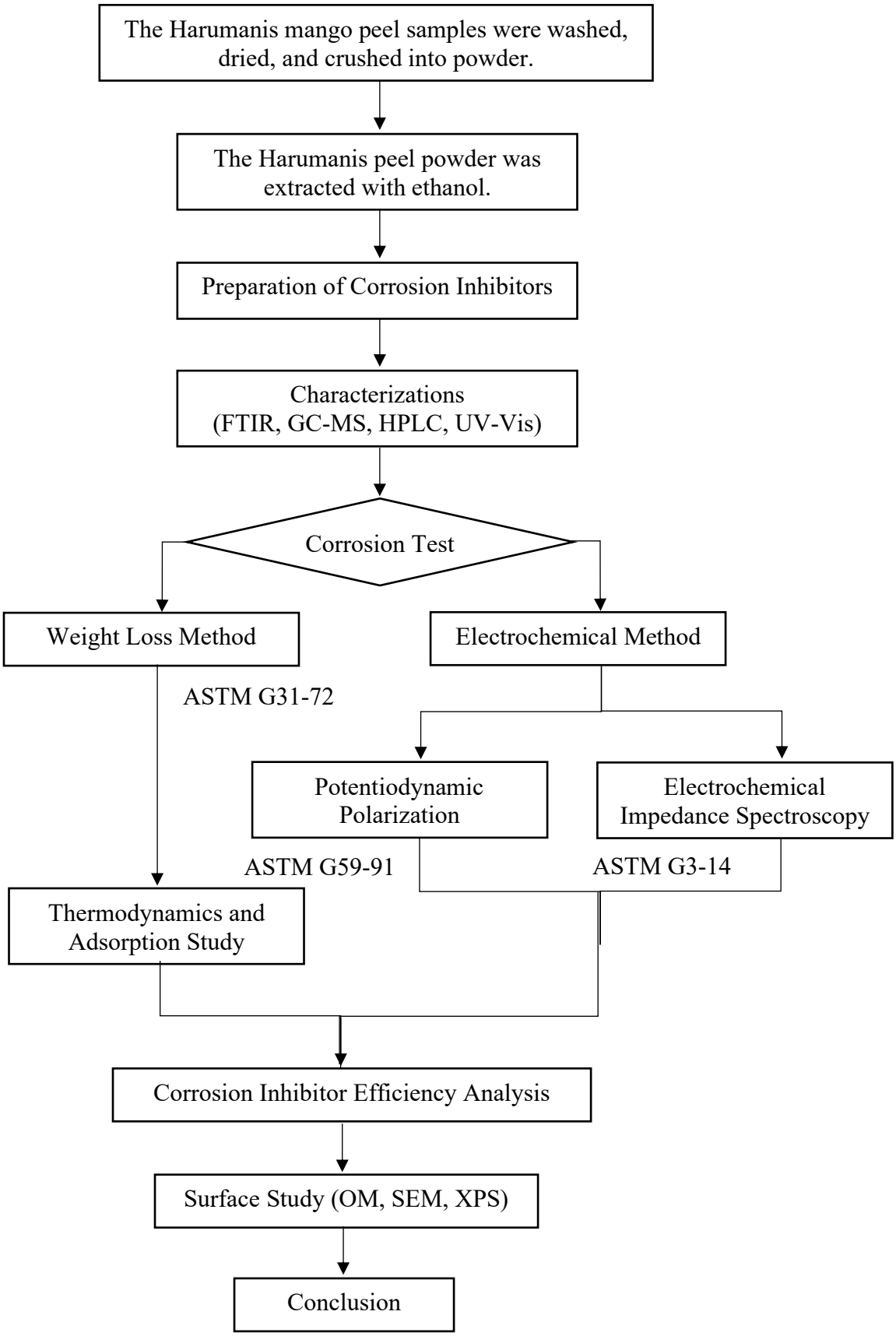
The Harumanis mango peel samples were washed, dried, and crushed into powder.
The Harumanis peel powder was extracted with ethanol.
Preparation of Corrosion Inhibitors
Characterizations (FTIR, GC-MS, HPLC, UV-Vis)
Corrosion Test
Weight Loss Method
Electrochemical Method
ASTM G31-72
Potentiodynamic Polarization
Electrochemical Impedance Spectroscopy
ASTM G59-91
ASTM G3-14
Thermodynamics and Adsorption Study
Corrosion Inhibitor Efficiency Analysis
Surface Study (OM, SEM, XPS)
Conclusion

# CHAPTER 4
# RESULTS AND DISCUSSION

## 4.1 Extraction of Harumanis Mango Peel Extracts (HMPE)

In this research, Harumanis mango peel extracts (HMPE) were extracted using solvent extraction. Solvent extraction was chosen for HMPE due to its efficiency, yield, and ability to sustain the bioactive compounds in the extracts. Solvent extraction has been found to yield higher amounts of phenolic compounds, flavonoids, carotenoids, and antioxidant activities compared to other methods (Garcia-Merdoza et al., 2015 & Javid et al., 2024). According to Javid et al. (2024), the total amount of phenolic compounds was significantly high in the mango when using hydroalcoholic solvent extraction. Besides that, solvent extraction can use less toxic solvents and reduce the environmental impacts compared to other methods like supercritical extraction, which need more energy and specialised equipment (Garcia-Mendoza et al., 2015).

First, 60 g of dried Harumanis mango peels was mixed in 500 mL ethanol-water (60:40). The aqueous ethanol was used as a solvent for this Harumanis mango peel extraction because of the ability of ethanol to give high yields of phytochemicals, including both polar and non-polar compounds such as phenolic compounds, flavonoids, terpenoids, and antioxidants (Kaczorba et al., 2021 & Mroz et al., 2023). In a study by Riaz et al. (2023), ethanol has been proven to yield higher amounts of bioactive compounds such as flavonoids and gallic acid. The gallic acid yield using ethanol extract from the study is 5.75 mg/g, which is significantly higher than the 3.14 mg/g obtained with water.

The ethanol/water ratio 60:40 also was chosen due to the effectiveness of the ratio in maximizing the extraction of the phenolic compounds and flavonoids (Chaiwarit et al., 2021). According to Lim et al., 2023, the 60:40 ratios also provide a balanced polarity that enhanced the solubility of both hydrophobic and hydrophilic compounds. Then. The HMP was immersed for 3 hours below 40ºC under stirring conditions. The aqueous ethanol was removed using rotary evaporator. After that, the HMPE powder was obtained by drying the crude product under 60ºC. Table 4.1 depicts the percentage yield of HMPE.

Table 4.1
Percentage Yield of HMPE

| Weight of HMPE before extraction (g) | Weight of HMPE after extraction (g) | Percentage yield (%) |
|---|---|---|
| 60.0000 | 11.3256 | 18.88 |

The percentage yield of 18.88% obtained in this study is consistent with the typical yields reported for mango peel extract. A similar study was found by Bala *et al.* (2022) for mango peel extract using ethanol as a solvent, in which the percentage yield obtained was 19.81%. Another study by Machado *et al.* (2022) also reported a percentage yield within this range, at 23.07%. Thus, the yield obtained in this study is consistent with previously reported values. However, variations in yield among the studies may be attributed to different in extraction parameters, such as solvent composition, extraction time, temperature, and the specific mango variety used.

## 4.2 Characterization of HMPE

The chemical compounds and functional groups present in HMPE that give inhibition to the corrosion were identified using FTIR, UV-Vis, HPLC, and GC-MS.

### 4.2.1 Fourier-transform Infrared Spectroscopy Analysis

The HMPE used as corrosion inhibitor was analysed by using FTIR to explore its active functional groups and identify those responsible for inhibiting mild steel corrosion. The presence of functional groups in HMPE was compared with that of the commercial standard chemical, mangiferin. Functional groups such as hydroxyl, carbonyl, and aromatic rings play a crucial role in adsorption and film formation on metal surfaces.

Figure 4.1 presents the FTIR spectra of both HMPE and mangiferin. The spectra reveal a broad band at 3358 and 3289 cm-1, signifying the existence of hydroxyl (OH) groups, which indicate the presence of phenolic and alcohol compounds capable of forming strong hydrogen bonds. These groups enhance adsorption onto metal surfaces, thereby creating a protective barrier against corrosive agents, a finding consistent with Karattu Veedu et al. (2019). Furthermore, the resemblance of these peaks indicates that

both HMPE and mangiferin contains hydroxyl groups, which are essential for their antioxidant and potential inhibitory properties. This discovery aligns with the findings of prior research by Karattu Veedu et al. (2019), who reported a significant concentration of phenolic compounds in the peel extract.

In addition, the peaks detected at 2924 and 2884 cm-1 shows the absorption of C-H sp3 stretching, indicating the distinctive features of aliphatic structures. These functional groups contribute to the stability and overall chemical compositions of the compounds. Furthermore, the sharp peak at 1705 cm-1 in the HMPE spectrum is indicative of carbonyl group, which is not prominently present in the mangiferin spectrum because of conjugation. This suggests the presence of significant compounds in HMPE that contain carbonyl functionalities such as ketones, aldehydes, carboxylic acids or esters. According to Jakha et al., 2024, the existence of these carbonyl compounds suggests a high amount of flavonoids.

Carboxylic acids, in particular, are known for their ability to hinder corrosion by forming protective layers on metal surfaces, effectively slowing down further corrosion (Thanh et al., 2020). In HMPE, carboxylix acid groups are likely to chelate Fe2+ ions, leading to the formation of insoluble complexes that block active corrosion sites. Moreover, the prominent peaks at 1410, 1485, 1600 and 1612 cm-1 pointed to the the existence of C=C stretching in aromatic rings. According to Pardede & Sofyan (2023), these aromatic compounds are recognised for their ability to inhibit corrosion and function as antioxidants.

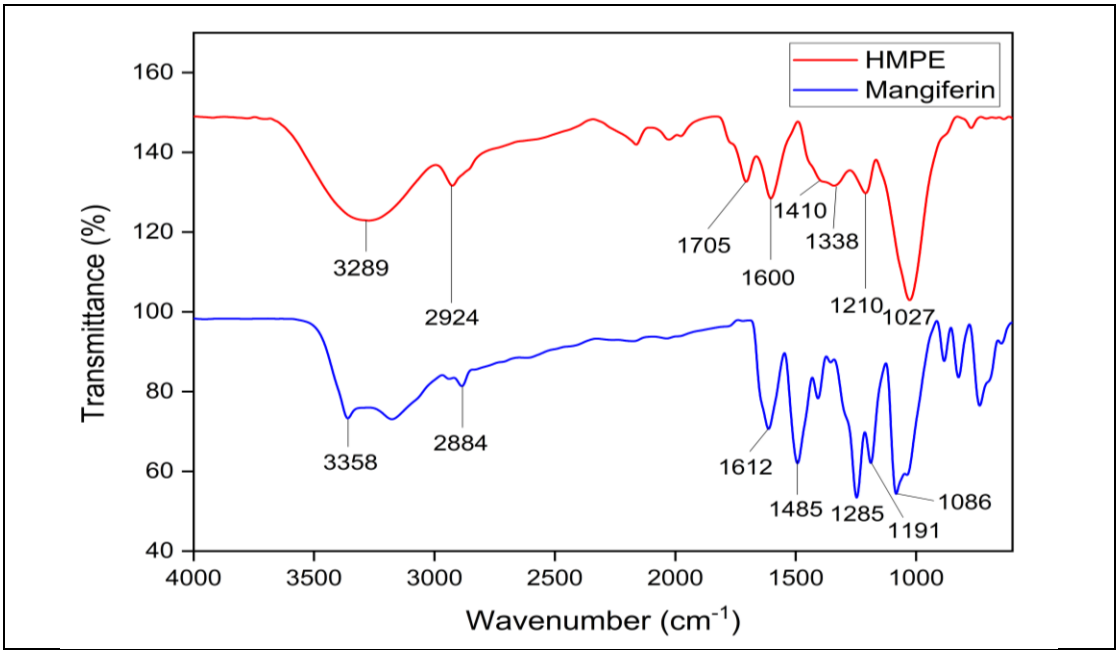


Figure 4.1 FTIR Spectrum of HMPE and Mangiferin Standard

Additionally, the peak at 1338 $cm^{-1}$ in HMPE may indicate the presence of C-N stretching vibrations, suggesting the presence of amine or amide groups. However, this peak could also originate from C-H bending or other C-O vibrations, requiring further analysis, such as NMR, for confirmation. This interpretation aligns with Parhizkar *et al.* (2017), who reported that amine and amide groups aid in creating a protective film on the metal surface, serving as a barrier against corrosive ions like chlorides.

The additional peaks at 1285, 1210, 1191, and 1086 in both samples confirm the presence of functional groups associated with C-O stretching vibrations. These peaks likely correspond to alcohols and ethers/esters. Notably, the sharp peak of 1027 $cm^{-1}$ strongly confirms the presence of C-O bond in HMPE. These peaks are commonly found in ethers, alcohols, and esters, and also indicate C-OH bending vibrations. These functional groups, commonly found in ethers, alcohols, and esters, enhance the chemical complexity and reactivity of the extracts.

A summary of the FTIR peaks and corresponding functional groups present in HMPE and mangiferin is provided in Table 4.2 for a detailed comparison.

Table 4.2
Summary of FTIR Peaks and Functional Groups Presence in HMPE and Mangiferin Standard

| Functional Groups | Samples | |
|---|---|---|
| | **HMPE** | **Standard Mangiferin** |
| O-H | 3358 $cm^{-1}$ | 3289 $cm^{-1}$ |
| C-H | 2924 $cm^{-1}$ | 2884 $cm^{-1}$ |
| C=O | 1705 $cm^{-1}$ | n.d. |
| C=C (Aromatic) | 1485 and 1600 $cm^{-1}$ | 1485 and 1612 $cm^{-1}$ |
| C-N | 1338 $cm^{-1}$ | n.d |
| C-O | 1210, 1027 $cm^{-1}$ | 1285, 1191, 1086 $cm^{-1}$ |

n.d. = not detected

### 4.2.2 Ultraviolet-visible Spectroscopy Analysis

It is essential to analyse the structure of a chemical compound in order to assess its potential as a corrosion inhibitor. Thus, studying the electronic structure and conjugation within molecules aids in evaluating the ability of compound to interact with a metal substrate. Therefore, UV-Vis analysis was conducted to detect the presence of a chromophore in HMPE that possesses a distinct electronic structure and conjugation. This step provides valuable insights about the compound's potential to inhibit corrosion, as a chromophore with these features is often suggests increased reactivity and effectiveness in interacting with metals (Zehra et al., 2023).

The electronic structure of the inhibitor plays an important role in the corrosion inhibitor. The presence of hetero atoms such as sulphur, oxygen, nitrogen, and phosphorus in the extract compound is electron-rich, allowing better adsorption onto the metal surface (Jano et al., 2021). These atoms are also high in electron density, which increases the coordination with vacant d-orbitals of metal atoms, forming a protective layer. The conjugation of the HMPE compound structure, such as aromatic rings and double bonds, also enhances the electron density, thus giving a stronger adsorption on the metal surface.

Figure 4.2 illustrates the UV-Vis spectrum of HMPE, displaying several absorption peaks corresponding to various chromophores present in the extract. The spectra indicated intense peaks at 275 nm and 287 nm. The 275 nm peak is associated with aromatic compounds. Kumar (2006) stated that benzene rings commonly absorb in this region because of π-π* transitions of the aromatic electrons. The delocalized π-electrons in the benzene ring can donate electrons to the metal d-orbitals of the metal. Thus, forming a stable protective layer that can inhibits the metal from corrosive agents (Amoko et al., 2021; Mohamed et al., 2021). The absorption peak at 287 and 302 nm indicates the presence of aromatic ring and carbonyl group (C=O). This may result from conjugated ketones or aldehydes found in the structure of the aromatic compounds in the extract.

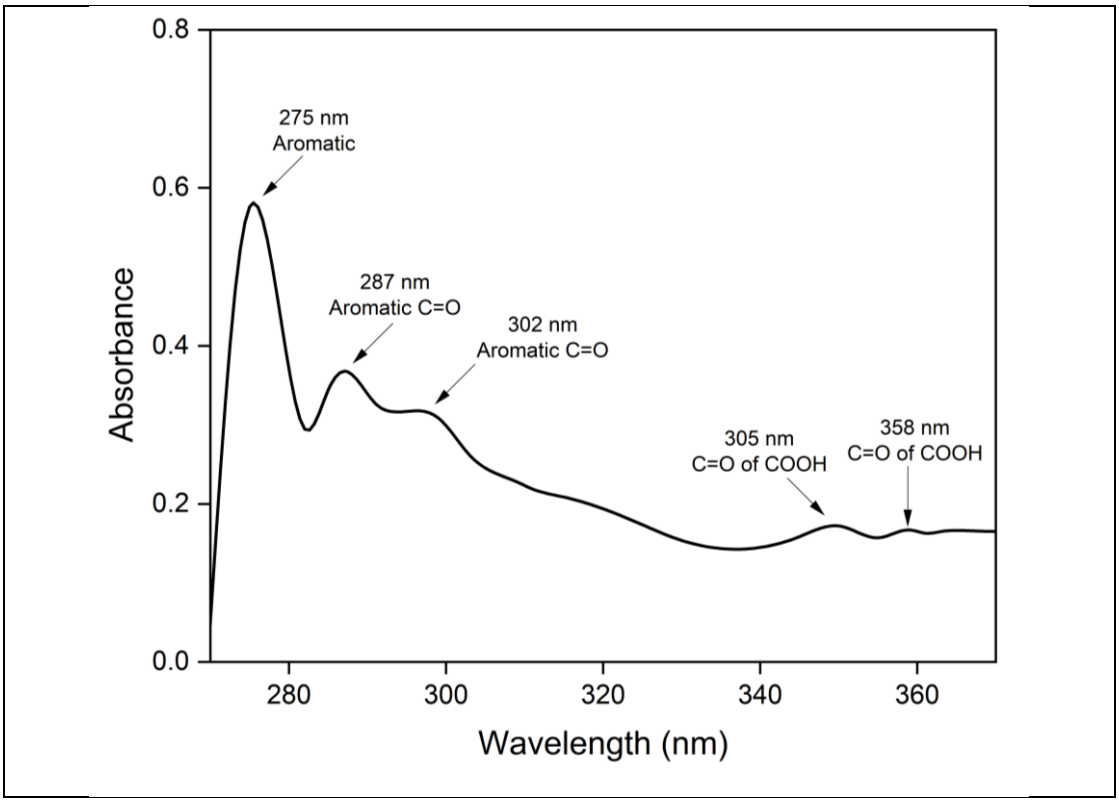


Figure 4.2 UV-Vis Spectra of HMPE

The absorption peaks detected at 305 and 358 nm can be attributed to the n-π* transition of C=O of the carboxylic acid groups. The lone pair of electrons on the oxygen atom in the carboxyl group shifts to the π*anti-bonding orbital of the C=O bond, which typically absorbs in this area. A study by Ramezanzadeh *et al*. (2019) also found similar absorption peaks appear in this region using mango leaf extract.

The UV-Vis results reveal that the compounds from HMPE have significant conjugation with aromatic rings, carbonyl groups, and carboxylic acid groups. These functional groups allow the compounds in HMPE to strongly adsorb on the metal surface, resulting in a stable and protective layer. This layer acts as a barrier, preventing the corrosive agents from penetrating the metal surface and thus inhibiting corrosion. The compounds' ability to absorb on the UV-Vis region, mainly due to the π-π* and n-π* transitions, indicates the compounds can interact strongly with the metal surface, which is necessary for efficient corrosion inhibition.

### 4.2.3 High-performance Liquid Chromatography Analysis

HPLC analysis holds significant importance in identifying the chemical compounds in HMPE. HPLC analysis allows for the separation and quantification of individual compounds in the extract, providing valuable information about the presence of key constituents. This analytical method is also crucial for identifying the specific chemical compounds responsible for the corrosion-inhibiting properties of mango peel extract, in line with its strategic use in corrosion protection.

Figure 4.3 illustrates the chromatogram of HMPE. The first peak obtained represent the ethanol solvent used. The sharp and high peak observed in the chromatogram at 3.400 minutes may correspond to gallic acid, as a similar peak at the same retention time found in the previous study (Marcillo-Parra et al., 2021). Next, the peak found at 3.994 minutes represents mangiferin as obtained in the standard. The concentration of mangiferin calculated in this HMPE is 8.45 µg mL-1.

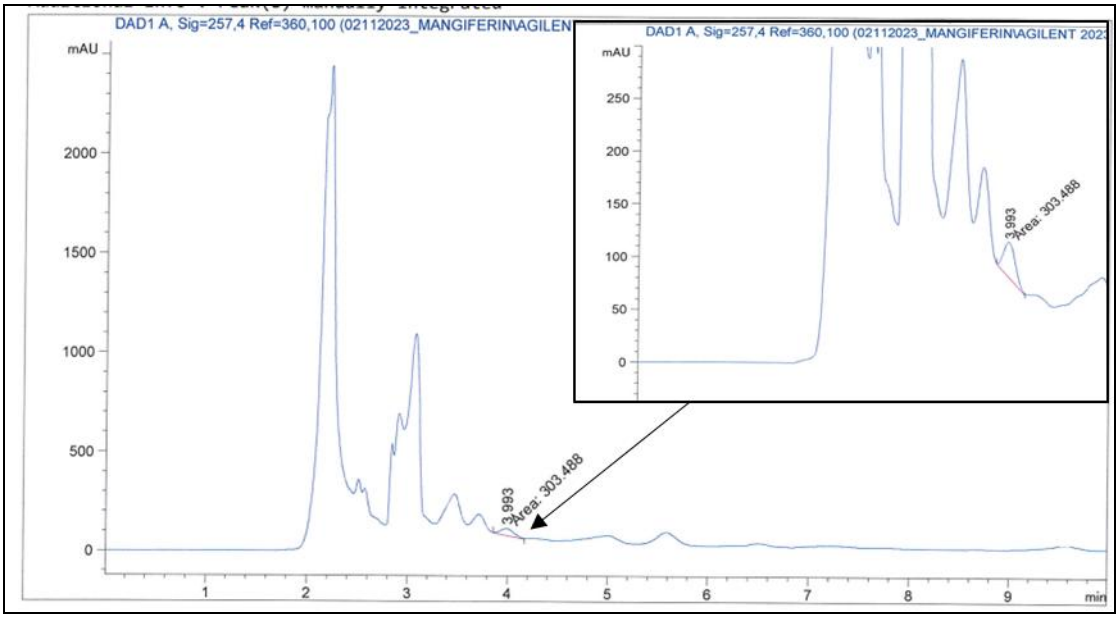

Figure 4.3 HPLC Chromatogram of HMPE

### 4.2.4 Gas Chromatography-Mass Spectrometry Analysis

The objective of using GC-MS analysis is to identified organic compounds in HMPE. These organic compounds can play various roles in the corrosion inhibition process. Table 4.3 depicts the chemical compounds detected by GC-MS in HMPE. The first compound, Benzaldehyde, 4-methyl-, oxime, (Z-)-, was detected at a retention time of 2.432 min. This compound has one aromatic ring attached with one oxime group. According to the Suttirak & Manurakchinakorn (2012), benzaldehyde, 4-methyl-, oxime found in mangosteen peel extract creates a protective film on the mild steel surfaces, serving as a barrier to shield the metal from corrosive agents, preventing direct contact.

The oxime group, consisting of the functional group C=N–OH, can act as both an electron acceptor and donor, thus enabling electron transfer within its interaction (Li *et al*., 2014). The nitrogen atom (N) bonded to an oxygen atom (O) through a double bond (N=O) can act as an electron donor due to its lower electronegativity than oxygen. In parallel, oxygen can attract electrons more strongly than nitrogen. However, in certain chemical environments, nitrogen can also act as an electron acceptor. Yet, the oxygen atom in the C=N–OH group is bonded to a hydrogen atom, forming an OH group. In this context, oxygen has the ability to donate electrons, particularly from the lone pair of electrons on the oxygen atom, making it an electron donor.

The second compound detected was 4-Ethylbenzoic acid, cyclohexyl ester, at a retention time of 2.666 min. The compound has two cyclic compounds with 1 COO ester compound connected to the ring. Esters are known to hydrolyze in aqueous environments, both of which may aid in the formation of a passive layer on the metal surface (Lamghafri *et al.*, 2024). Besides that, the aromatic ring attached also can help in electron donation to the metal surface, increasing the adsorption and creating a protective layer.

The alkene compounds 1-Dodecene and 5-Octadene (E) detected at the retention times 10.468 and 16.278 min also contribute to the inhibition of mild steel. The double bond in alkenes can adsorb onto the metal surface via π-electrons. According to Alonso *et al*. (2015), the π-electrons from the double bonds in alkenes allow strong interactions with metal surfaces, resulting in the formation of robust alkyl layers that increase hydrophobicity.

The presence of phenol and derivatives such as phenol, 2,5-bis (1,1-dimethylethyl) detectected at retention time of 19.284 is also important. This is due to the phenolic compounds are known for their antioxidant properties and their ability to adsorb on to metal surfaces to form a protective barrier against corrosive agent (Gerard *et al*., 2021, Salleh *et al*., 2021, Njoku *et al*., 2024).

Table 4.3
Chemical Compounds Detected by GC-MS in HMPE

| Retention Time (min) | Compound | Chemical Structure | % |
|---|---|---|---|
| 2.432 | Benzaldehyde, 4-methyl-, oxime, (Z-) - | 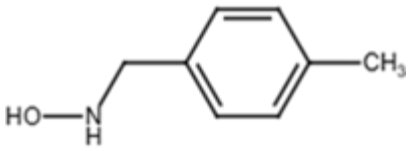 | 13.13 |
| 2.666 | 4-Ethylbenzoic acid, cyclohexyl ester | 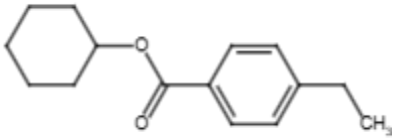 | 8.22 |
| 10.468 | 1-Dodecene |  | 14.84 |
| 16.278 | 5-Octadene, (E) - | 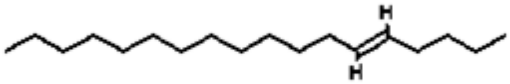 | 17.00 |
| 19.284 | Phenol, 2,5-bis (1,1-dimethylethyl) | 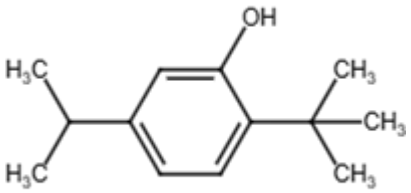 | 37.42 |
| 21.320 | Oxalic acid, allyl octadecyl ester | 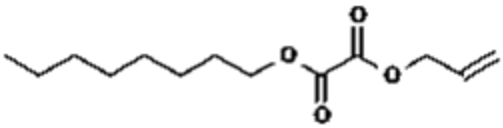 | 9.38 |

### 4.2.5 Summary of Characterization of HMPE

Table 4.4
Summary of Characterization of HMPE

| Analysis Method | Main Findings | Significance of Corrosion Inhibitor |
|---|---|---|
| FTIR | Functional groups identified: O-H (hydroxyl), C=O (carbonyl), C=C (aromatic), C-N (amine/amide), C-O (ether/alcohol/ester) | These functional groups aid in adsorption on the metal surfaces, forming a protective barrier. |
| UV-Vis | Peaks at 275, 287, 302, 305, and 358 nm, indicating aromatic compounds, carbonyls, and carboxyl groups | $\pi$-$\pi^*$ and n-$\pi^*$ transitions in the HMPE compounds enhance electron density, thus, improve metal surface interaction and formation of protective layer. |
| HPLC | Presence of mangiferin and gallic acid | Mangiferin and gallic acid contribute to antioxidant and corrosion inhibition |
| GC-MS | Compounds identified: Benzaldehyde, 4-Ethylbenzoic acid, alkenes, phenol derivatives, oxalic acid esters. | These compounds form protective films, adsorb onto metal surfaces, and enhance corrosion resistance |

## 4.3 Corrosion Test

### 4.3.1 Weight Loss Measurements Analysis

#### *4.3.1.1 Corrosion Inhibition in Acidic Medium*

Figure 4.4 demonstrates the corrosion rate graph for mild steel in a 0.5 M HCl in the presence of HMPE inhibitor. The trend shows that the corrosion rates decrease as the HMPE inhibitor increases. The highest corrosion rate was shown by the low HMPE concentration. It also can be observed that, for each concentration of HMPE, the corrosion rate tends to increase with time. The lowest corrosion rate was shown by the highest HMPE concentration (350 ppm) at all immersed time studied.

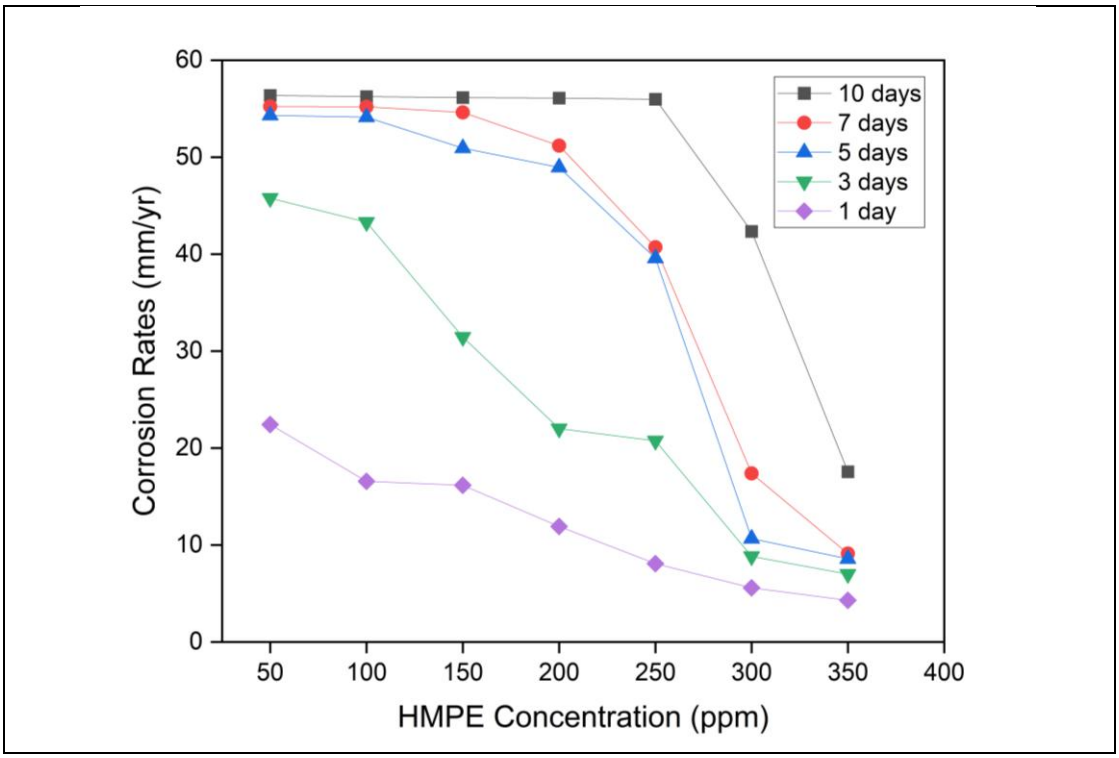


Figure 4.4 Corrosion Rates (mm/yr) of Mild Steel in 0.5 M HCl and in the Presence of HMPE Corrosion Inhibitor at Different Concentration and Immersion Time

Immersion of mild steel for 1 day shows the corrosion rates decrease as the concentration of HMPE increases, with the lowest corrosion rate at 350 ppm. This is because the increase in concentration of the HMPE resulted in a higher surface coverage of the adsorbed extract on the mild steel surface. Thus, the high surface coverage will hinder the acid attack on the surface and consequently slowed down the dissolution of

mild steel (Jimoh & Usman, 2021). Increasing the immersion time to 3 days, the corrosion rates also decrease as the concentration of the HMPE inhibitor rises. However, the corrosion rate values, 7 mm/yr are higher than the 1 day immersion, (4 mm/yr). This phenomenon is presenting the moderate dissolution of mild steel.

As the immersion time is further increased to 5, 7, and 10 days, the corrosion rates was still decline as the concentration of HMPE increases. This situation can be seen clearly when 200 to 350 ppm HMPE was applied in the HCl medium. The corrosion rates which show about 48 to 55 mm/yr has drastically decrease to only less than 20 mm/yr. However, they are higher than the corrosion rates observed during the 1 day and 3 days' immersion which about less than 50 mm/yr at low HMPE concentration and less than 10 mm/yr at high HMPE concentration. This occurrence is because the protective effect of HMPE inhibitor diminishes over time, which might be due to the degradation or desorption of the HMPE corrosion inhibitor molecules from the mild steel surface. Consequently, the mild steel was subjected to the acidic medium, thus, it led to greater exposure of the mild steel surface to the corrosive environment, resulting in the higher dissolution of metal (Al-Baghdadi *et al*., 2021).

Figure 4.5 shows the corrosion inhibition efficiency of mild steel in 0.5 M HCl with the presence of the HMPE corrosion inhibitor at different concentrations and immersion times. As the HMPE concentration rise up, the IE% increases significantly from 3% to 88% for all the time immersion as the concentration of the HMPE increases from 50 to 350 ppm. For example, the immersion of mild steel for 1 day gives highest IE% in the range of 45-90% at all HMPE concentrations. The highest inhibition efficiency of 88% can be seen at 350 ppm. The extension of time to 3 days of immersion also shows a gradual increase in IE% in the range of 10-86% with an increase in the HMPE concentration. However, for 5 to 10 days of immersion time, the IE% was mostly lower than 20% at low concentrations of HMPE (50-200 ppm). Meanwhile, at a high concentration of HMPE (250-350 ppm), the IE% values are mostly higher than 20% at all-time exposure.

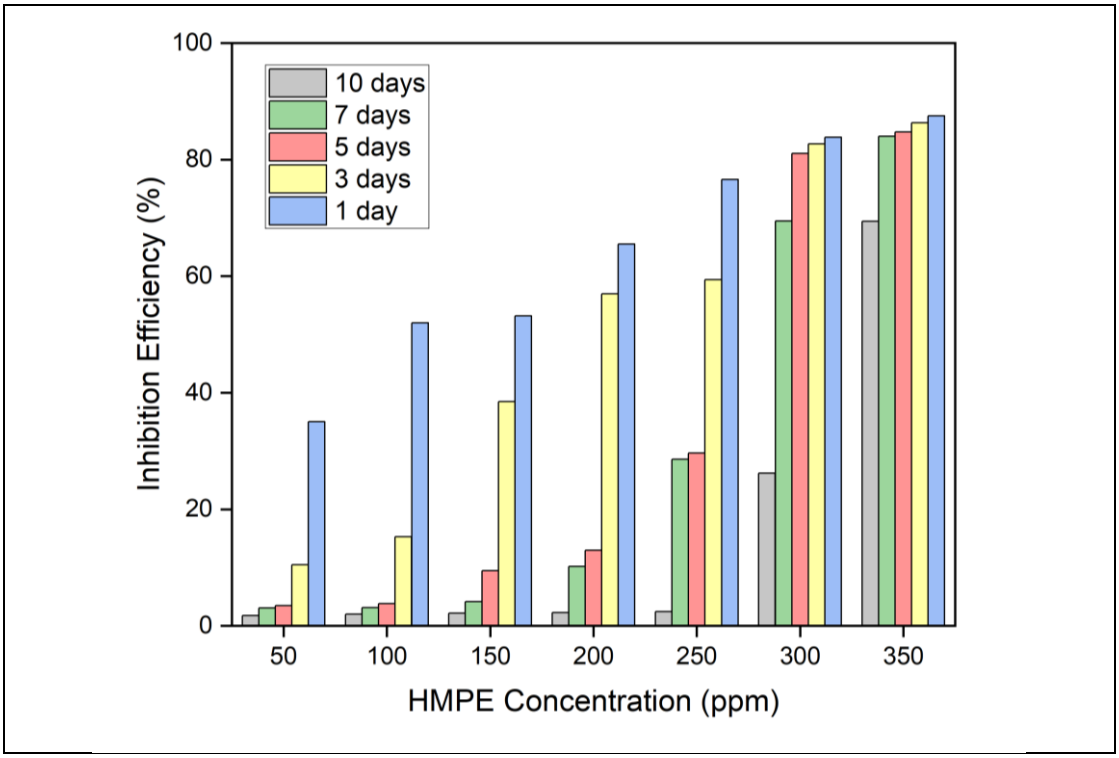


Figure 4.5 Corrosion Inhibition Efficiency (IE%) of Mild Steel in 0.5 M HCl and in the Presence of HMPE Corrosion Inhibitor at Different Concentration and Immersion Time

This finding shows that the corrosion inhibition efficiency of mild steel is dependent on the concentration of HMPE and immersion time. The high concentrations of HMPE can give high IE% in a short term immersion time. The increased in corrosion rate over the time could also indicate that HMPE inhibitor is unable to form a stable complex with the steel or that its protective layer is subject to breakdown in the acidic environment of 0.5 M HCl.

#### *4.3.1.2 Corrosion Inhibition in Near-Neutral Medium*

Figure 4.6 depicts the graph of corrosion rate against the concentrations of HMPE inhibitor. According to the graph, the corrosion rates decline as the concentration of HMPE inhibitor increase up to 250 ppm, but the corrosion rates start to rise beyond 250 ppm for all time immersions. For instances, the lowest corrosion rates, 0.18 mm/yr can be seen at 250 ppm at 1 day immersion. Despite the decrease in corrosion rates as the concentration increase, the corrosion rates value is generally higher with longer exposure times at 3, 5, 7 and 10 days immersion. The highest corrosion rates, 0.69 mm/yr obtained are at 10 days' immersion.

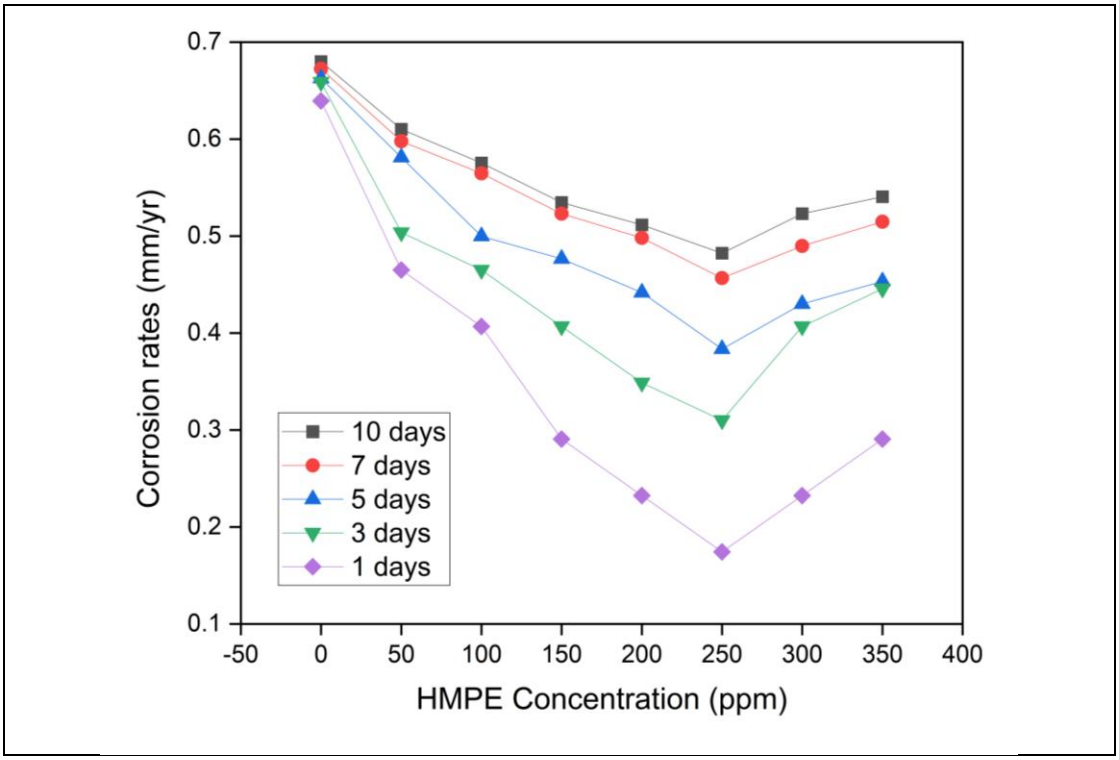


Figure 4.6 Corrosion rates (mm/yr) of Mild Steel in 0.6 M NaCl and in the Presence of HMPE Corrosion Inhibitor at Different Concentration and Immersion Time

The results also show that the increasing corrosion rates over time affect the performance of HMPE inhibitors due to the ongoing corrosion process. It can be seen that in only 1 day immersion, the corrosion rate value was drastically decrease from 0.65 to 0.18 mm/yr as concentration increase from 50-250 ppm. As the concentration increase to 350 ppm, the corrosion rates value increase to 0.28 mm/yr. This is happened due to the desorption process of adsorbed HMPE molecules. The interaction among the HMPE molecules with the anions and cations in the bulk solution leads to mutual attraction due to Van der Waals effect. Therefore, the weak adsorption has made the mild steel surfaces were exposed to NaCl and increase the rate of corrosion. The same situation has shown in all immersion time studied. The increase in corrosion rates after 250 ppm might be due to the maximum possible coverage of the metal surface by the inhibitor, which the addition of the concentration beyond this will not yield additional benefits (Miralrio & Espinoza Vazquez, 2020).

Figure 4.7 shows the graph depicting the corrosion inhibition efficiency of mild steel in 0.6 M NaCl in the presence of different concentration and immersion time. The graph illustrates the rise in HMPE concentration leads to an increase in IE% up to a certain point. For example, the highest inhibition efficiency of 73% was achieved at 250 ppm at 1 day immersion. For longer immersion time, the highest IE% obtained are

also at 250 ppm, before it starts to decrease. The similar trend of IE% value also shown as the immersion time was extended.

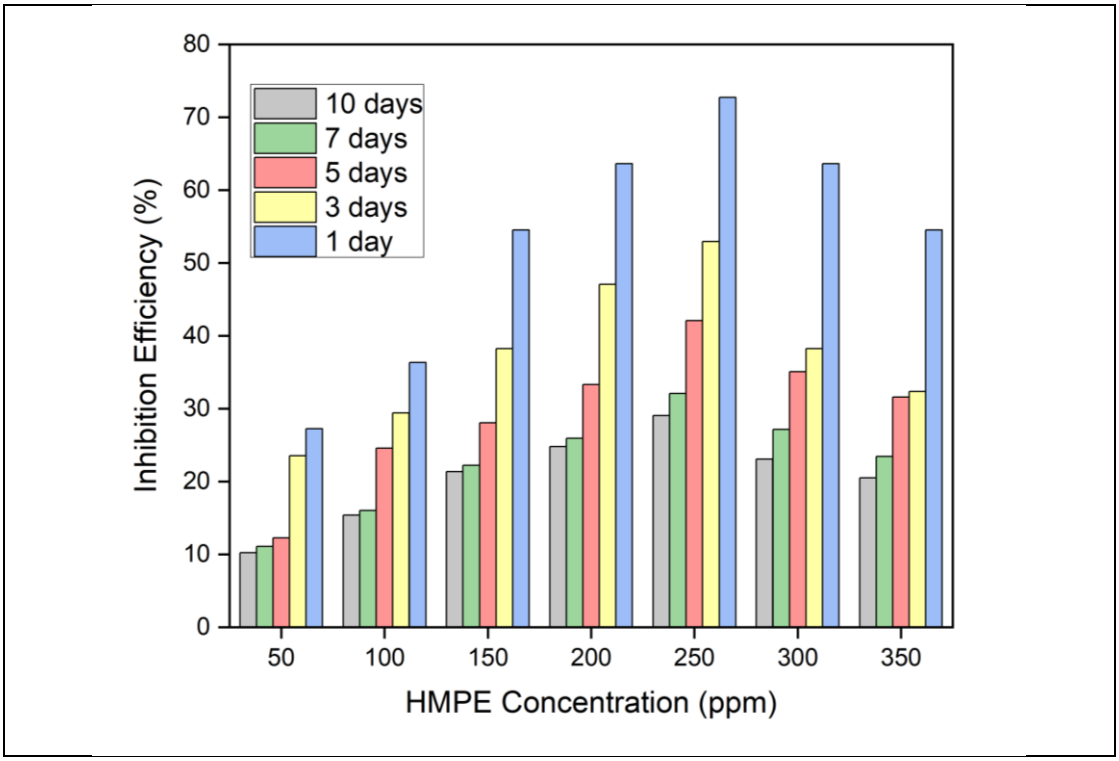


Figure 4.7 Corrosion Inhibition Efficiency (IE%) of Mild Steel in 0.6 M NaCl and in the Presence of HMPE Corrosion Inhibitor at Different Concentration and Immersion Time

However, the IE% value start to decline at the application of 300 - 350 ppm according to the excess in inhibitor molecules. This circumstance happened due to the interaction among the HMPE molecules in the bulk solution. The Van der Waals interaction may occur within the HMPE molecules, leading to molecular aggregation, which can reduce their availability in the corrosive medium. Below the 250 ppm HMPE, the inhibitor molecules were sufficiently enough to inhibit the mild steel corrosion by giving 10-70% IE at all immersion times. Over the time, the efficiency of the HMPE inhibitor start to decrease. This might due to the breakdown of the inhibitor layer or the saturation of the metal surface, where additional inhibitor cannot adsorb and thus does not contribute to increased efficiency (Hossain *et al.,* 2023).

#### *4.3.1.3 Effect of Temperature*

The effect of temperature was also studied in this research. Figure 4.8 illustrates the graph of corrosion inhibition efficiency of mild steel in 0.5 M HCl and in the presence of HMPE inhibitor for 3 hours at different temperatures (303, 313, 323, and 333 K). According to the graph, the IE% increases as the concentration of HMPE inhibitor increases for all temperatures studied. At lower concentrations, such as 50 ppm, the IE% is rather low at all temperatures, with the highest IE% observed at 303 K. However, as the HMPE inhibitor concentration increases, the IE% begins to rise significantly, especially at 200 ppm and above. The highest IE% recorded is 97% at 350 ppm for 303 K.

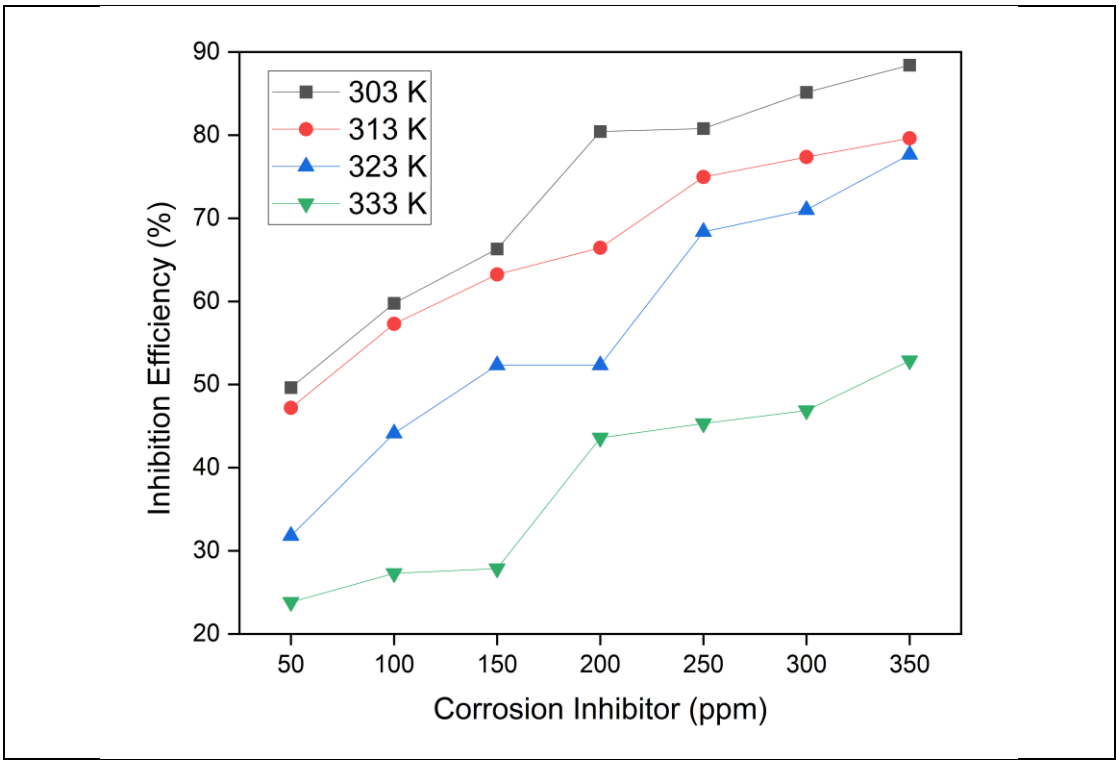


Figure 4.8 Corrosion Inhibition Efficiency (IE%) of Mild Steel in 0.5 M HCl and in the presence of HMPE Corrosion Inhibitor at Different Temperature

Despite that, the IE% is signinficantly lower at higher temperature, particularly at 333 K, where the IE% does not exceed 60% even at 350 ppm. This suggests that the efficiency of HMPE as a corrosion inhibitor declines as temperature rises, probably due to the increased in kinetic energy in the molecule, resulting to higher corrosion rate or

degradation of the HMPE inhibitor molecules at higher temperature (Mamand *et al.,* 2023).

Figure 4.9 depicts the graph of corrosion inhibition of mild steel immersed in 0.6 M NaCl with and without the presence of HMPE inhibitor for 4 hours at different temperatures. Based on the graph, the IE% rose for all temperatures studied until 250 ppm, with the highest efficiency obtained at 89% (303 K). However, the IE% started to decrease after more concentration of HMPE was added at 300 ppm and 350 ppm. The results are in line with the previous weight loss study with different immersion times where the optimum concentration is also at 250 ppm due to the inhibitor reaching its maximum coverage on the metal surface. Thus, increasing the concentration further may cause the HMPE inhibitor to desorb.

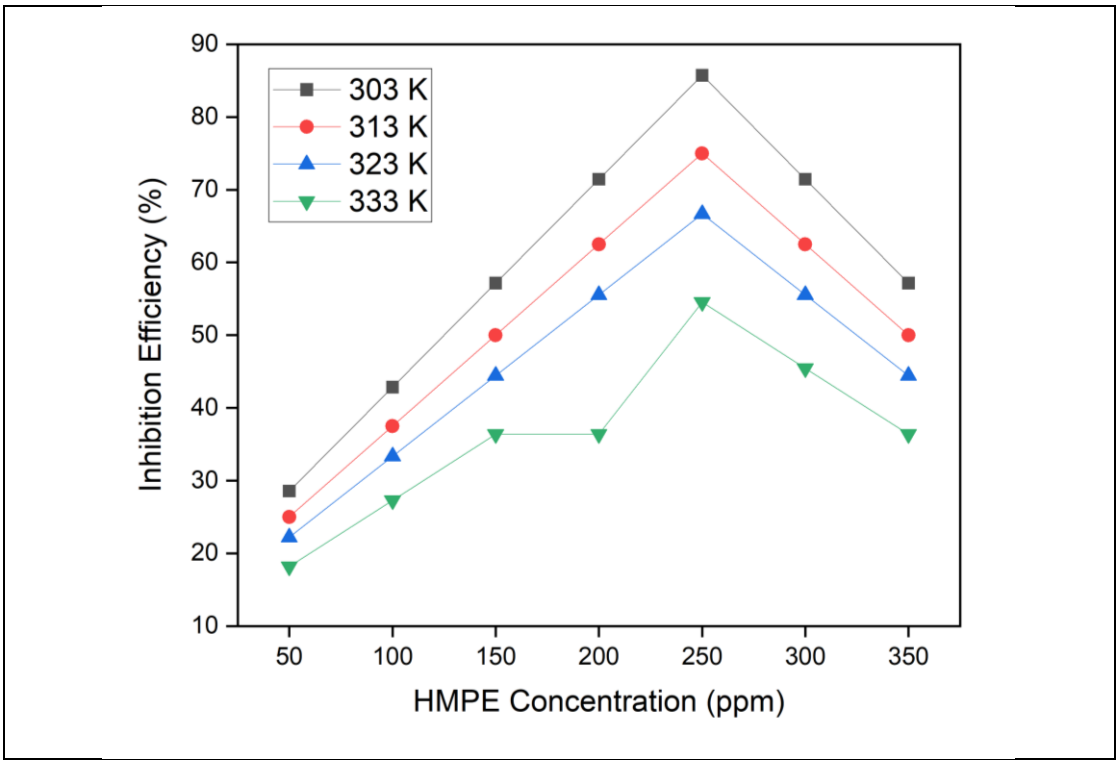


Figure 4.9 Corrosion Inhibition Efficiency (IE%) of Mild Steel in 0.6 M NaCl and in the Presence of HMPE Corrosion Inhibitor at Different Temperature

The IE% also declines as the temperature increases. The higher IE% observed at 303 K implies that the adsorption of HMPE inhibitors on a mild steel surface is more effective at lower temperatures. This is because at higher temperatures (333 K), the kinetic energy of the molecules increases. Therefore, this increased kinetic energy can

weaken the interactions between the HMPE inhibitor molecules and the metal surface, allowing the inhibitor to desorb from the metal surface.

### 4.3.2 Potentiodynamic Polarization Analysis

In this study, the potentiodynamic polarization test was conducted to further demonstrate the effectiveness of HMPE inhibitor by studying the reaction on anodic and cathodic parts of electrochemical process. This analysis is to support the finding from the weight loss results which indicate that the HMPE corrosion inhibitor is effective in inhibiting mild steel corrosion in acidic medium.

#### *4.3.2.1 Corrosion Inhibition in Acidic Medium*

Figure 4.10 displays the Tafel plots graph of the mild steel in 0.5 M HCl in the presence of HMPE inhibitor. The graph shows that both the anodic and cathodic branches have shifted towards lower current densities, indicating that the HMPE inhibitor has reduce the rate of oxidation and reduction process. In this case, HMPE has act to decrease the rate of metal dissolution (oxidation) and also inhibit the rate of hydrogen evolution (reduction). Therefore, HMPE is said to be effective in reducing the rate of corrosion. There is a slight shift in the corrosion potential ($E_{corr}$) with increasing of HMPE concentration. Nevertheless, there is no significant different in the corrosion potential value, showing that HMPE functions as a mixed-type inhibitor, impacting both anodic and cathodic processes.

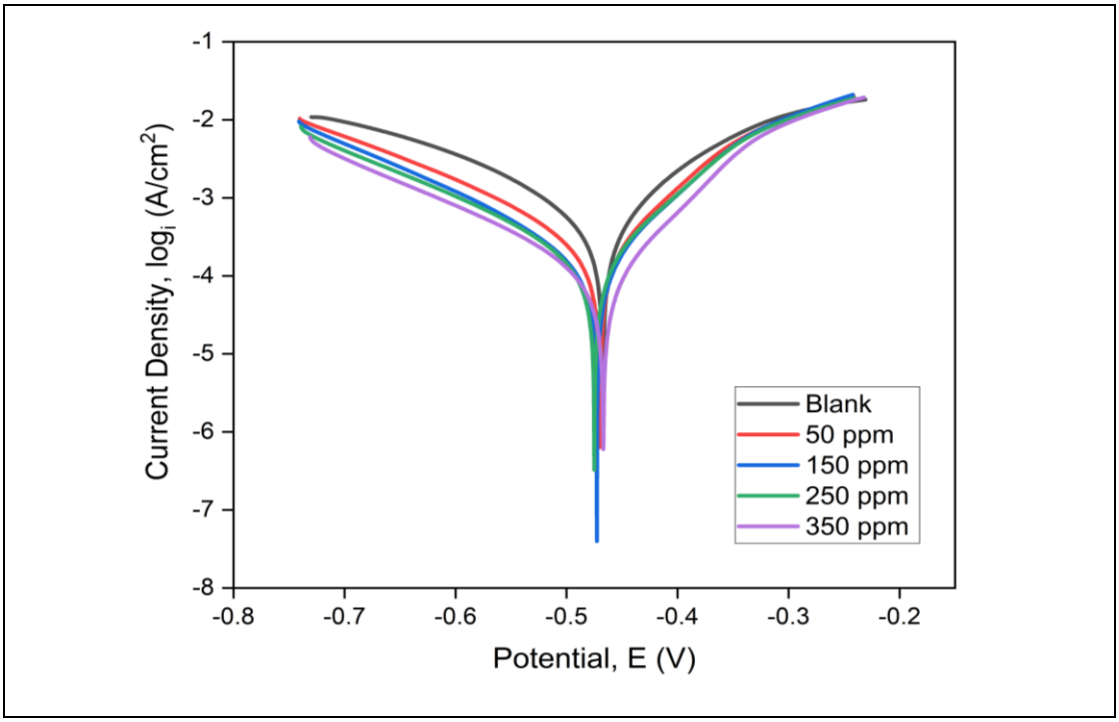


Figure 4.10 Tafel Plots for the Corrosion of Mild Steel in 0.5 M HCl and in the Presence of HMPE Corrosion Inhibitor in Different Concentration

Table 4.5 shows the result of potentiodynamic polarization for mild steel in 0.5 M HCl in the presence and absence of HMPE. The data provides the informations of the kinetic parameters specifically the corrosion current density ($i_{corr}$), corrosion potential ($E_{corr}$), anodic slopes ($\beta_a$), cathodic slopes ($\beta_c$), corrosion rates, and corrosion inhibition efficiency. Analysis has shown that the $i_{corr}$ values decrease from 447.3 µA cm$^{-2}$ (0.5 M HCl) to 35.99 µA cm$^{-2}$ with the addition and increase in concentration of HMPE inhibitor. Corrosion rate values also decrease from 208.22 mpy to 16.75 mpy with the concentration of HMPE, supporting the $i_{corr}$ results. In addition, the tafel slopes ($\beta_a$ and $\beta_c$) with increasing inhibitor concentration suggest that HMPE is influencing both anodic and cathodic processes. According to the Table 4.5, the $E_{corr}$ values exhibit a slight shift toward more positive potentials, with no significant changes observed at the highest concentration of 350 ppm, where the $E_{corr}$ is -467.60 mV. The corrosion IE% also rise with the concentration of HMPE, reaching up to 91.95% at 350 ppm, which shows a high level of inhibition efficiency at this concentration.

Table 4.5
Potentiodynamic Polarization Analysis Results of Mild Steel in 0.5 M HCl and in the Presence of HMPE Corrosion Inhibitor.

| Corrosion Inhibitor (HMPE) | $E_{corr}$ (mV) | $i_{corr}$ (µA $cm^{-2}$) | $\beta_a$ (mV $dec^{-1}$) | $\beta_c$ (mV $dec^{-1}$) | CR (mm/yr) | IE % |
|---|---|---|---|---|---|---|
| 0 ppm | -467.73 | 447.3 | 97.9 | 160.1 | 5.29 | 0 |
| 50 ppm | -469.93 | 161.5 | 85.4 | 181.9 | 1.91 | 63.89 |
| 150 ppm | -473.39 | 112.03 | 67.7 | 143.8 | 1.33 | 74.95 |
| 250 ppm | -472.77 | 68.96 | 74.1 | 165.8 | 0.82 | 84.58 |
| 350 ppm | -467.60 | 35.99 | 64.1 | 112.5 | 0.43 | 91.95 |

A higher $E_{corr}$ value indicates that the inhibitor has caused the metal surface to become slightly more noble. It may cause by the inhibitor is impacting the anodic reaction by potentially creating a protective layer that hinders the metal from dissolving easily (Al-Amiery *et al*., 2023). Even so, the small changes in the $E_{corr}$, which are below 85 mV as per ASTM standards, indicate that HMPE is not substantially altering the thermodynamics of the corrosion process but is affecting both the anodic and cathodic reactions (Dube-Johnstone *et al*., 2023). This behaviour is characteristic of a mixed-type inhibitor. The small increase in $E_{corr}$ and the Tafel slopes indicate that HMPE slows down both the anodic metal dissolution and the cathodic hydrogen evolution reactions. At the concentration of 350 ppm, HMPE showed the highest inhibition efficiency and the lowest corrosion rates. This suggests that the phenolic compounds present in the extract, such as mangiferin and gallic acid, are effective in reducing corrosion even at low concentrations.

In this analysis, the results obtained are consistent with a prior study conducted by Ramezanzadeh *et al*. (2019), which investigated the use of mango leaf extract as a corrosion inhibitor for mild steel in 1 M HCl. The results showed that both the anodic and cathodic branches exhibited a shift towards lower current densities. This finding indicates the mixed inhibitory effects caused by the mango leaf inhibitor on the mild steel and for our cases, HMPE. Despite that, the $E_{corr}$ values obtained from their study are moving slightly towards the cathodic side. Thus, the cathodic hydrogen evolution reaction rate can be considered as the dominant effect of mango leaf extract inhibitors. The IE% obtained is also high, at 92%, which is almost identical to the 91.95% observed

in our study on HMPE. These significant inhibitory effects are due to the organic compounds in the mango leaf extract, such as mangiferin, gallic acid, and iriflophenone, whose functional groups contain many heteroatoms, such as oxygen.

Similarly, Rocha *et al.* (2014) conducted a study utilizing orange peel and mango peel extract as corrosion inhibitors for carbon steel in 1 M HCl. From their studies, both cathodic and anodic current densities were lower than the blank, and the Ecorr shifted slightly to a more positive value, indicating that this extract functions as a mixed-type inhibitor with predominantly effect anodic properties. The highest IE% calculated from the icorr values for the mango peel and orange peel extract are 96% and 91%, respectively. This inhibitory effect might be because of the antioxidant compounds in the extract, such as polyphenols, vitamin C, and carotenoids.

#### *4.3.2.2 Corrosion Inhibition in Near-Neutral Medium*

Figure 4.11 shows the polarization curves for the corrosion of mild steel in 0.6 M NaCl in the presence and absence of HMPE corrosion inhibitor in different concentration. The corrosion current density (icorr) declined indicating a reduction in the corrosion rates, with the addition of HMPE corrosion inhibitor. The corrosion potential (Ecorr) also shifts towards more positive values at the presence of HMPE inhibitor. A positive shift in Ecorr when an inhibitor is present usually suggests a predominantly anodic type of inhibition, where the inhibitor is more efficient at decreasing the anodic reaction, which involves the metal dissolving process (Rehioui et al., 2021).

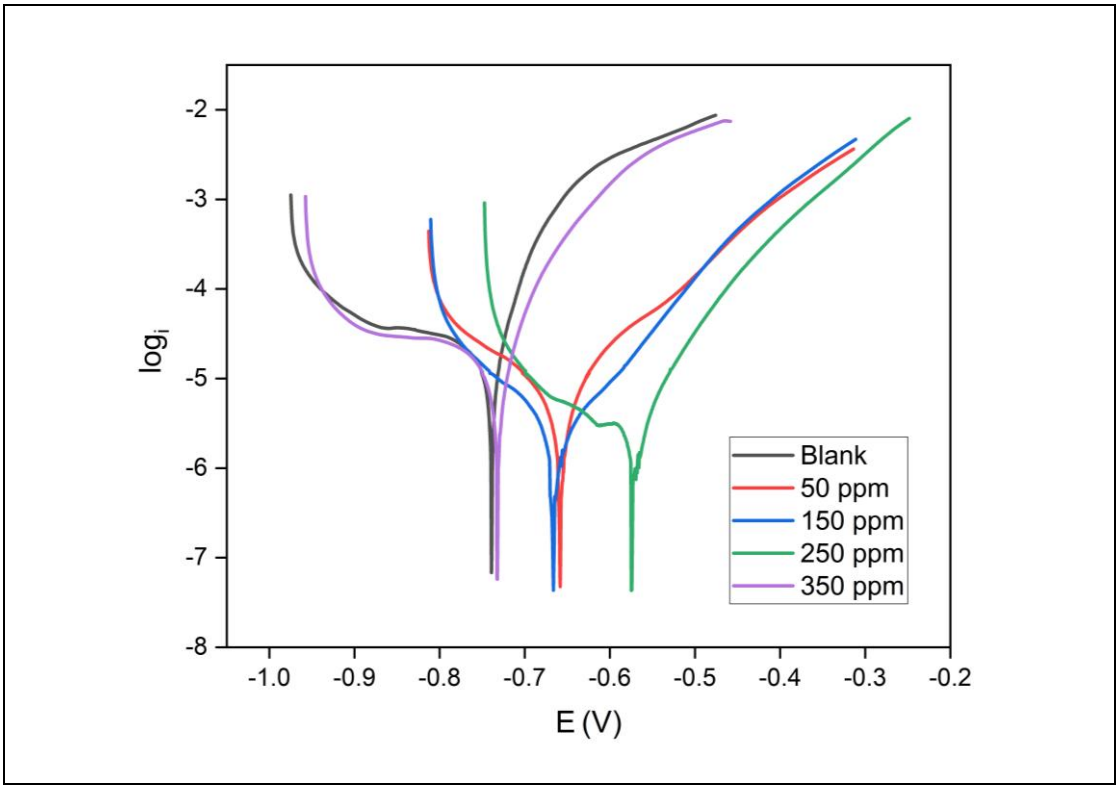


Figure 4.11 Tafel plots for the Corrosion of Mild Steel in 0.6 M NaCl and in the Presence of HMPE Corrosion Inhibitor in Different Concentration

According to the potentiodynamic polarization data (Table 4.6), the mild steel sample subjected in the blank 0.6 M NaCl has the highest $i_{corr}$ and most negative $E_{corr}$ values, this indicates it has the highest corrosion rate among the samples. The best performance of the mild steel corrosion inhibition was identified at 250 ppm HMPE, where it exhibits the lowest corrosion rates (0.819 mpy) and the maximum IE% (84.42%). Additionally, the data illustrates that the $i_{corr}$ values begin to rise beyond 250 ppm, resulting in increasing the corrosion rates and reduction of the IE%. This situation indicates that higher concentrations may not offer greater protection. There might be an optimal concentration range for HMPE inhibitory action. This may be caused by the formation of other complex interactions on the steel surfaces that limit the inhibitor's effectiveness.

Table 4.6
Potentiodynamic Polarization Analysis Results of Mild Steel in 0.6 M NaCl and in the Presence of HMPE Corrosion Inhibitor.

| Corrosion Inhibitor (HMPE) | $E_{corr}$ (mV) | $i_{corr}$ (µA $cm^{-2}$) | $\beta_a$ (mV $dec^{-1}$) | $\beta_c$ (mV $dec^{-1}$) | CR (mm/yr) | IE % |
|---|---|---|---|---|---|---|
| 0 ppm | -737.45 | 11.3 | 31.87 | 13.26 | 0.13 | 0 |
| 50 ppm | -658.44 | 3.48 | 14.91 | 12.86 | 0.04 | 69.20 |
| 150 ppm | -575.38 | 2.30 | 8.98 | 11.78 | 0.03 | 79.65 |
| 250 ppm | -574.15 | 1.76 | 17.21 | 11.09 | 0.02 | 84.42 |
| 350 ppm | -732.34 | 7.06 | 28.63 | 14.40 | 0.09 | 37.52 |

The $E_{corr}$ values of the inhibited mild steel samples shift towards more positive values compared to the mild steel sample reacted in blank 0.6 M NaCl, indicating that the inhibitor may be affecting the anodic reaction. This suggests that the HMPE could be acting as an anodic inhibitor, or at least has a significant inhibiting effect on the anodic process. This indicates that the inhibitor is hindering the metal's ability to release electrons and enter the solution as metal ions. However, since there is a slightly shift in $E_{corr}$ values, typically less than 85 mV as per ASTM standard, HMPE can be classified as a mixed-type inhibitor with predominantly anodic.

The finding is in line with Budiarsa *et al.,* 2024 who investigated the red dragon fruit peel extract as a corrosion inhibitor in 0.6 M NaCl. According to the research, the red dragon fruit peel extract has been identified as an anodic type inhibitor. Thus, this extract can reduce the corrosion rate by forming a protective oxide film on the metal surface to prevent further oxidation that can lead to corrosion. The mechanism of the extract components on the steel surface influences the electrochemical behaviour of the metal in a near-neutral environment.

### 4.3.3 Electrochemical Impedance Spectroscopy Analysis

#### *4.3.3.1 Corrosion Inhibition in Acidic Medium*

EIS provides insights into the electrochemical processes at the metal or solution interface by measuring the impedance of the system at different frequencies. Figure 4.12 illustrates the Nyquist plot show the impedance behaviour of mild steel in 0.5 M HCl with the addition of HMPE at different concentration. According to the plots, the diameter of the semicircle rises with the concentration of HMPE, which means the charge transfer resistance ($R_{ct}$) increase. This indicate that the HMPE is effectively increasing the resistance to charge transfer, which correlates with a decrease in the corrosion rates. In potentiodynamic polarization, the potential sweep disturbs the surface and the inhibitor film, so small changes in corrosion potential are masked, but in EIS, the near-equilibrium measurement allows slight adsorption of the mango peel to shift the mixed potential, causing the slight changes in corrosion potential observed.

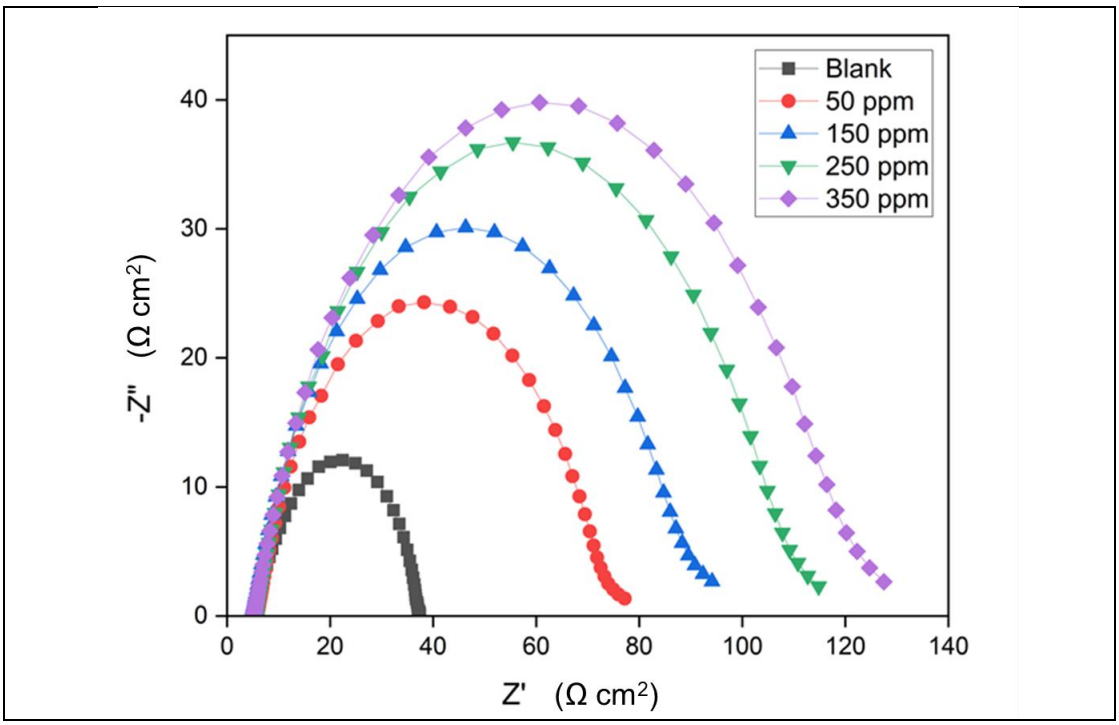


Figure 4.12 Nyquist Plots for the Corrosion of Mild Steel in 0.5 M HCl and in the Presence of HMPE Corrosion Inhibitor in Different Concentration

Table 4.7 displays the impedance parameters for the corrosion of mild steel in 0.5 M HCl with the HMPE inhibitor. The parameters consist of solution resistance ($R_s$),

charge transfer resistance ($R_{ct}$), constant phase element (CPE), CPE exponent (n), and inhibition efficiency (IE%). The $R_s$ values remain relatively constant, indicating that the inhibitor does not have a significant impact on the solution resistance. The $R_{ct}$ values rise with increasing concentrations of HMPE, validating the pattern seen in the Nyquist plot. In addition, the CPE values, which are linked with capacitance, typically decrease as $R_{ct}$ increases. The greatest level of inhibition efficiency (IE%) was achieved at a high concentration of HMPE, specifically 75.29%.

Table 4.7
Impedance Parameters for the Corrosion of Mild Steel in 0.5 M HCl and in the Presence of HMPE Corrosion Inhibitor in Different Concentration.

| **Corrosion Inhibitor (HMPE)** | **$R_s$ ($\Omega$ cm$^2$)** | **$R_{ct}$ ($\Omega$ cm$^2$)** | **CPE (F cm$^2$)** | **n** | **IE %** |
|---|---|---|---|---|---|
| 0 ppm | 20.768 | 33.04 | 0.0041 | 0.657 | 0 |
| 50 ppm | 23.496 | 75.08 | 0.0005 | 0.763 | 56.00 |
| 150 ppm | 19.376 | 95.87 | 0.0009 | 0.753 | 65.54 |
| 250 ppm | 22.488 | 111.60 | 0.0004 | 0.769 | 70.39 |
| 350 ppm | 20.556 | 133.70 | 0.0006 | 0.740 | 75.29 |

The data indicates that HMPE is an efficient corrosion inhibitor for mild steel in 0.5 M HCl. The inhibitor probably functions by adsorbing onto the steel surface, forming a barrier that impedes the corrosion process. The rise in $R_{ct}$ and the decline in CPE as inhibitor concentration increases may suggest the formation of a protective film on the steel surface. The IE% also can be explained by the adsorption of HMPE molecules on the metal surface, leading to a decrease in the active sites for the corrosive reaction.

#### *4.3.3.2 Corrosion Inhibition in Near-Neutral Medium*

Figure 4.13 shows a Nyquist plot illustrating the corrosion of mild steel in 0.6 M NaCl with and without various concentrations of HMPE corrosion inhibitor. The plot show a depressed semicircle compared to the plot in HCl. This is because the non-uniform adsorption of the HMPE caused by the distruption of chloride ions in NaCl.

The semicircle with the smallest diameter corresponds to the lowest $R_{ct}$ and therefore the highest corrosion rate. Increasing the concentration of HMPE results in larger semicircle diameters, which suggest higher $R_{ct}$ values and consequently lower corrosion rates. At 350 ppm, the semicircle decreases in size, which goes against the anticipated pattern. This result is consistent with the findings from potentiodynamic polarization and weight loss experiments.

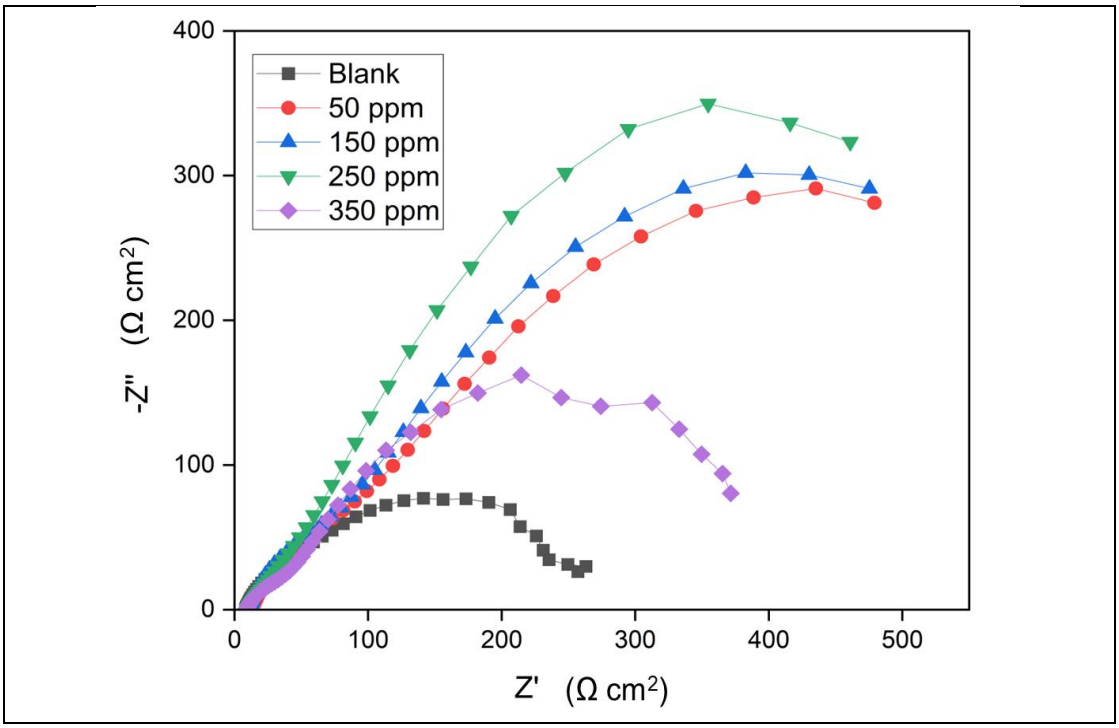


Figure 4.13 Nyquist Plots for the Corrosion of Mild Steel in 0.6 M NaCl and in the Presence of HMPE Corrosion Inhibitor in Different Concentration

According to Table 4.8, $R_s$ a consistent value regardless of the concentrations. The $R_{ct}$ values increase with the concentration of the inhibitor up to 250 ppm, validating the observations from the Nyquist plot that the inhibitor's effectiveness rises up to this point. At 350 ppm, the $R_{ct}$ decreases, as indicated by the smaller semicircles in the Nyquist plot, implying reduced effectiveness of the inhibitor at higher concentrations. Furthermore, the inhibitor efficiency demonstrates an increase in corrosion protection up to 250 ppm (90.29%) in the IE%, but then decreases, supporting the conclusion that the inhibitor's effectiveness diminishes at higher concentrations.

Table 4.8
Impedance Parameters for the Corrosion of Mild Steel in 0.6 M NaCl with and without the Presence of HMPE Corrosion Inhibitor in Different Concentration.

| **Corrosion Inhibitor (HMPE)** | **$R_s$ ($\Omega$ $cm^2$)** | **$R_{ct}$ ($\Omega$ $cm^2$)** | **CPE (F $cm^2$)** | **n** | **IE %** |
|---|---|---|---|---|---|
| 0 ppm | 8.056 | 267.7 | 0.004101 | 0.657 | 0 |
| 50 ppm | 12.01 | 1122.0 | 0.005424 | 0.5864 | 76.14 |
| 150 ppm | 9.327 | 1197.0 | 0.005792 | 0.6027 | 77.64 |
| 250 ppm | 9.76 | 2758.0 | 0.00763 | 0.6038 | 90.29 |
| 350 ppm | 8.427 | 677.0 | 0.006235 | 0.5463 | 60.46 |

The rise in impedance as the HMPE concentration increases indicates that the inhibitor functions by inhibiting the active corrosion sites on the metal surface or by creating a complex compound with metal ions, both of which would lower the metal dissolution rate. The decrease in $R_{ct}$ at concentrations exceeding 250 ppm may result from the saturation of adsorption sites on the steel surface. This could cause HMPE molecules to aggregate instead of adsorb, potentially resulting in a less efficient corrosion inhibition layer.

### 4.3.4 Summary of Corrosion Analysis

Table 4.9 shows the summary of corrosion analysis obtained from the corrosion test, WL, PP, and EIS in both 0.5 M HCl and 0.6 M NaCl.

Table 4.9
Summary of Corrosion Test

| Corrosion Analysis | 0.5 M HCl | 0.6 M NaCl |
|---|---|---|
| Weight Loss Analysis | High corrosion rates observed for blank. After the addition of HMPE inhibitor, the corrosion rates reduce. The IE% increase as the concentration of HMPE increase. The highest IE% obtained was 88% at 350 ppm. | Lower corrosion rates than HCl observed for blank, but the addition of HMPE inhibitors still show a reduction in weight loss. There is an optimum concentration of the HMPE observed. The IE% increase as the concentration of HMPE increase up to 250 ppm before it starts to decrease. The highest IE% obtained was 73% at 250 ppm. |
| Potentiodynamic Polarization Analysis | HMPE acted as a mixed-type inhibitor reducing bothe the anodic metal dissolution and cathodic hydrogen evolutions. The highest IE% obtained was 92% at 350 ppm. | HMPE acted as a mixed-type inhibitor with predominantly anodic. The highest IE% obtained was 84% at 250 ppm. |
| Electrochemical Impedance Spectroscopy Analysis | The $R_{ct}$ increase after the addition of HMPE, indicating increase in IE%. The highest IE% obtained was 76% at 350 ppm. | The $R_{ct}$ increase after the addition of HMPE up to 250 ppm before it started to decrease. The highest IE% obtained was 90% at 250 ppm. |

## 4.4 Corrosion Surface Study Analysis

### 4.4.1 Observation via Optical Microscope

In this subchapter, the analysis of the observation of mild steel surface structure was discussed. Throughout the discussion, the concentration of HMPE ranging from 50 to 100 ppm was classified as low concentration, meanwhile 150 to 250 ppm as moderate concentration, and 300 and 350 ppm as high concentration. The classification of the 3 ranges of HMPE concentration was done in this subchapter to ensure the observation and analysis are more focused and systematic.

#### *4.4.1.1 Corrosion Inhibition in Acidic Medium*

Figure 4.14 (a) and (b) display the microscopic images of mild steel surfaces in 0.5 M HCl (blank) at different immersion time. The metal samples without inhibitors show significant corrosion after 1 day immersion seems to intensify after 10 days. The steel surface looks very rough and formed uneven structure. The rapid degradation of mild steel surface for both 1 day and 10 days immersion in HCl solution is due to the highly aggressive environment of acid.

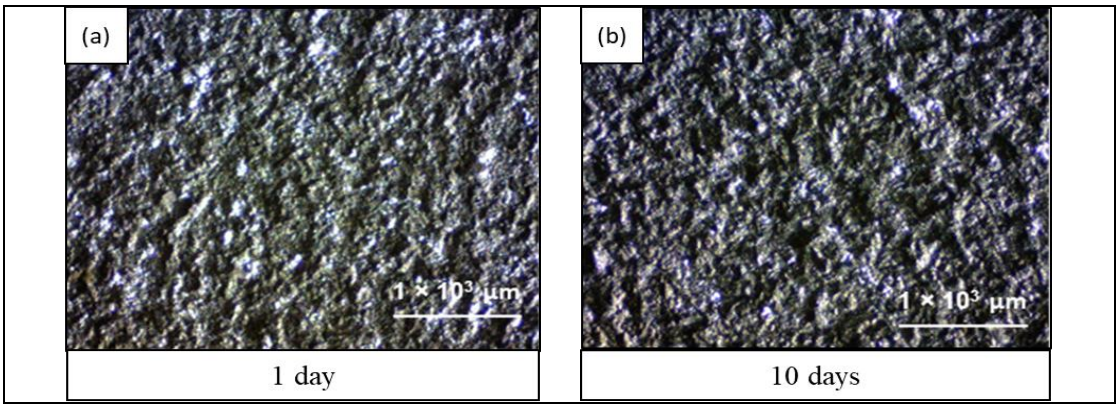


Figure 4.14 Optical Microscopic Images of Mild Steel Surface in 0.5 M HCl (blank) for; (a) 1 day and (b) 10 days Immersion

Figure 4.15 (a), (b), (c), and (d) show the mild steel surface after the addition of the HMPE corrosion inhibitor at lower concentrations of 50 ppm and 100 ppm for 1 day and 10 days of immersion. The steel surface at 1 day immersion for both HMPE concentrations show less corroded structure compared to the mild steel surface without

inhibitor, indicating 10 to 15% inhibition efficiency as calculated from the weight loss test. After 10 days, the protective effect appears to have diminished, as the roughness of the surface remained visible.

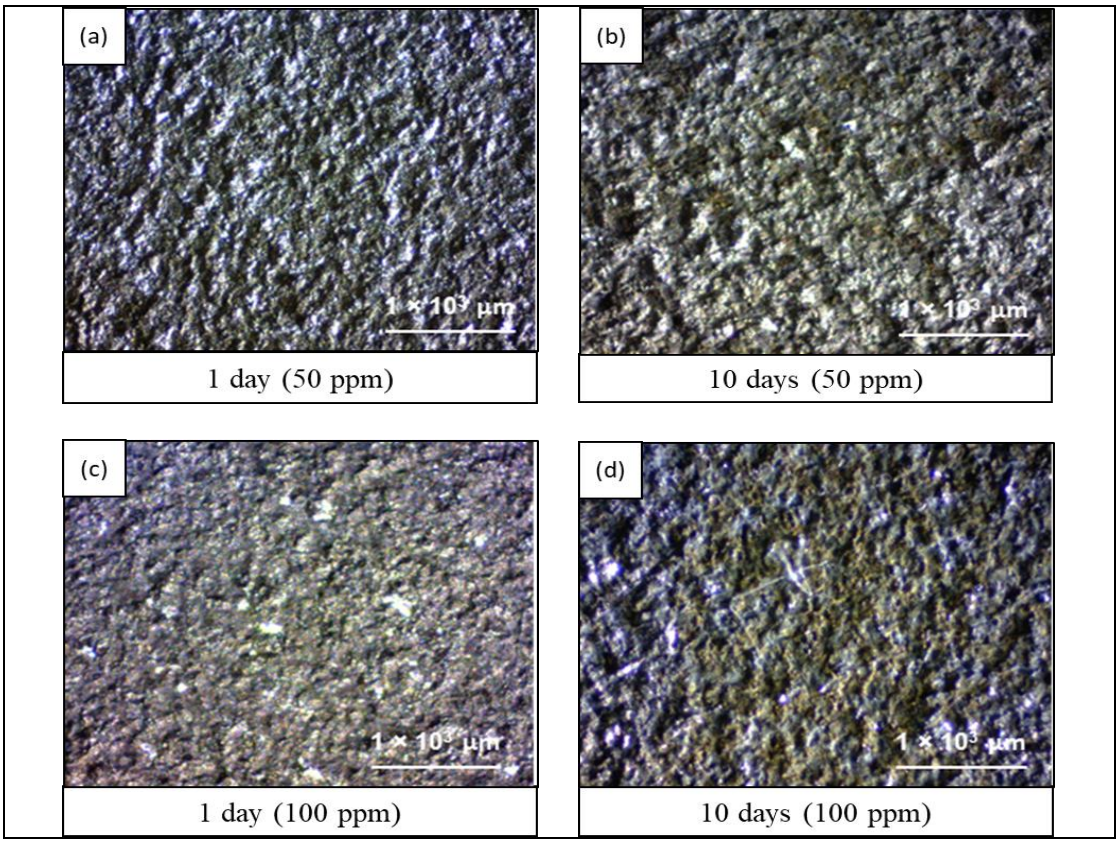


Figure 4.15 Optical Microscopic Images of Mild Steel Surface in 0.5 M HCl in the Presence of low HMPE Concentrations; (a) 50 ppm for 1 day Immersion (b) 50 ppm for 10 days Immersion (c) 50 ppm for 1 days Immersion and (d) 100 ppm for 10 days Immersion

Figure 4.16 (a) to (f) depict the microscopic images of mild steel surface in the presence of 150 to 250 ppm for 1 day and 10 days. Following the addition of concentrations of HMPE from 150 to 250 ppm, the steel surface shows smoother than the blank surface after being immersed for 1 day as shown in the Figure 4.16 (a), (c), and (e). Also, after 10 days of immersion, the mild steel surface shows improvement compared to the blank and lower concentrations of HMPE.

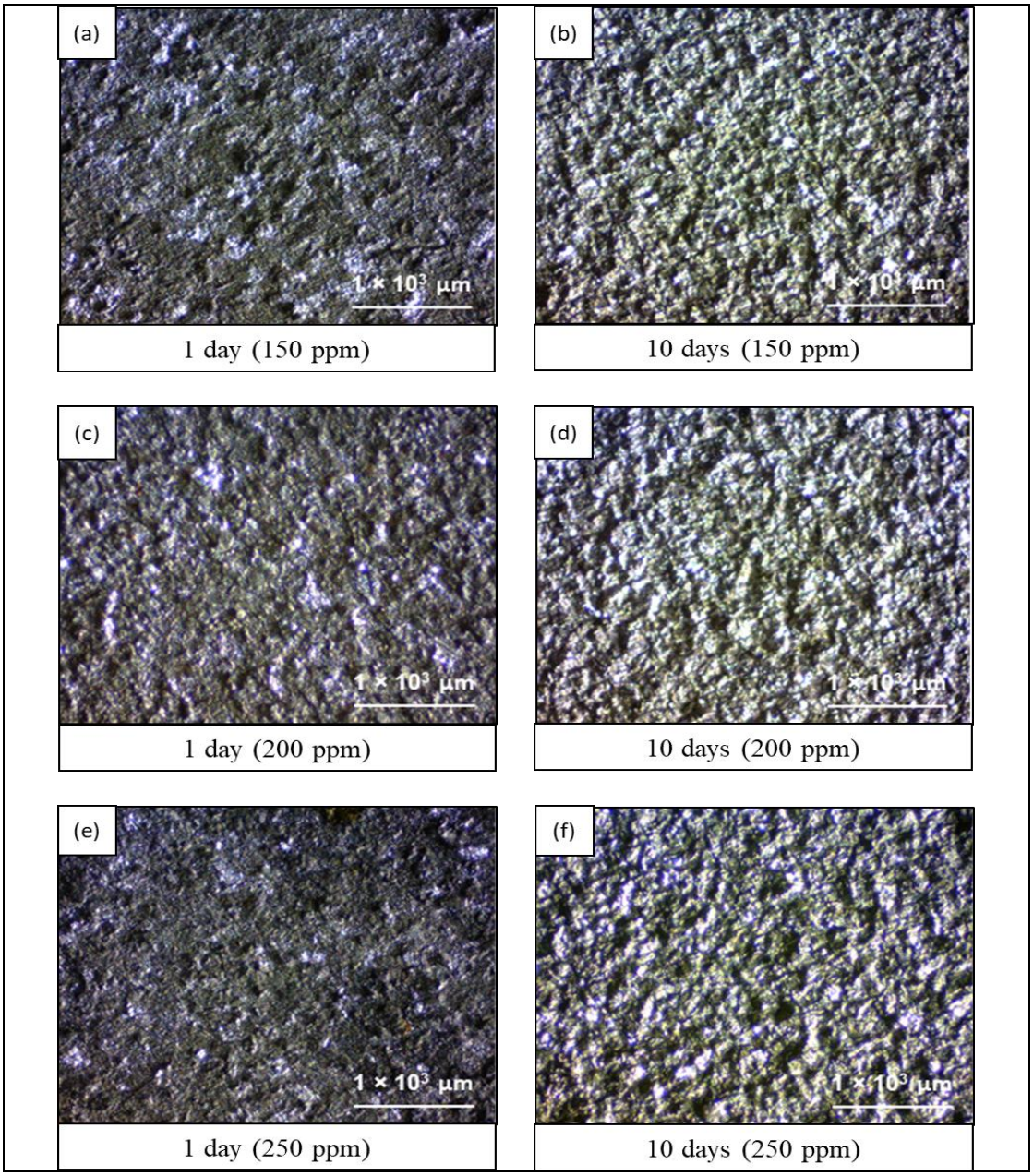


Figure 4.16 Optical Microscopic Images of Mild Steel Surface in 0.5 M HCl in the Presence of Moderate HMPE Concentrations; (a) 150 ppm for 1 day Immersion (b) 150 ppm for 10 days Immersion (c) 200 ppm for 1 day Immersion (d) 200 ppm for 10 days Immersion (e) 250 ppm for 1 day Immersion and (f) 250 ppm for 10 days Immersion

The mild steel corrosion becomes notably inhibited and exhibits minimal roughness at higher concentrations of HMPE at 300 and 350 ppm as shown in Figure 4.17 (a), (b), (c), and (d), surpassing the improvements seen at lower concentrations. This demonstrating an enhanced inhibition effect after 1 day of immersion. Following 10 days of immersion at 300 and 350 ppm, the mild steel surface also shows considerable improvement compared to the blank HCl solution and lower

concentrations of HMPE. Despite this, the surface retains more roughness compared to the smoother appearance after 1 day of immersion.

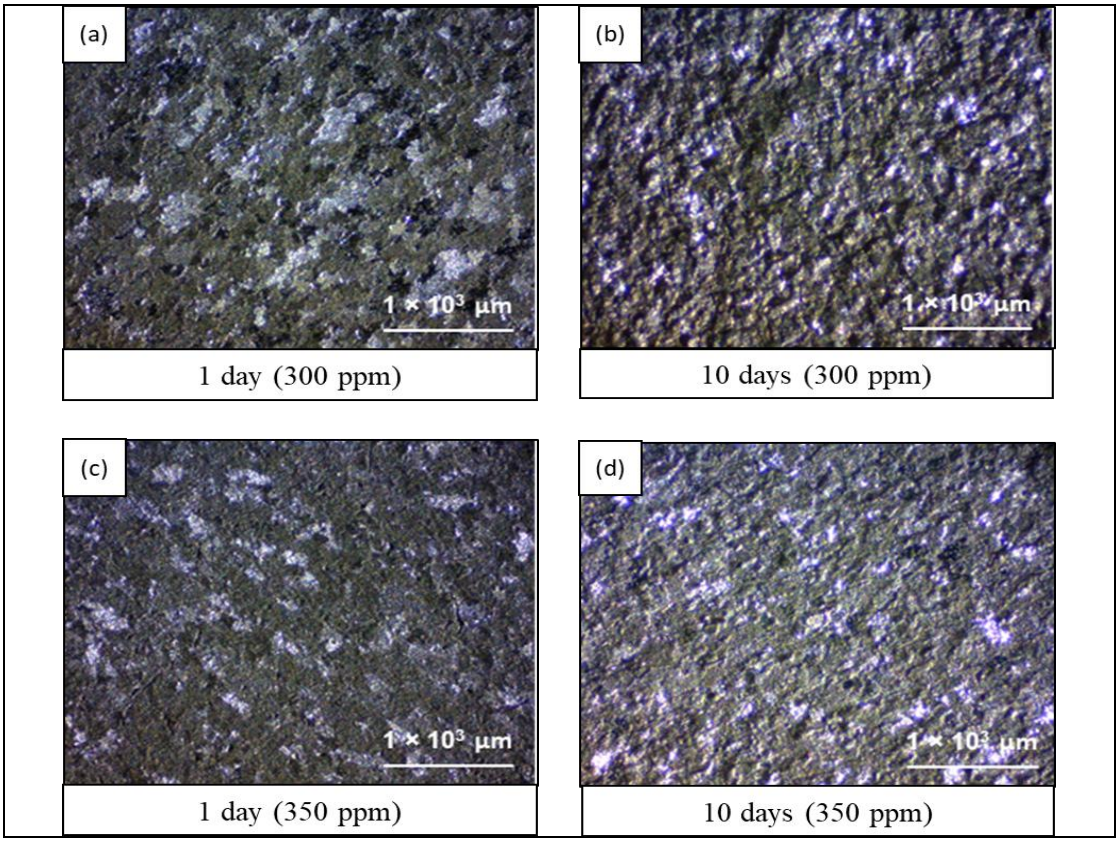


Figure 4.17 Optical Microscopic Images of Mild Steel Surface in 0.5 M HCl in the Presence of High HMPE Concentrations; (a) 300 ppm for 1 day Immersion (b) 300 ppm for 10 days Immersion (c) 350 ppm for 1 days Immersion and (d) 350 ppm for 10 days Immersion

The mild steel surface for both 1 and 10 days immersion in 0.5 M HCl in the presence of HMPE inhibitor shows improvement compared to the blank. The rapid degradation of mild steel surface for both 1 day and 10 days immersion in blank HCl solution is due to the highly aggressive environment of acid. The addition of low HMPE concentration (50 and 100 ppm), for 1 day immersion, exhibits a decline in corrosive structure on the surface. This prove the effectiveness of the HMPE as corrosion inhibitor. However, the effectiveness diminishes, as the roughness of the surface become evident after 10 days of immersion, which probably due to the insufficient concentration of HMPE inhibitor. As previously revealed from the weight loss analysis, the IE% was reduced from 54% to 2%. As the concentration of HMPE increase to 150 and 350 ppm, the corrosion inhibition of mild steel surface gradually improves and the surface becomes smoother, indicating the formation of the organic protective HMPE

inhibition layer on the mild steel surface (Hossain *et al*., 2022). Despite this, over prolonged immersion (10 days), the mild steel surface persistently rough even at higher concentration of HMPE. This situation is probably due to the decreased in availability of the HMPE molecule for the adsorption on the mild steel surface, resulting to the decline in inhibitory effect (Aljibori *et al.*, 2024).

#### *4.4.1.2 Corrosion Inhibition in Near-Neutral Medium*

Figure 4.18 (a) and (b) displays the microscopic images of mild steel surfaces after exposure in 0.6 M NaCl for 1 day and 10 days immersion. The mild steel surface in the blank NaCl solution, shows yellowish-orange color with extensive pitting spots after 1 day of immersion. However, after 10 days, the mild steel surface turns black.

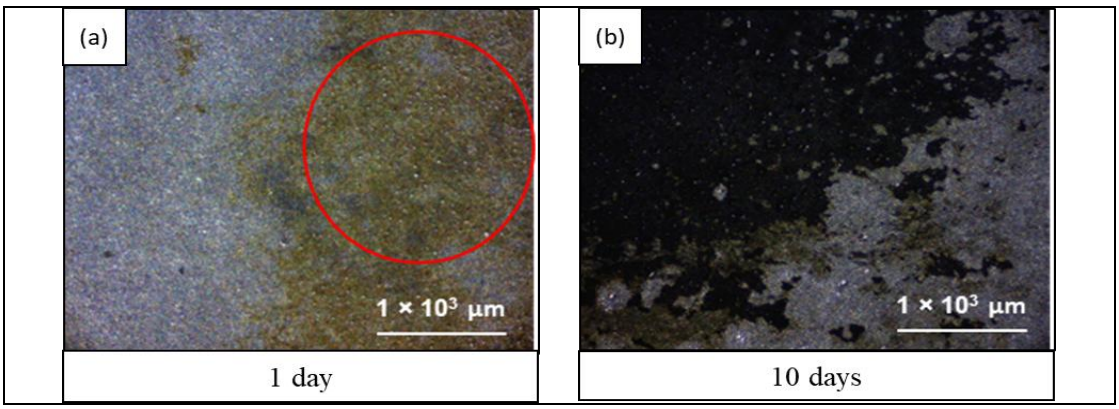


Figure 4.18 Optical Microscopic Images of Mild Steel Surface in 0.6 M NaCl Blank for; (a) for 1 day Immersion (b) for 10 days Immersion

The addition of the HMPE inhibitor at the concentration of 50 ppm (Figure 4.19 (a)) has formed several pitting spots (as shown in circle) and a sign of yellowish corrosion product are still apparent after 1 day. Figure 4.19 (b) reveals an immersion after 10 days the surface remains yellow with many pitting spots. Increasing the HMPE inhibitor concentration from 50 ppm to 100 ppm for 1 day immersion leads to development of smaller & less pitting spots. The yellow coloration on the mild steel surface remains visible after 10 days immersion but has decreased in intensity.

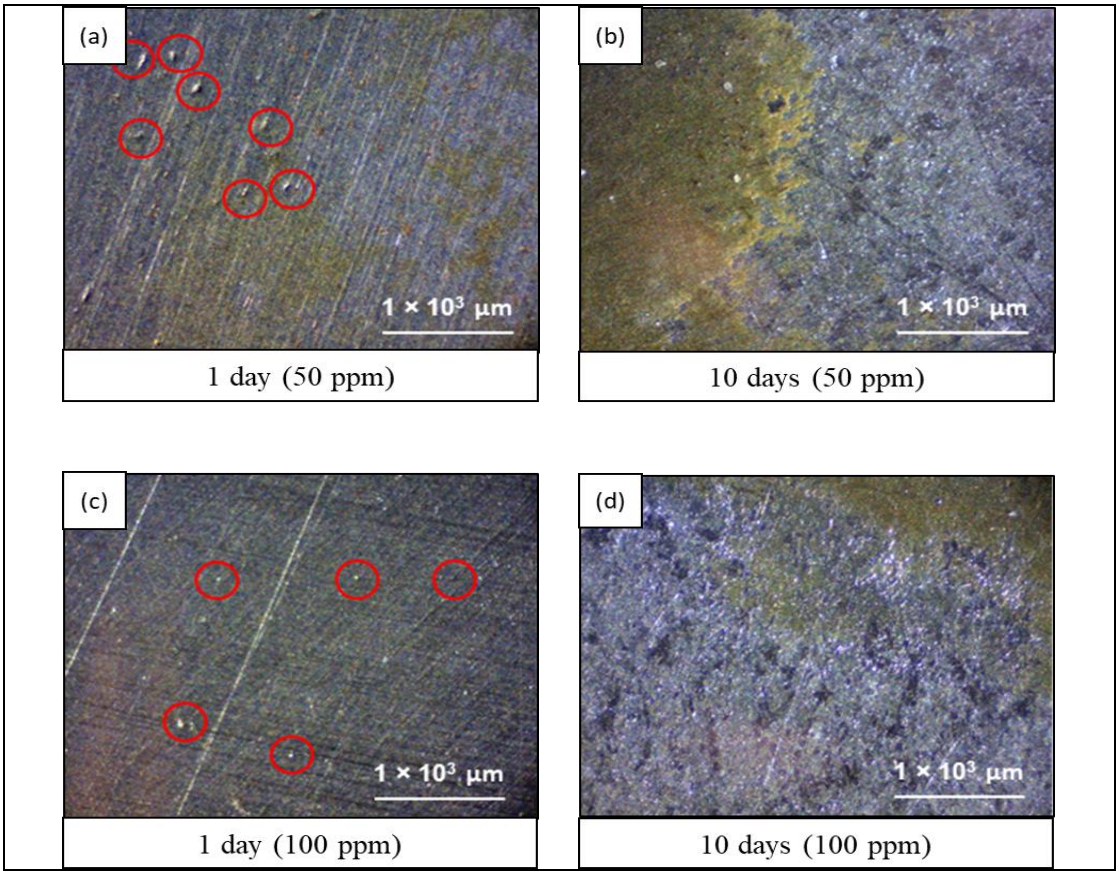


Figure 4.19 Optical Microscopic Images of Mild Steel Surface in 0.6 M NaCl in the Presence of Low HMPE Concentration; (a) 50 ppm for 1 day Immersion (b) 50 ppm for 10 days Immersion (c) 100 ppm for 1 days Immersion and (d) 100 ppm for 10 days Immersion

Figure 4.20 (a) and (c) display the immersion of mild steel at 150 to 200 ppm of HMPE, shows notable improvement without any noticeable pitting spots within 1 day of immersion. After 10 days, the pitting spots are reduced and become smaller as shown in Figure 4.20 (b) and (d). At a higher concentration of 250 ppm, the surface of the mild steel almost similar to its original surface as shown in Figure 4.20 (e), exhibiting a significant inhibition effect. After 10 days (Figure 4.20 (f)), the surface is getting smoother with invisible pitting spots, although the condition after 1 day showed less corrosion effect.

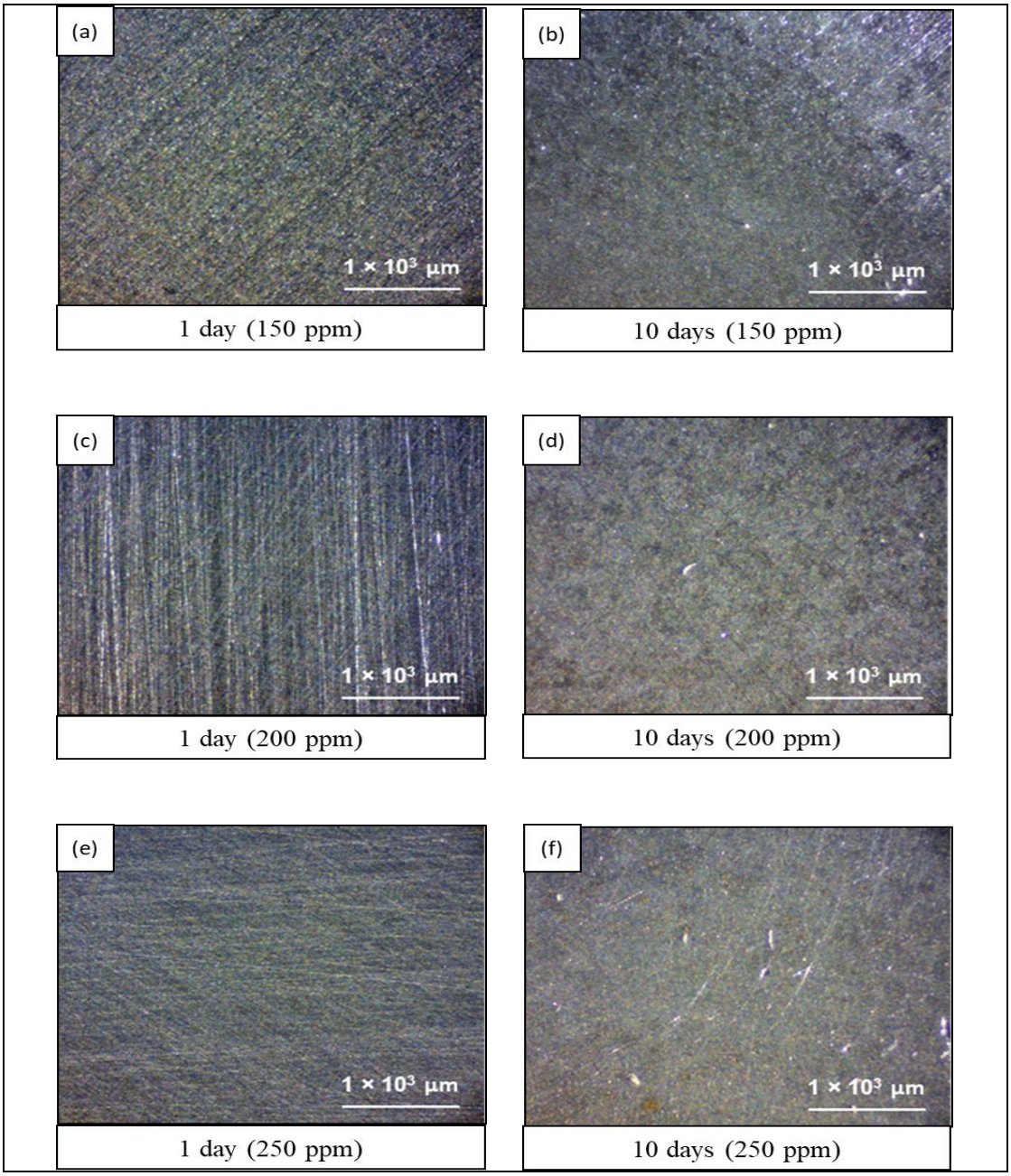


Figure 4.20 Optical Microscopic Images of Mild Steel Surface in 0.6 M NaCl in the Presence of Moderate HMPE Concentration (a) 150 ppm for 1 day Immersion (b) 150 ppm for 10 days Immersion (c) 200 ppm for 1 days Immersion (d) 200 ppm for 10 days Immersion (e) 250 ppm for 1 day Immersion and (f) 250 ppm for 10 days Immersion

Despite this, Figure 4.21 (a) to (d) show the mild steel surface at the presence of higher concentrations of HMPE in 300 and 350 ppm. The surface of the mild steel begins to deteriorate, becoming less smooth compared to the surface in 250 ppm for 1 day of immersion. After 10 days, the regression becomes more noticeable, as the surface depicts several pitting spots.

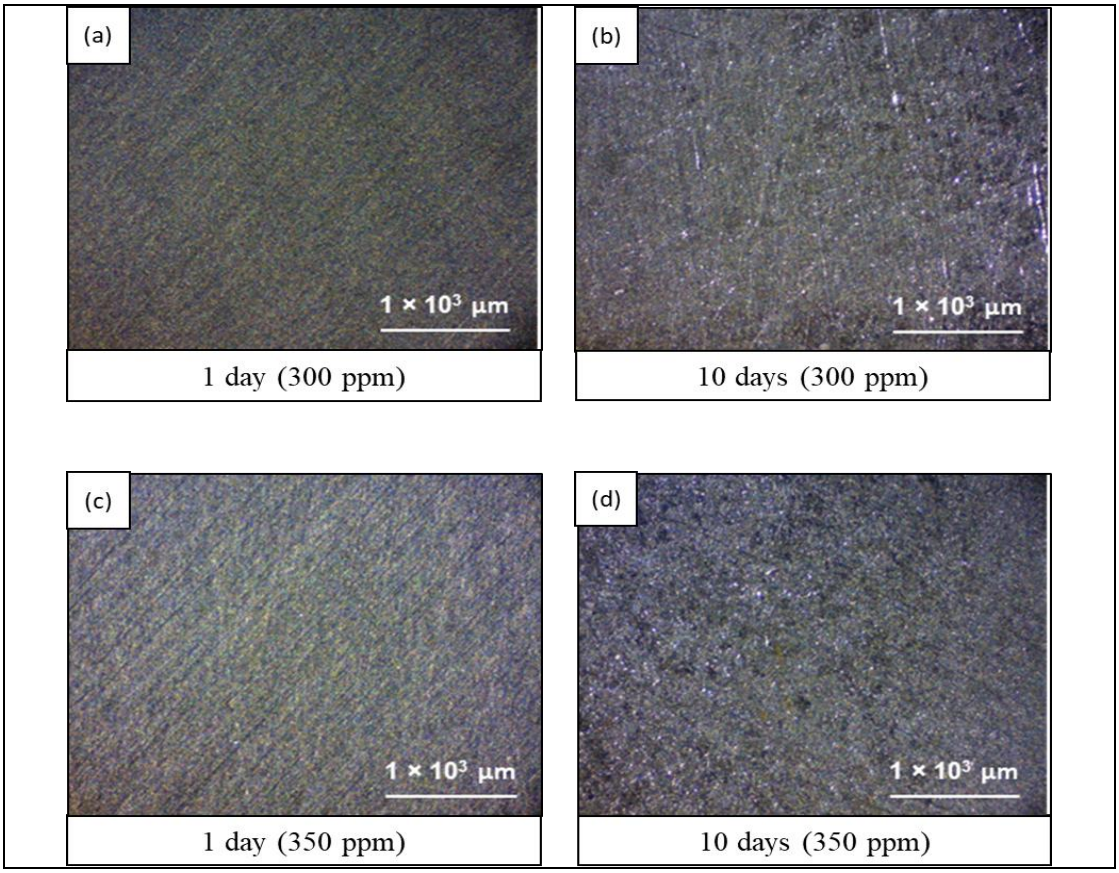


Figure 4.21 Optical Microscopic Images of Mild Steel Surface in 0.6 M NaCl in the presence of High HMPE Concentrations; (a) 300 ppm for 1 day Immersion (b) 300 ppm for 10 days Immersion (c) 350 ppm for 1 days Immersion (d) 350 ppm for 10 days Immersion

The mild steel surface starts to turns yellow after the immersion in NaCl for 1 day without the presence of the inhibitor, denoting the presence of rust. However, after prolonged immersion of 10 days, the mild steel turns black, indicating the presence of iron oxides of magnetite ($Fe_3O_4$) (Bozovic *et al*., 2020). After the addition of HMPE inhibitor at a low concentration of 50 to 100 ppm, the mild steel surface showed slight improvement at 1 day immersion but still corroded at 10 days of immersion. This is probably due to the formation of HMPE inhibitors protective film which is weakly developed. This situation allows some chloride ions penetrating into the film and attack the surface, consequently causes pitting. At 250 ppm, the mild steel surface reveal to be as smooth as the original mild steel for 1 day of immersion, which signifies the more effective inhibiting action of HMPE in NaCl, aligned with the results of IE% from weight loss (73%) and electrochemical tests (84 and 90%). Despite this, for 10 days of immersion, the mild steel surface moderately deteriorate even it was better than lower concentration. This is because HMPE inhibitor molecule desorbs through the interface

of the protective layer the longer immersion time (Vorobyova *et al*., 2022). The higher concentration of 300 and 350 ppm displays the mild steel surface begins to relapse for both 1 day and 10 days of immersion. This phenomenon is due to the formation of a complex HMPE compound but possibly less adherent which can cause uneven coverage, then allowing the corrosion progress.

### 4.4.2 Scanning Electrons Microscope

SEM is essential for evaluating the effectiveness of HMPE as corrosion inhibitor on the mild steel surface, as it provides high-resolution images on the surface before and after treatment. SEM also can be used to observe the surface morphology and detect the signs of corrosion such as pitting, cracks, or roughness on the mild steel.

#### *4.4.2.1 Corrosion Inhibition in Acidic Medium*

Figure 4.22 (a), (b), and (c) depicts the morphology images of SEM for mild steel in 0.5 M HCl and in the presence of HMPE inhibitor. The image in Figure 4.19 (a) shows the mild steel immersed in 0.5 M HCl which appears highly corroded with significant roughness on the surface. The addition of lower concentration HMPE, the mild steel surface reveals less corroded area compared to the blank, suggesting partial protection by the inhibitor. The addition of higher concentration of HMPE shows the inhibitor provides significant protection against corrosion as the mild steel surface displays minimal corrosion and smooth.

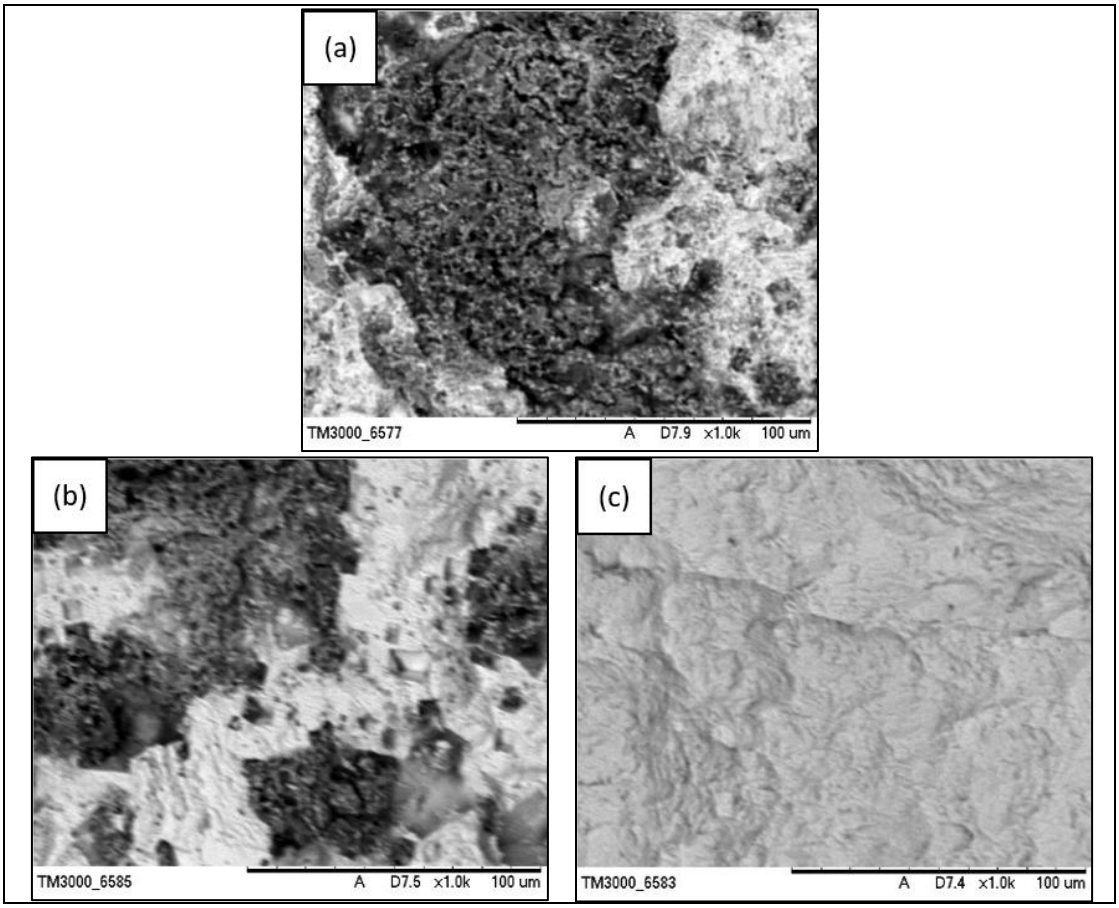

Figure 4.22 SEM Morphology Images of Mild Steel in a) 0.5 M HCl blank b) 0.5 M HCl + Low Concentration of HMPE c) 0.5 M HCl + High Concentration of HMPE

According to Deghani *et al*., (2020), the highly aggressive chloride ions can easily permeate the metal surface and corrode the steel for the uninhibited sample. Thus, this is aligned with the rough morphology displays for the blank sample and the presence of highly porous surface. The addition of HMPE inhibitor in lower concentration still shows the presence of porous surface although better than the blank. This situation is probably because the concentration of HMPE provided are insufficient to give protection to the mild steel surface. However, the addition of higher concentration of HMPE inhibitor depicts a uniform and smoother surface. Thus, the lesser damage of the mild steel surface may be attributed to the adsorption of HMPE inhibitors, which reduces the interaction between the corrosive ions and the mild steel surface, resulting in a lower dissolution rate (Alimohammadi *et al*., 2023). This result was in agreement with the %IE from the potentiodynamic polarization test (92%).

#### *4.4.2.2 Corrosion Inhibition in Near-Neutral Medium*

The morphological images for mild steel in the blank 0.6 M NaCl and in the presence of HMPE inhibitor are shown in Figure 4.23. The mild steel surface exposed in 0.6 M NaCl shows severe damaged. The image depicts localized corrosion pits and rough texture. The addition of HMPE inhibitor at a lower concentration exhibits the reduction in pitting spots to generally smaller than the mild steel in 0.6 M NaCl. This shows that the HMPE is effective in mitigating the corrosion. At a higher concentration of HMPE, the mild steel surface exhibits only minimal small pitting and becomes notably smoother compared to the both mild steel samples in lower concentration of HMPE and without HMPE.

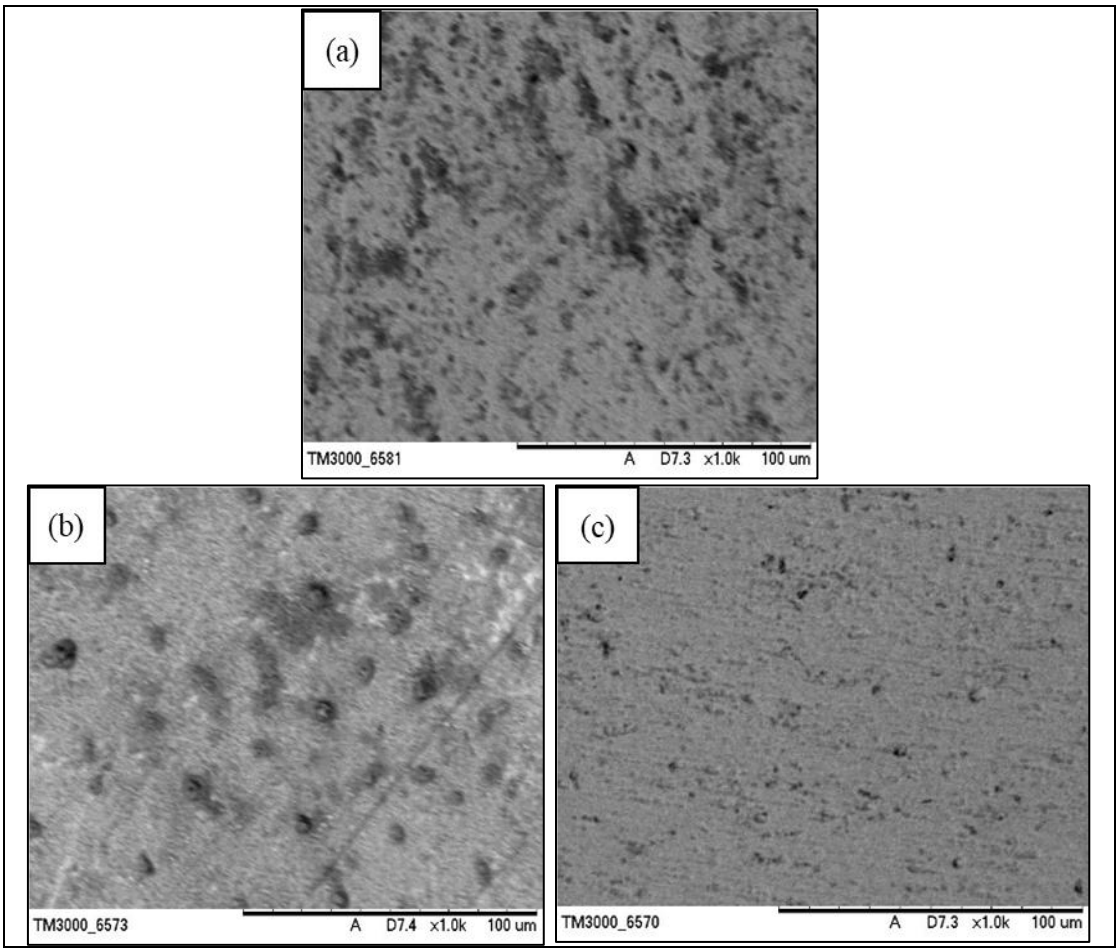


Figure 4.23 SEM Morphology Images of Mild Steel in a) 0.6 M NaCl Bank b) 0.6 M NaCl + Low Concentration of HMPE c) 0.6 M NaCl + High Concentration of HMPE

The severe pitting corrosion depicts on the mild steel surface in the 0.6 M NaCl of the absence HMPE potrayed the obvious degradation. Compared to the blank sample,

the addition of HMPE inhibitor at lower concentration displays better mild steel surface with smaller pits than blank with the %IE from weight loss and potentiodynamic polarization which is 73% and 90% respectively. This improvement is due to the presence of adsorbed HMPE inhibitor molecules, which verifies the formation of protective film (Shyamvarnan *et al*., 2021). Despite that, the mild steel surface is likely highly corroded if compared to the high concentration of HMPE inhibitor. This occurrence is caused by the mild steel dissolution process was significantly reduced in the presence of higher concentration of HMPE, which resulted in a smoother mild steel surface (Vorobyova & Skiba, 2019).

### 4.4.3 X-Ray Photoelectron Spectroscopy

The X-ray photoelectron spectroscopy (XPS) analysis was conducted to verify the adsorption of HMPE on the surface of mild steel and to evaluate the chemical characteristics of the interface between the inhibitors and the steel surface.

#### *4.4.3.1 Corrosion Inhibition in Acidic Medium*

Figure 4.24 shows the XPS result of mild steel in 0.5 M HCl in the presence of HMPE. Based on the graph, the peak obtained around 710 eV is associated with oxide products of $Fe_2O_3$ or $Fe_3O_4$. The highest and sharpest peak, around 529 eV, signifies the iron oxides ($Fe_2O_3$ or $Fe_3O_4$). The N 1s and C 1s peaks are attributed to the organic compounds in the HMPE that help in the inhibition process.

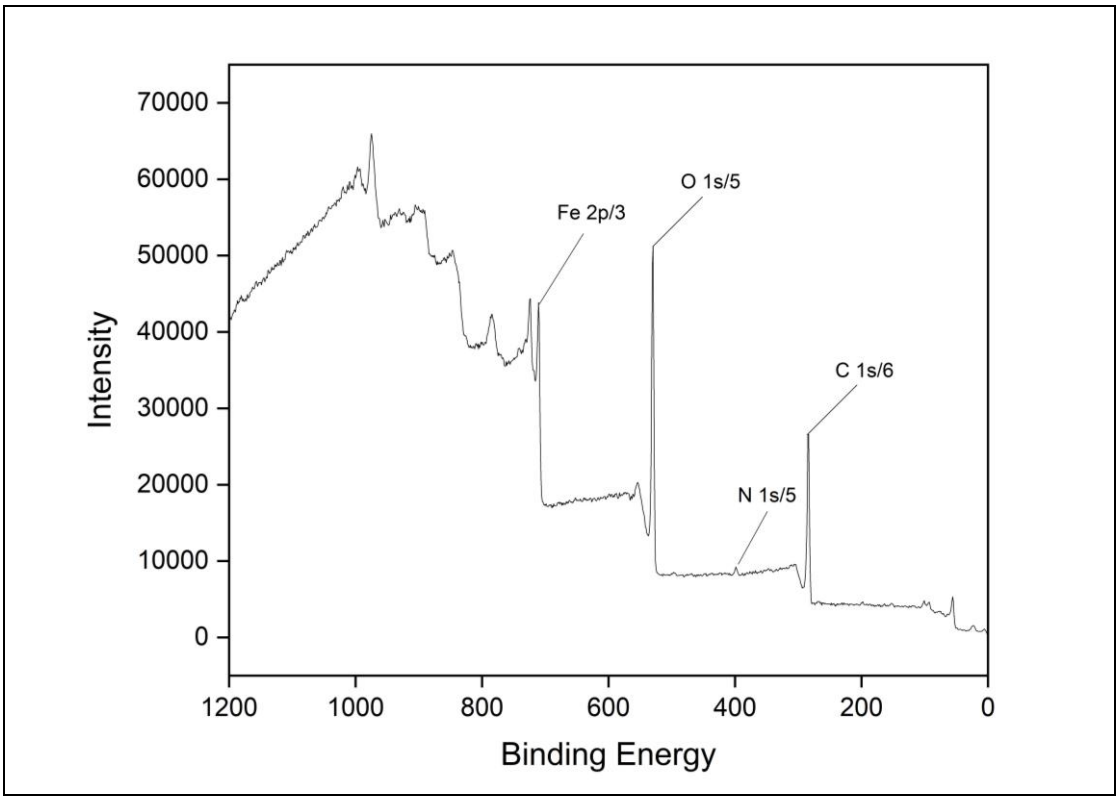


Figure 4.24 XPS Spectra of Mild Steel in 0.5 M HCl in the Presence of HMPE

According to the XPS profile details, binding energy, and chemical bonding presented in Figure 4.25 and Table 4.10, the C1s spectrum shows sp2 carbon (70.7%), with contributions from C-N/C-O (16.3%), carbonyl group (3.0%), and metal carbide

peak (10.0%). This shows that the organic layer from HMPE is mainly double-bonded or aromatic, also with heteroatom-containing carbons interacting on the surface. The O1s peaks indicate a dominant C=O/Fe-O-C (56.3%) and Fe-O components from $Fe^{2+}$ and $Fe^{3+}$, suggesting that the HMPE inhibitors are chemically bonded to the oxide through oxygen. In the N1s region, the distribution of nitrogen species reveals that pyrolic nitrogen (45.6%), followed by Fe-N bonding (12.0%), pyridinic nitrogen (9.1%), and a small proportion of quaternary nitrogen (7.2%). This shows that the lone pairs from n atoms directly coordinate with the Fe atom's surface by donating electron density to empty Fe orbitals, which forms the Fe-N bond. Lastly, the Fe2p envelope contains only $Fe^{2+/}Fe^{3+}$ signals, while metallic $Fe^{0}$ is not present. This observation confirms that the mild steel surface is fully covered by a mixed oxide or oxyhydroxide layer linked with the organic inhibitor film.

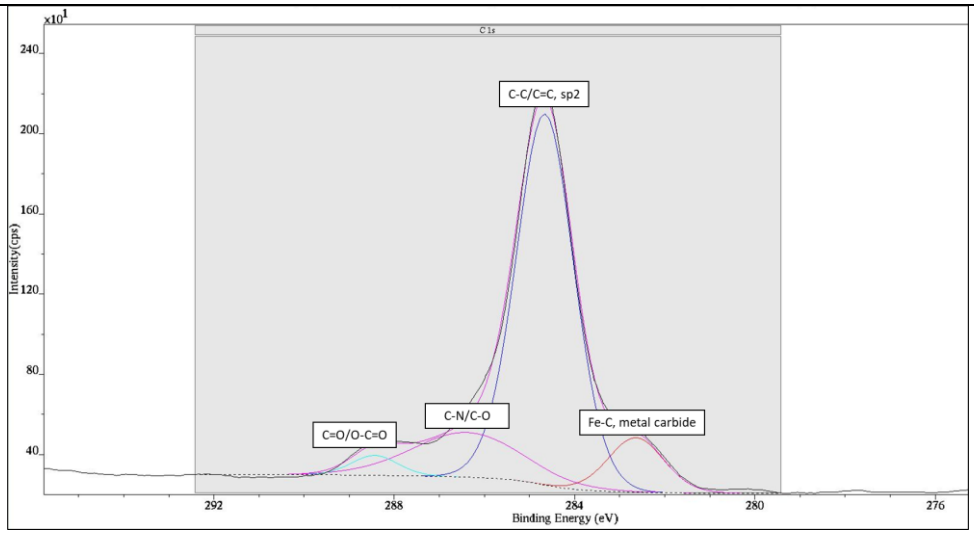


(a)

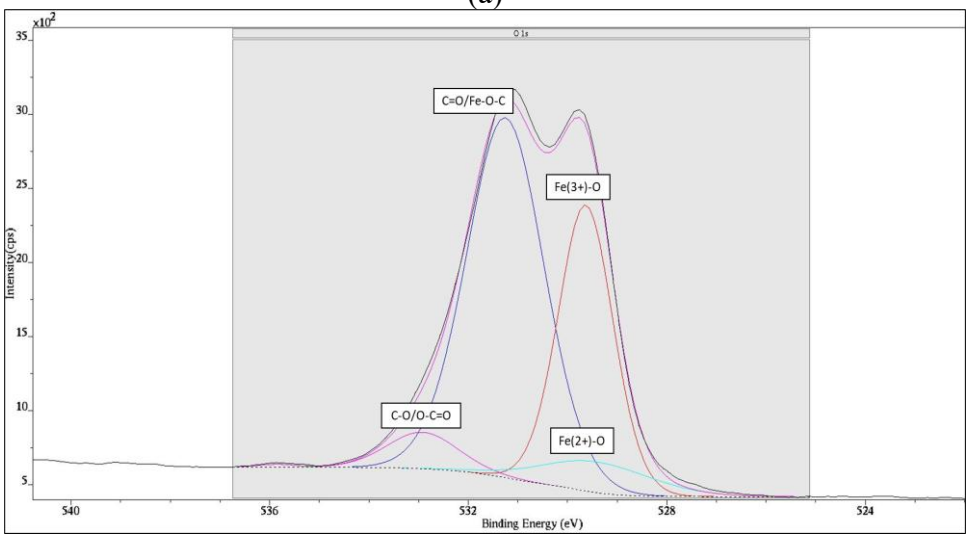


(b)

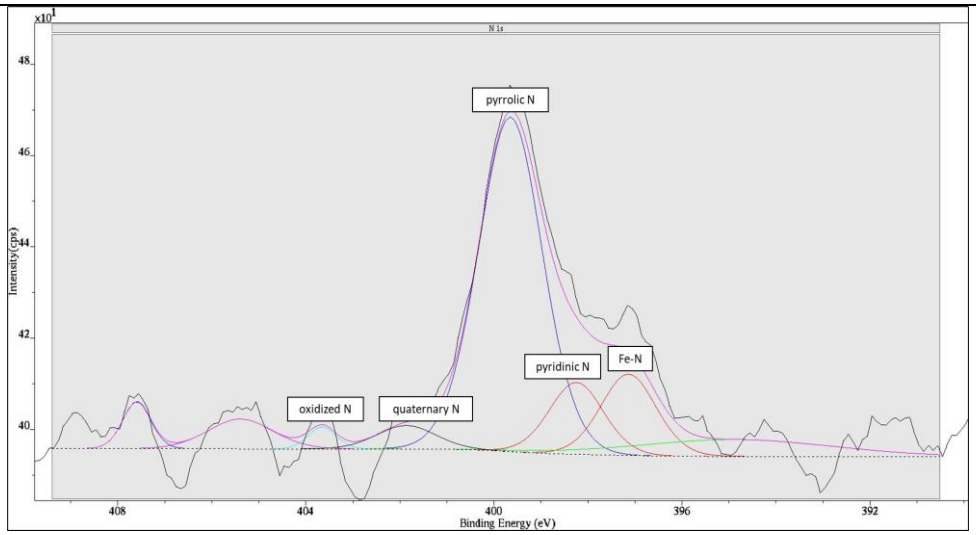


(c)

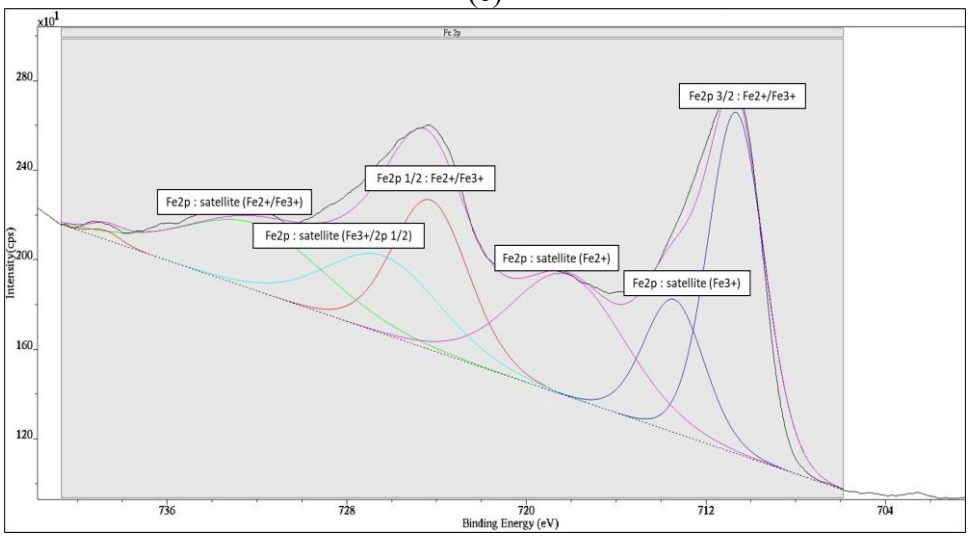


(d)

Figure 4.25 XPS Profile Details (a) C1s (b) O1s (c) N1s (d) Fe2p on Spectra of Mild Steel in 0.5 M HCl in the Presence of HMPE

Table 4.10
Binding Energy and Chemical Bonding of Mild Steel in 0.5 M HCl in the Presence of HMPE.

| Sample | Binding Energy (eV) | Chemical bonding |
|---|---|---|
| C 1s | 282.7 (10.0%) | Fe-C, metal carbide |
| | 284.7 (70.7%) | C-C, C=C, sp2 |
| | 286.4 (16.3%) | C-N / C-O |
| | 288. 4 (3.0%) | C=O / O-C=O |
| O 1s | 529.4 (6.7%) | Fe (2+)-O |
| | 529.6 (31.6%) | Fe (3+)-O |
| | 531.3 (56.3%) | C=O / Fe-O-C |
| | 532.9 (5.2%) | C-O / O-C=O |
| N 1s | 397.2 (12.0%) | Fe-N |
| | 398.3 (9.1%) | pyridinic N |
| | 399.6 (45.6%) | pyrrolic N |
| | 401.9 (7.2%) | quaternary N |
| | 403.7 (3.7%) | oxidized N |
| Fe 2p | 710.7 (26.9%) | Fe2p 3/2: $Fe^{2+}/Fe^{3+}$ |
| | 713.5 (12.5%) | Fe2p: satellite ($Fe^{3+}$) |
| | 718.1 (19.7%) | Fe2p: satellite ($Fe^{2+}$) |
| | 724.3 (16.0%) | Fe2p 1/2: $Fe^{2+}/Fe^{3+}$ |
| | 726.4 (12.5%) | Fe2p: satellite ($Fe^{3+}$, 2p1/2) |
| | 732.1 (13.2%) | Fe2p: satellite ($Fe^{2+}/Fe^{3+}$) |

#### *4.4.3.2 Corrosion Inhibition in Near-Neutral Medium*

Figure 4.26 depicts the XPS spectra of mild steel in 0.6 M NaCl in the presence of the HMPE inhibitor. According to the graph, the peak Fe 2p/1 and 2p/3 obtained around 710 and 721 eV represents the existence of iron salts and oxide products, including $Fe_2O_3$, $Fe_3O_4$, and FeOOH. The intense peak obtained at around 530 eV for O 1s indicates the presence of oxides or hydroxides. Therefore, it is confirmed that the HMPE inhibitor is absorbed into the oxides or hydroxides layer, possibly $Fe_2O_3$ or FeOOH, rather than directly onto the exposed surface of mild steel (Baux et al., 2018). The N 1s and C 1s peaks indicate the presence of organic compounds from the HMPE inhibitor that aid in the inhibition process. The intense peak of C 1s at around 289 eV confirm the presence of C = C, C – C, and also C = O in the HMPE inhibitor.

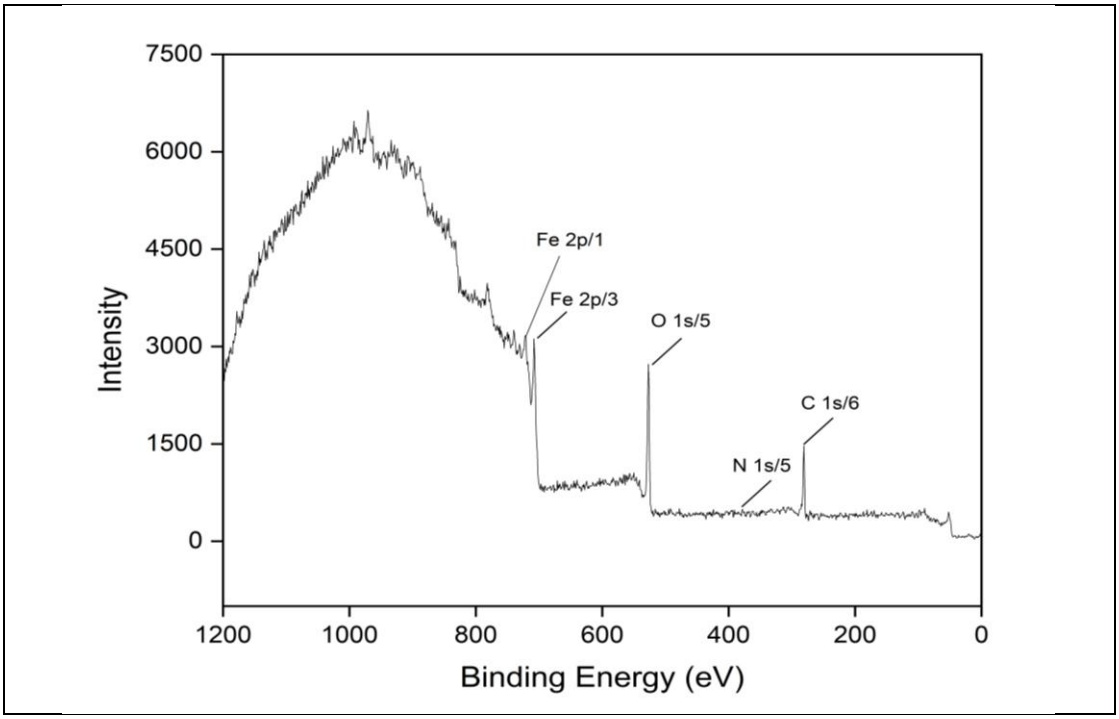


Figure 4.26 XPS Spectra of Mild Steel in 0.6 M NaCl in the Presence of HMPE

As a result, the XPS analysis reveals that the HMPE inhibitor adsorbed into the oxides or hydroxides layers first. The adsorption process helps maintain the oxide layer and prevent it from being easily disturbed. Thus, these adsorbed inhibitors create an additional protective layer over the oxides layer. This layer acts as a physical barrier, reducing the penetration of corrosive agents into the mild steel surface. Therefore, the combined effect of adsorption and the formation of a protective layer improves the

corrosion resistance of mild steel by effectively reducing both oxidation and corrosion (Pham Van *et al.*, 2024). This highlights the effectiveness of HMPE in forming a protective barrier against corrosion on the mild steel surface.

The detailed XPS profile, binding energy, and chemical bonding of mild steel in 0.6 M NaCl in the presence of HMPE have been depicted in Figure 4.26 and Table 4.11. The C1s spectrum in NaCl depicts $sp^2$ carbon (67.3%) along with $sp^3$ C–H component (14.8%) and stronger carbonyl or ester features (9.7%), suggesting a mixture of carbon types that includes aromatic rings, aliphatic group chains, and oxygenated groups. The O1s spectrum is mainly composed of oxygen from organic groups (C–O/O–C=O, 56.3%), followed by Fe–O–C/C=O (40.3%), with the pure Fe–O (11%), which is small indicating that the oxide layer on the steel surface is thin and the surface film is covered more by the organic film formed by the inhibitor. In the N1s region, Fe–N/Fe–N–C bonds are dominant (57.6%), with smaller contributions from pyridinic and quaternary nitrogen, indicating that the HMPE inhibitor mainly binds to the mild steel surface by forming strong chemical bonds between nitrogen and iron. Lastly, the Fe 2p spectrum reveals a combination of different iron oxidation states along with a signal for metallic iron ($Fe^0$) and iron carbide (Fe–C) around 706.5 eV. This indicates that the protective film formed on the steel surface is not uniform or fully developed, resulting to some areas of the underlying metal exposed to chloride ions.

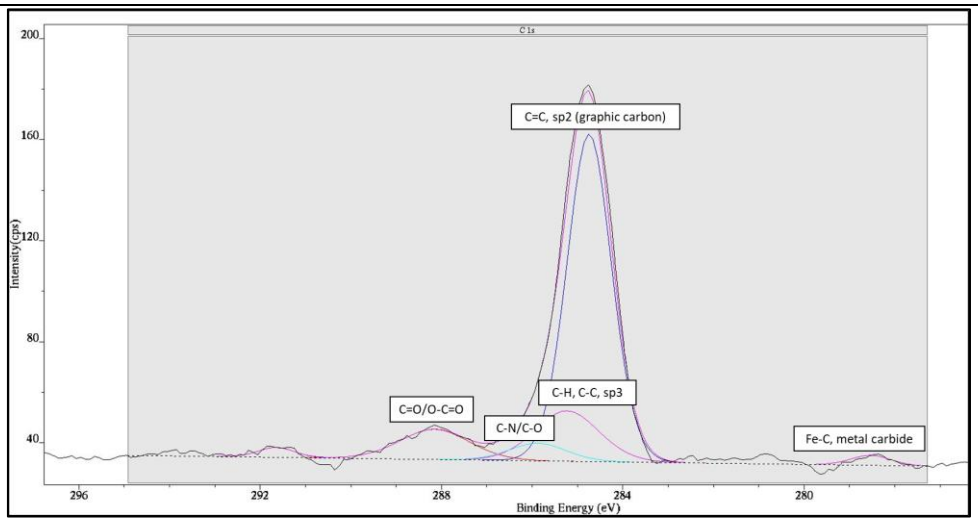
C 1s
C=C, sp2 (graphic carbon)
C-H, C-C, sp3
C=O/O-C=O
C-N/C-O
Fe-C, metal carbide
Intensity(cps)
Binding Energy (eV)

(a)

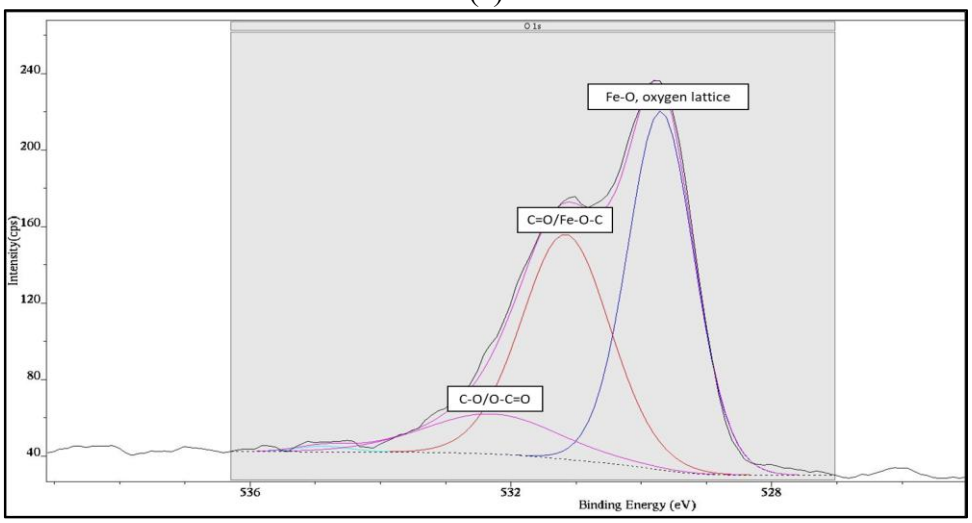
O 1s
Fe-O, oxygen lattice
C=O/Fe-O-C
C-O/O-C=O
Intensity(cps)
Binding Energy (eV)

(b)

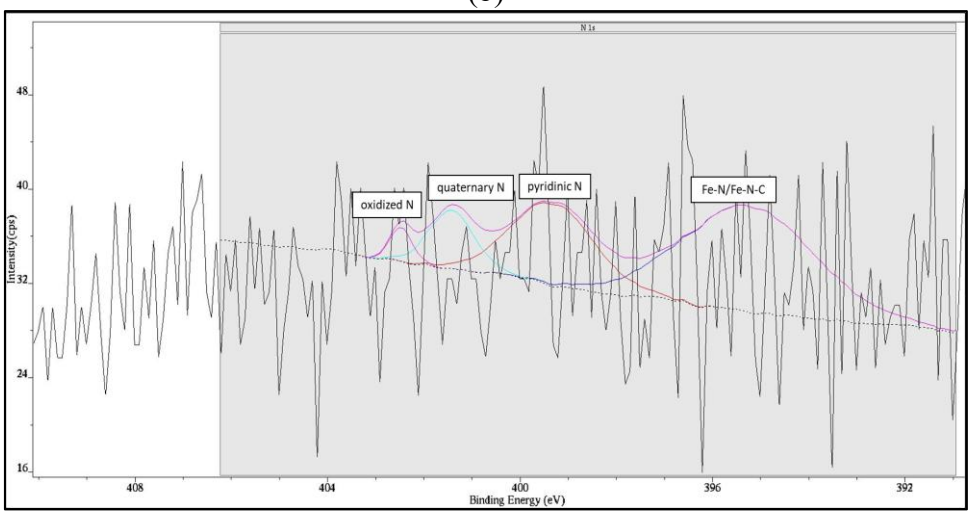
N 1s
oxidized N
quaternary N
pyridinic N
Fe-N/Fe-N-C
Intensity(cps)
Binding Energy (eV)

(c)

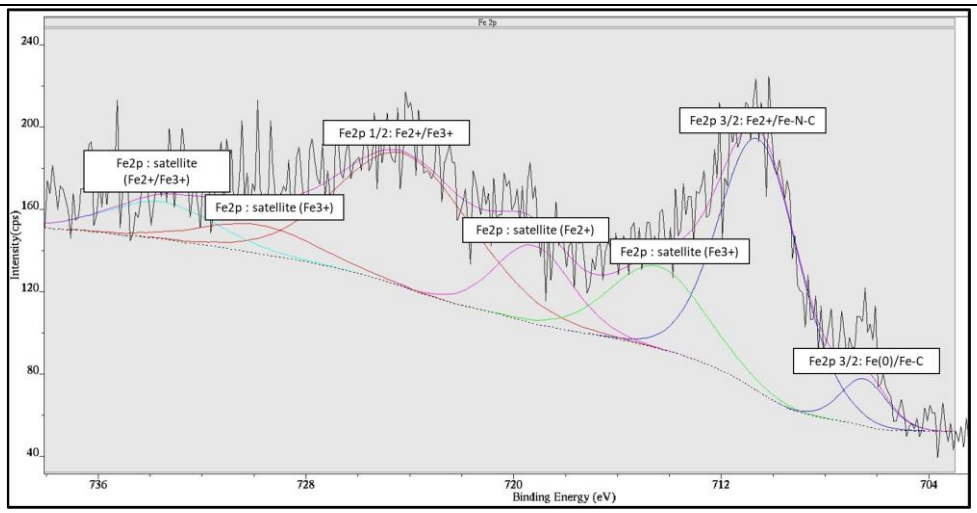


(d)

Figure 4.27 XPS Profile Details (a) C1s (b) O1s (c) N1s (d) Fe2p on Spectra of Mild Steel in 0.6 M NaCl in the Presence of HMPE

Table 4.11
Binding Energy and Chemical Bonding of Mild Steel in 0.6 M NaCl in the Presence of HMPE.

| Sample | Binding Energy (eV) | Chemical bonding |
|---|---|---|
| C 1s | 278.5 (1.8%) | Fe-C, metal carbide |
| | 284.8 (67.3%) | C=C, sp2 |
| | 285.2 (14.8%) | C-H, C-C, sp3 |
| | 285.9 (4.6%) | C-N / C-O |
| | 288. 1 (9.7%) | C=O / O-C=O |
| O 1s | 529.7 (11.0%) | Fe-O |
| | 531.2 (40.3%) | C=O / Fe-O-C |
| | 532.3 (56.3%) | C-O / O-C=O |
| N 1s | 395.3 (57.6%) | Fe-N / Fe-N-C |
| | 399.3 (28.3%) | pyridinic N |
| | 401.4 (11.0%) | quaternary N |
| | 402.5 (3.1%) | oxidized N |
| Fe 2p | 706.5 (3.6) | Fe2p 3/2: Fe(0) / Fe-C |
| | 710.6 (32.9.9%) | Fe2p 3/2: $Fe^{2+/}$Fe-N-C |
| | 714.4 (12.6%) | Fe2p: satellite ($Fe^{3+}$) |
| | 719.2 (9.6%) | Fe2p: satellite ($Fe^{2+}$) |
| | 724.2 (29.4%) | Fe2p 1/2: $Fe^{2+}$/$Fe^{3+}$ |

| | | |
|---|---|---|
| | 729.8 (5.4%) | Fe2p: satellite ($Fe^{3+}$) |
| | 733.5 (6.6%) | Fe2p: satellite ($Fe^{2+}/Fe^{3+}$) |

### 4.4.4 Summary of Surface Study

Table 4.12 summarized the result for both the surface study from OM, SEM, and XPS analysis in this chapter.

Table 4.12
Summary of Surface Study.

| Aspect Viewed | 0.5 M HCl | 0.6 M NaCl |
|---|---|---|
| Types of corrosion | General corrosion with pitting and roughness structure | Localized corrosion with some visible pitting |
| Effect on surface without HMPE inhibitor | Severe surface damage, rough with deep pits | Surface damage less than HCl, moderate pitting |
| Effect on surface with HMPE inhibitor | Significant improvement, smaller pits at lower concentration of inhibitor, smoother surface at higher concentration of inhibitor | Surface damage reduces, fewer pits and smoother surface at lower concentration of inhibitor, surface almost likely no damage at higher concentration of inhibitor |
| Mechanism of corrosion in blank solution | Hydrogen ions in the acid attack on the mild steel surface leading to metal dissolution and pitting | Chloride ions in NaCl attack on the mild steel surface leading to localized pitting corrosion |
| Mechanism of corrosion inhibition with HMPE inhibitor | HMPE adsorbs on the mild steel surface, forming a protective film that prevents active corrosion sites and reduces metal dissolution and pitting corrosion. | HMPE forms a mostly organic-rich protective layer with strong Fe–N coordination over a thin oxide layer, preventing chloride ions from penetrating the steel surface and significantly reducing localized pitting corrosion. |

## 4.5 Adsorption Isotherm Analysis

### 4.5.1 Langmuir Isotherm

#### *4.5.1.1 Corrosion Inhibition in Acidic Medium*

The Langmuir adsorption plots in Figure 4.28 show the adsorption behavior of HMPE at different temperatures in 0.5 M HCl. According to the graph, the plots are approximately linear for all temperatures, indicating the adsorption of HMPE on mild steel adheres well to the Langmuir adsorption isotherm model. The slopes of the lines also increases as the temperature rise, indicating that higher concentrations of HMPE are required to achieve the same surface coverage at higher temperature.

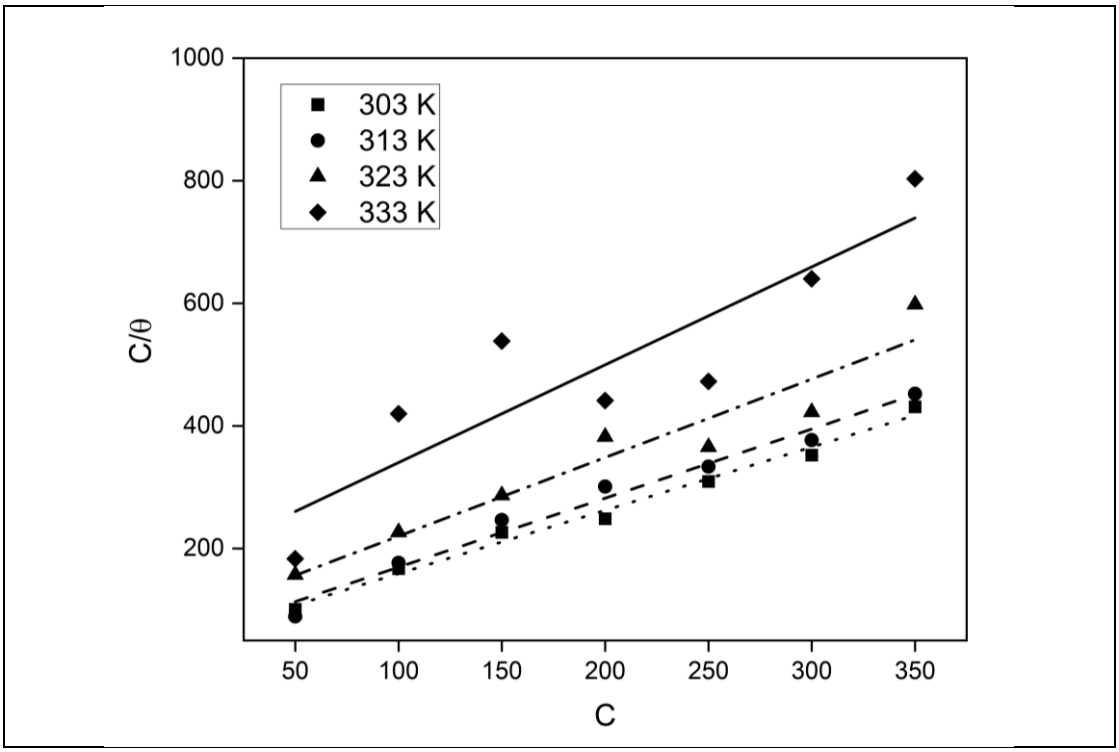


Figure 4.28 Langmuir Plots of HMPE on Mild Steel in 0.5 M HCl

Table 4.13 depicted the Langmuir adsorption parameters data obtained from the plots. The intercept values, which are inversely correlated to the adsorption equilibrium constant (Kads), reveal that larger intercepts at higher temperatures correspond to a drop in Kads. Thus, this suggest that the adsorption becomes less favourable as temperature increase (Ituen et al., 2017). The correlation coefficient (R2) values reveal the fit quality of the Langmuir adsorption model to the experimental data. The R2 values in the data

in the range of 0.7962 to 0.9876, suggest a strong correlation with the Langmuir model. The closer the $R^2$ values equal to 1 indicates a strong agreement between the experimental data and the Langmuir equation (Go *et al*., 2020, & Ayoola *et al*., 2022). However, an $R^2$ value below than 0.99 indicates slight deviation from an ideal adsorption behaviour due to the surface heterogeneity and mixed adsorption mechanisms but the model still reasonably describes the system.

Table 4.13
Langmuir Adsorption Parameters of HMPE on Mild Steel in 0.5 M HCl.

| **Temperature (K)** | **Slope** | **Intercept ($1/K_{ads}$)** | **$K_{ads}$** | **$R^2$** | **$\Delta G_{ads}$ (kJ $mol^{-1}$)** |
|---|---|---|---|---|---|
| 303 | 1.032 | 55.86 | 0.0179 | 0.9876 | -24.65 |
| 313 | 1.126 | 57.01 | 0.0175 | 0.9806 | -25.42 |
| 323 | 1.281 | 92.24 | 0.0108 | 0.9228 | -25.01 |
| 333 | 1.596 | 180.65 | 0.0055 | 0.7962 | -24.02 |

The Langmuir assumption was shown to be an excellent fit for the adsorption of HMPE at temperatures 303 and 313 K. According to the Langmuir postulation, it can be suggestes that the HMPE adhered to the surface of mild steel through monolayer adsorption. From the Langmuir assumption, it can be revealed that the HMPE molecules do not interact between each other, showing no attractive and repulsive forces between them, and the adsorption of the HMPE molecules and mild steel surface were homogeneous (Al-Ghouti & Da'ana, 2020, Go et al., 2020). The reason for this behaviour can be attributed to the HMPE molecule that possess various advantageous characteristic for significant adsorption. These include the existence of heteroatoms such as O and N, numerous phenol groups, and benzene rings.

Nevertheless, the rise in temperature to 333 K has prevented the $R^2$ values from approaching unity. This behaviour indicated that the HMPE molecules began to collide with each other and had a lower inclination to adhere to the surface. This occurrence can be related to the lower values of $K_{ads}$ which suggests weaker interaction between the HMPE molecules and mild steel surface. Therefore, the corrosion inhibition efficiency become lower even at highest concentration due to the minimal amount of adsorbate would be adsorbed at 333 K. Thus, this can be attributed to the fact that higher

temperatures might cause desorption or less stable adsorption of HMPE on the steel surface.

The Gibbs free energy ($\Delta G_{ads}$) can determined the characteristics of adsorption molecules on the metal surface. The negative $\Delta G_{ads}$ values at all temperatures indicate that the adsorption process of HMPE onto the mild steel surface is spontaneous. However, the decrease in the magnitude of $\Delta G_{ads}$ with increasing temperature suggests reduced spontaneity, which aligns with the decreasing of $K_{ads}$ values. The $\Delta G_{ads}$ value also can provide insights of the type of adsorption. According to Deghani & Ramezanzadeh (2022), if the $\Delta G_{ads}$ is more negative than -40 kJ $mol^{-1}$, the adsorption is considered chemisorption, which involved the chemical bond. In parallel, if the adsorption is less negative than -20 kJ $mol^{-1}$, the adsorption is considered physisorption, which involves weaker van der Waals forces or electrostatic interactions. However, if the $\Delta G_{ads}$ is between -20 kJ $mol^{-1}$ and -40 kJ $mol^{-1}$, it can be mixed-type of physisorption and chemisorption. In this case, the $\Delta G_{ads}$ is between -24.02 to -25.42 kJ $mol^{-1}$, which indicate that the adsorption of HMPE is mixed-type.

#### *4.5.1.2 Corrosion Inhibition in Near-Neutral Medium*

Figure 4.2 9 depicted the plots of C/θ vs C for the Langmuir adsorption of HMPE on mild steel in 0.6 M NaCl. The graph exhibit a nearly linear plots for the corrosion inhibition of HMPE in all temperatures, suggesting that the adsorption of HMPE on the mild steel follows the Langmuir adsorption isotherm model.

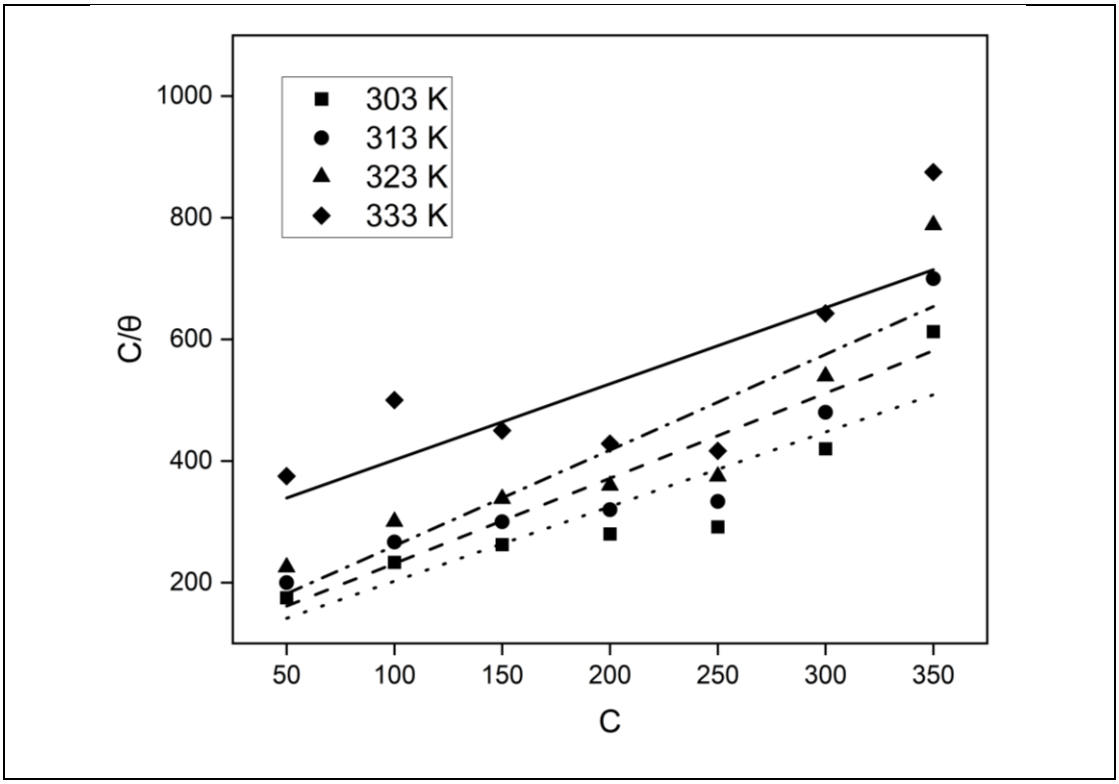


Figure 4.29 Langmuir Plots of HMPE on Mild Steel in 0.6 M NaCl

The data in Table 4.14 shows the parameters of Langmuir adsorption for HMPE on mild steel. The data reveals that the $K_{ads}$ values reduce as the temperature increases. The decrease in $K_{ads}$ with rising temperature indicates that HMPE inhibitor molecules' adsorption is less efficient at higher temperatures. This phenomenon is probably due to the kinetic energy of the inhibitor molecules increasing, overcoming the adsorption forces that bind the HMPE molecules on the mild steel surface, resulting in a decrease in adsorption affinity and, thus, a decrease in inhibition efficiency (Bouiti *et al*., 2022).

Table 4.14
Langmuir Adsorption Parameters of HMPE on Mild Steel in 0.6 M NaCl.

| Temperature (K) | Slope | Intercept ($1/K_{ads}$) | $K_{ads}$ | $R^2$ | $\Delta G_{ads}$ (kJ $mol^{-1}$) |
|---|---|---|---|---|---|
| 303 | 1.2253 | 79.9631 | 0.0125 | 0.8103 | -23.76 |
| 313 | 1.4302 | 91.4286 | 0.0109 | 0.8104 | -24.19 |
| 323 | 1.5748 | 103.0064 | 0.0097 | 0.8089 | -24.64 |
| 333 | 1.2514 | 276.5992 | 0.0036 | 0.5890 | -22.67 |

The $R^2$ values obtained are in the range of 0.8104 to 0.8089 for 303 to 323 K, implying a good fit for the Langmuir adsorption model and thus verifying the model's postulations, such as monolayer adsorption and homogeneous surface sites. However, as the temperature rises to 333 K, the $R^2$ value significantly drops to 0.5890. This value drop at higher temperatures illustrates that the Langmuir model's assumptions are less valid, most likely due to greater molecular mobility and potential interactions between adsorbed molecules.

The $\Delta G_{ads}$ values for the adsorption of HMPE on mild steel in 0.6 M NaCl are consistently negative at all temperatures studied, indicating that the adsorption of HMPE inhibitor on mild steel is a spontaneous process. The $\Delta G_{ads}$ values obtained are in the range of -22.67 to -24.64 kJ $mol^{-1}$, which implies the $\Delta G_{ads}$ is between -20 and -40 kJ $mol^{-1}$, suggesting a mixed-type adsorption mechanism. Mixed-type adsorption means the adsorption of HMPE inhibitor molecules on mild steel involves both physisorption and chemisorption. The mixed mode adsorption enables HMPE molecules to form a protective film on the mild steel surface using both weak Van der Waals forces and stronger chemical bonds, thus increasing its efficiency as a corrosion inhibitor.

### 4.5.2 Temkin Isotherm

#### *4.5.2.1 Corrosion Inhibition in Acidic Medium*

Figure 4.30 presents the Temkin adsorption plots of HMPE at different temperatures in 0.5 M HCl. According to the graph, the plots were scattered if compared to Langmuir adsorption isotherm. However, the line remain shows a linear trend which suggesting that Temkin isotherm is a reasonable model to explain the adsorption process of HMPE on mild steel. The linear lines on the graph also shows as temperature increase, the surface coverage also decline, implying the adsorption tendency also decrease. Thus, the HMPE is more effective at lower temperature.

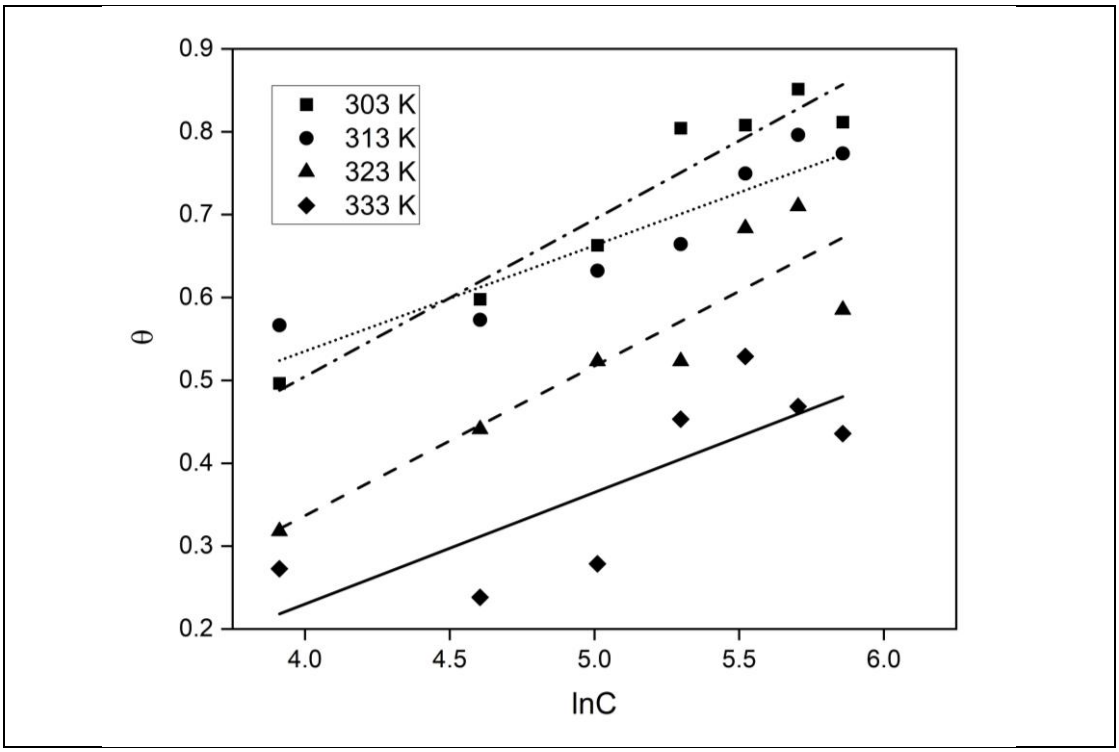


Figure 4.30 Temkin Plots of HMPE on Mild Steel in 0.5 M HCl

Table 4.15 displays the parameters of Temkin adsorptions of HMPE on mild steel in 0.5 M HCl. The table shows the slope and intercept values of the Temkin graphs that can be used to find the values of $K_{ads}$. The $K_{ads}$ values decrease as temperature increase, which suggest the HMPE inhibitor work better in lower temperature. The $R^2$ values for 303 K is the highest (0.9324), which present the model is better fit at lower temperature. However, the $R^2$ values of Langmuir isotherms is

much higher and closer to 1. Thus, Langmuir isotherm is better fit to describe the adsorption mechanism of HMPE inhibitor of mild steel in 0.5 M HCl.

Table 4.15
Temkin Adsorption Parameters of HMPE on Mild Steel in 0.5 M HCl.

| **Temperature (K)** | **Slope** | **Intercept ($1/K_{ads}$)** | **$K_{ads}$** | **$R^2$** | **$\Delta G_{ads}$ (kJ $mol^{-1}$)** |
|---|---|---|---|---|---|
| 303 | 0.1898 | -0.1365 | 0.4872 | 0.9324 | -8.3064 |
| 313 | 0.1277 | -0.0992 | 0.4599 | 0.8515 | -8.4304 |
| 323 | 0.1806 | -0.3856 | 0.1182 | 0.8250 | -5.0513 |
| 333 | 0.1347 | -0.3088 | 0.1010 | 0.6358 | -4.7723 |

#### *4.5.2.2 Corrosion Inhibition in Near-Neutral Medium*

Figure 4.31 presents the plots of surface coverage (θ) vs. ln C for the Temkin adsorption isotherms of HMPE on mild steel at different temperatures in 0.6 M NaCl. The graph shows that the surface coverage decreases as the temperature increases, implying that the HMPE inhibitor adsorbs better at lower temperatures. The linear lines obtained for each temperature indicate that the adsorption of HMPE does follow the Temkin adsorption isotherms. However, based on the graph alone, the Langmuir adsorption isotherm appears to be a better fit than the Temkin isotherm. Nevertheless, further discussion of the slopes, intercepts, and correlation coefficients is necessary to obtain the final conclusions about the fitting of the adsorption isotherms.

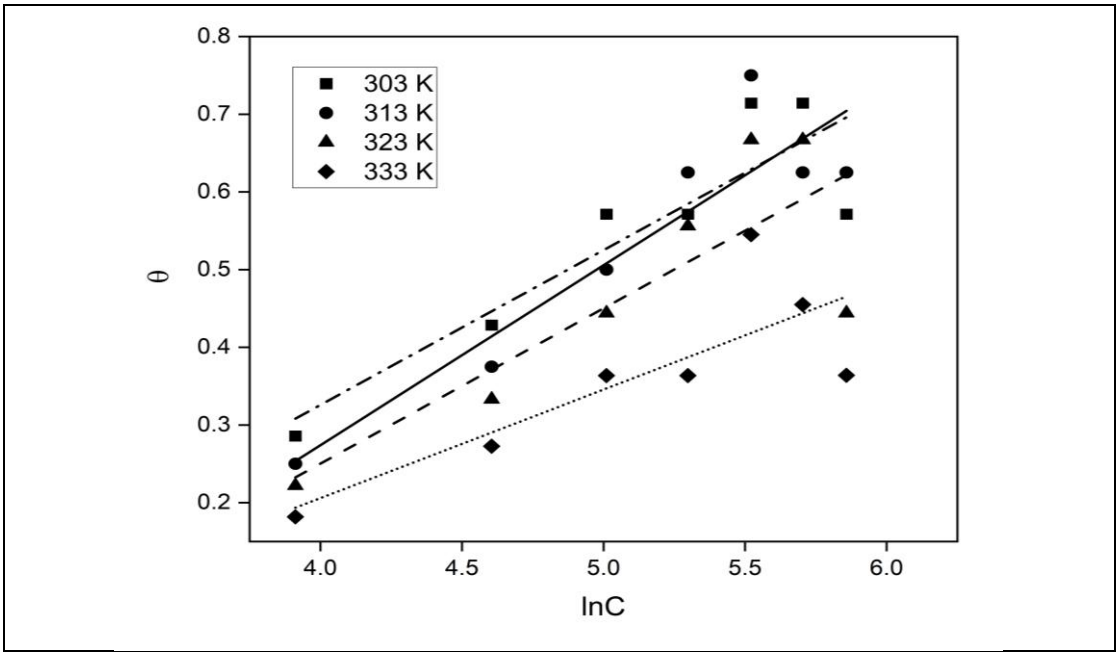


Figure 4.31 Temkin Plots of HMPE on Mild Steel in 0.6 M NaCl

Table 4.16 presents the values of slope, intercept, $K_{ads}$, $R^2$, and $\Delta G_{ads}$ of Temkin isotherms parameters for HMPE on mild steel in 0.6 M NaCl. The $K_{ads}$ values at a lower temperature of 303 K is the highest. Thus, it signifies greater adsorption, which indicates higher IE%. The $R^2$ values range between 0.6643 and 0.7986, suggesting a moderate fit for the Temkin isotherm model. The $\Delta G_{ads}$ values (-3.1218 to -4.1270 kJ $mol^{-1}$) are all negative, indicating a spontaneous adsorption process. However, the forces are weaker compared to the Langmuir model due to the more negative $\Delta G_{ads}$ values. Therefore, while both models suggest spontaneous adsorption, the Langmuir model indicates stronger adsorption interactions than the Temkin model.

Table 4.16
Temkin Adsorption Parameters of HMPE on Mild Steel in 0.6 M NaCl.

| **Temperature (K)** | **Slope** | **Intercept ($1/K_{ads}$)** | **$K_{ads}$** | **$R^2$** | **$\Delta G_{ads}$ (kJ $mol^{-1}$)** |
|---|---|---|---|---|---|
| 303 | 0.1993 | -0.4713 | 0.0940 | 0.7986 | -4.1614 |
| 313 | 0.2316 | -0.6525 | 0.0598 | 0.7159 | -3.1218 |
| 323 | 0.2000 | -0.5498 | 0.0640 | 0.6765 | -3.4038 |
| 333 | 0.1396 | -0.3526 | 0.0800 | 0.6643 | -4.1270 |

## 4.6 Mechanism of Corrosion Inhibition of Mild Steel by HMPE

### 4.6.1 Corrosion Inhibition in Acidic Medium

Figure 4.32 shows the mechanism of mild steel in an acidic medium where the metal surface undergoes an anodic reaction. Iron (Fe) from the mild steel loses electrons and dissolves into $Fe^{2+}$ in the solutions. Then, the electrons flow to the cathodic sites, where the hydrogen ions ($H^+$) from HCl gain electrons to form hydrogen gas ($H_2$). The chloride ions ($Cl^-$) from HCl accelerate the corrosion process by interacting with $Fe^{2+}$ ions to form $FeCl_2$, which dissolves away. Thus, preventing any oxide formation. Therefore, to inhibit the corrosion process, the corrosion inhibitor was added to prevent the dissolution of mild steel surfaces.

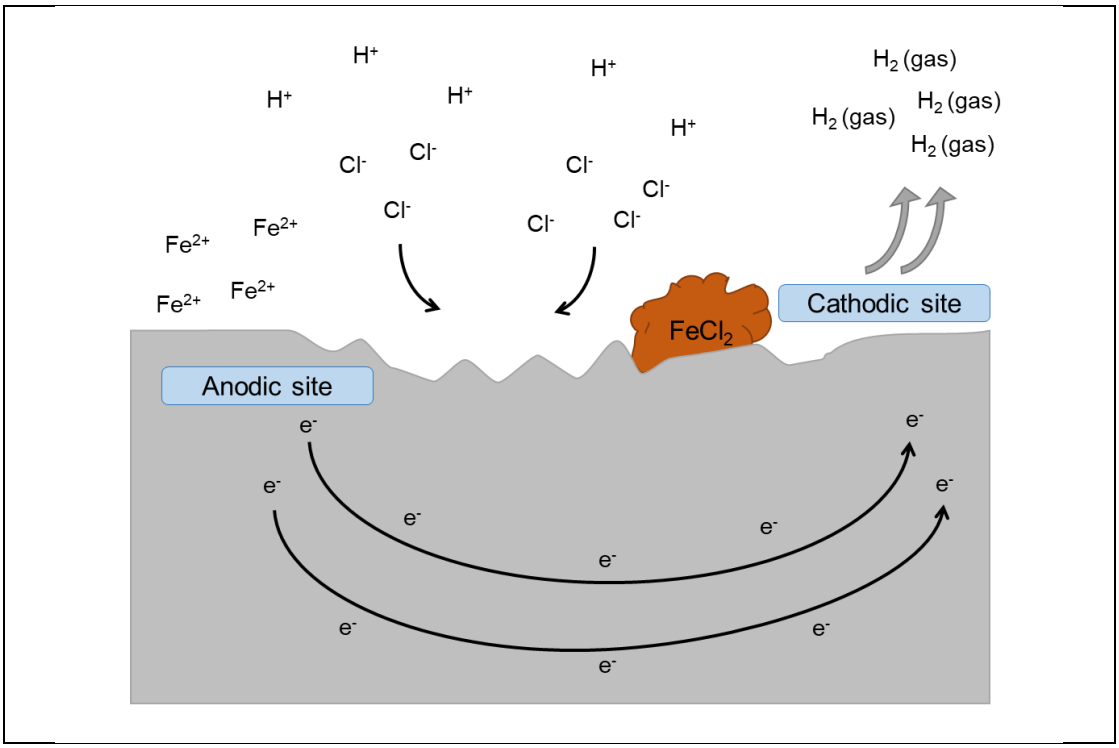


Figure 4.32 Mechanism of Mild Steel in Acidic Medium

Figure 4.33 shows the mechanism of mild steel corrosion inhibition in the presence of the HMPE inhibitor in an acidic medium. The addition of the HMPE inhibitor bioactive compound in the corrosive medium (HCl) interacts with the metal surface by adsorption process, forming a protective layer. The inhibition occurs through a combination of physisorption and chemisorption. First, the chloride ions from HCl adsorb onto the metal surface, making it negatively charged. Then, the protonated

HMPE molecule electrostatically attaches to the surface. This initial physisorption process forms a weak, reversible protective layer on the mild steel surface. Chemisorption occurs after increasing the concentration of the inhibitor, where the functional groups, such as hydroxyl and carbonyl, interact with Fe atoms, forming stable Fe-O and Fe-C bonds. This irreversible process aids in preventing Fe dissolution and blocking $Cl^-$ ions.

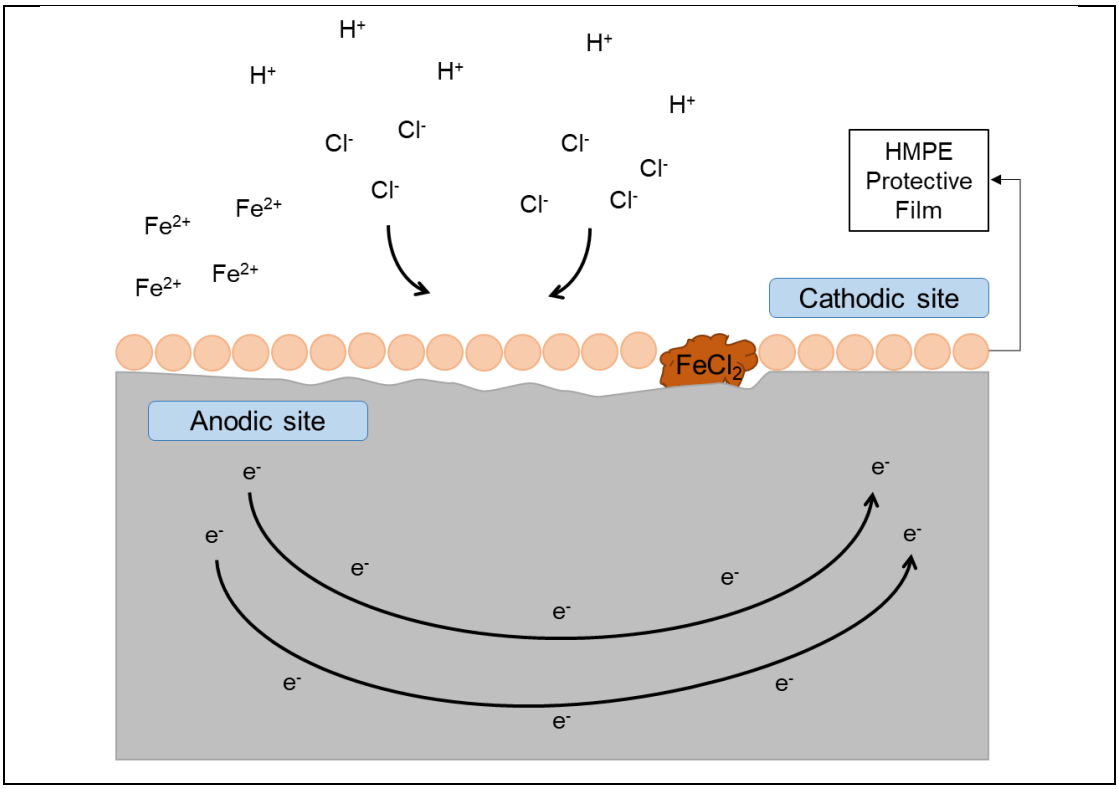


Figure 4.33 Mechanism of Mild Steel Corrosion Inhibition in Acidic Medium with the Presence of HMPE Inhibitor

This mechanism also has been reported by Pinto et al. (2022) that study on Tamarindus indica pericarp extract as a green corrosion inhibitor for mild steel in hydrochloric acid. In the study, the bioactive compounds in the extract at lower concentrations initially adsorb onto the metal surface through weak electrostatic interactions, forming a temporary protective layer. As the concentration increases, functional groups such as hydroxyl and carbonyl interact in stronger chemical interactions with iron atoms, likely forming a stable Fe–O and Fe–C bonds. This chemisorbed layer acts as a protective barrier, significantly reducing the metal dissolution. Additionally, the formation of this inhibitor film effectively blocks the approach of aggressive chloride ions ($Cl^-$) present in the acidic medium, as confirmed

by SEM-EDX analysis, which showed decreased $Cl^-$ presence on the inhibited steel surface.

### 4.6.2 Corrosion Inhibition in Near-Neutral Medium

Figure 4.33 displays the mechanism of mild steel corrosion in a near-neutral environment. In NaCl, the corrosion mechanism begins with the dissolution of iron, where Fe loses electrons to form $Fe^{2+}$. Then, the released electrons move to cathodic sites and reduce the dissolved oxygen in water, producing hydroxide ions ($OH^-$) which react with $Fe^{2+}$ to produce iron hydroxide ($Fe(OH)_2$). The iron hydroxide forms can further oxidize to produce $Fe_2O_3$ or $Fe_3O_4$. The presence of $Cl^-$ ions in NaCl quickens the corrosion by destabilizing the passive film on the mild steel surface and promoting localized attack, leading to pitting corrosion.

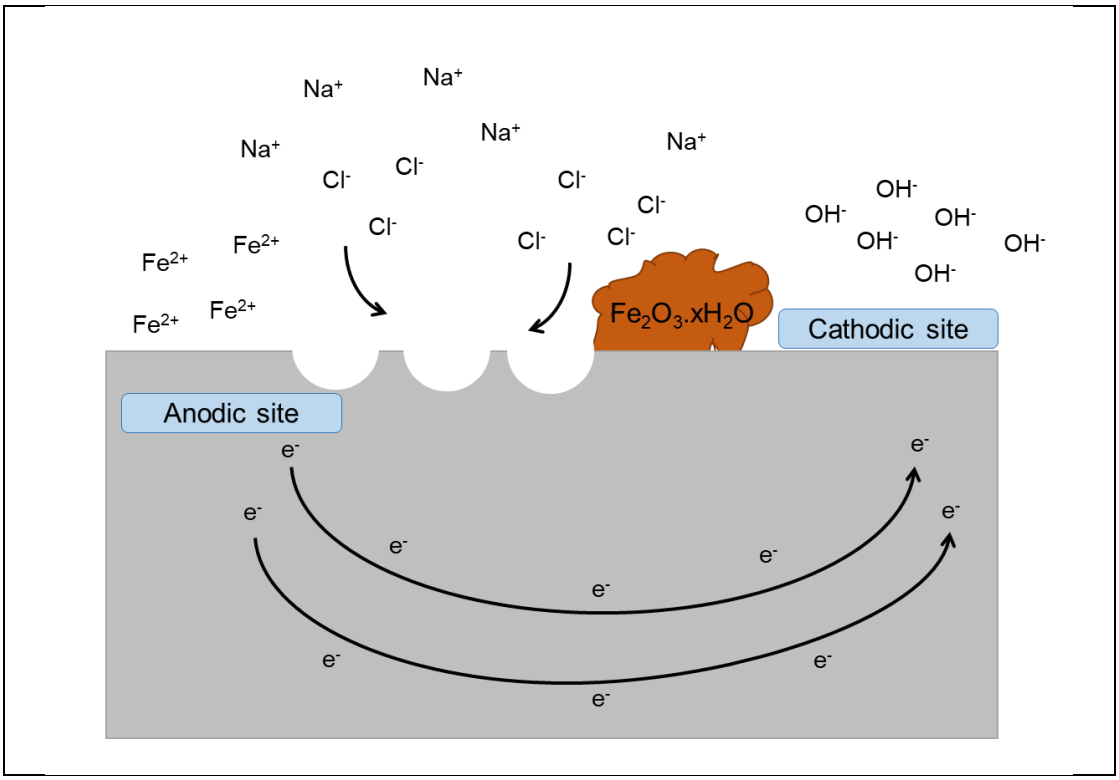


Figure 4.34 Mechanism of Mild Steel in Near-Neutral Medium

Figure 4.35 depicts schematic diagrams of the mild steel mechanism in the near-neutral medium in the presence of an HMPE inhibitor. When HMPE is introduced into the system, the inhibition occurs through a two-step adsorption process: physisorption followed by chemisorption. Initially, the protonated bioactive compounds in HMPE

inhibitor adsorb onto the steel surface via weak electrostatic interactions such as Van de Waals forces, forming a temporary barrier. As concentration of HMPE increases, chemisorption happened, where the extract's functional groups (hydroxyl, carbonyl, and aromatic rings) form strong Fe–O–C bonds with Fe atoms, stabilizing the protective layer. The potentiodynamic polarization results confirm HMPE as a mixed-type inhibitor, suppressing both anodic and cathodic reactions.

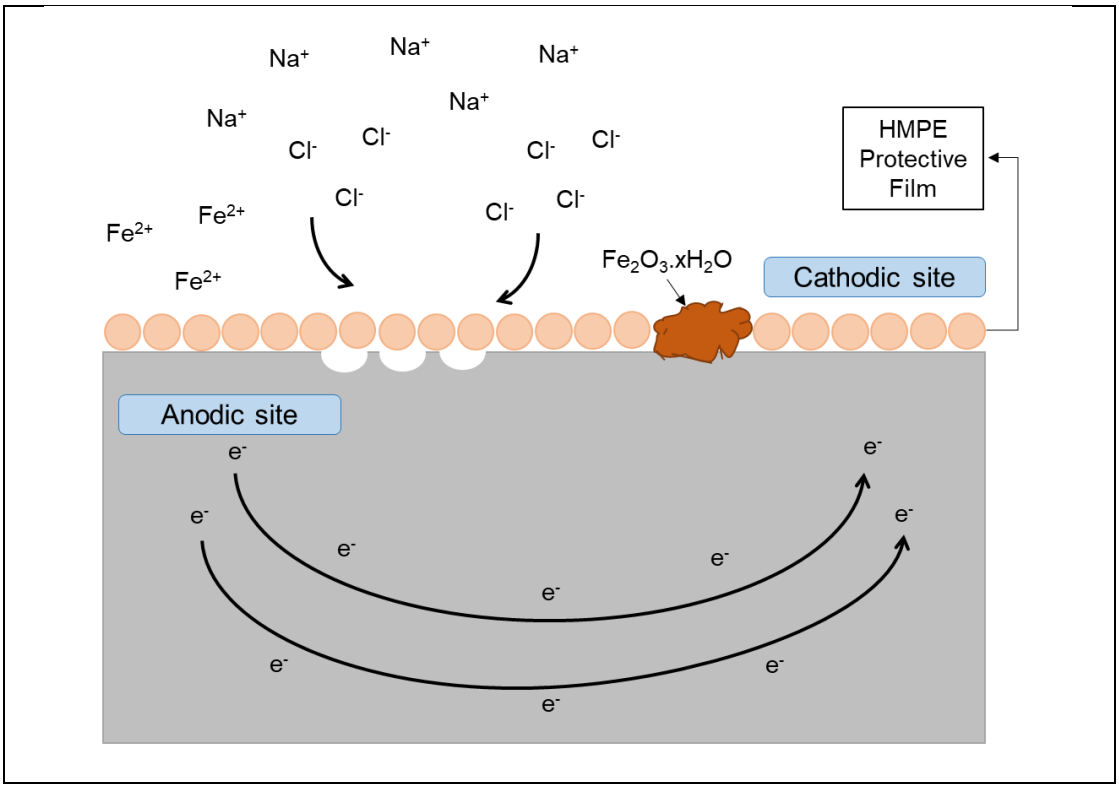


Figure 4.35 Mechanism of Mild Steel in Near-Neutral Medium in the Presence of HMPE Inhibitor

A similar two-step adsorption mechanism also has been found using other plant-based inhibitors. A study by Vorobyova *et al.* (2021) using peach pomace extract as a corrosion inhibitor has reported an initial physisorption stage, where the bioactive molecules such as flavonoids and phenolic acids adsorb weakly onto the steel surface through electrostatic interactions, forming a preliminary barrier. Then, after increased exposure over time, the compounds undergo oxidation, leading to chemisorption, in which more stable polymerized products form strong bonds with the steel surface, increasing the protection. Similarly, another study by Vorobyova *et al.* (2023) reported that agri-food waste extracts also inhibit corrosion through a dual mechanism involving initial physisorption followed by chemisorption, where functional groups like hydroxyl,

carbonyl, and aromatic rings interact chemically with Fe atoms. Both studies confirmed the formation of a protective layer and identified the inhibitors as mixed-type, suppressing both anodic and cathodic reactions parallel to the inhibition behaviour of the HMPE inhibitors.

# CHAPTER 5
# CONCLUSION

## 5.1 Conclusion

As a conclusion, the three objectives of this study were achieved. The first objective is to identify and characterize the chemical compounds and functional groups of HMPE. The Harumanis mango peel has been extracted using 60% ethanol. A lot of functional groups such as C-H, C=O, aromatic C=C, COOH, and C-N have been found in HMPE. Chemical compounds such as gallic acid and mangiferin have also been detected. These functional groups and chemical compounds found in HMPE highlight its potential as a green organic corrosion inhibitor.

The second objective is to evaluate the inhibition efficiency of HMPE as a corrosion inhibitor for mild steel in acidic and near-neutral media. In this study, three corrosion tests (weight loss, potentiodynamic polarization test, and electrochemical impedance spectroscopy tests) have been done to evaluate the IE% of HMPE as a corrosion inhibitor in acidic and near-neutral media. The IE% increased as the HMPE concentration increased for the weight loss test. The highest IE% obtained was 88% at 350 ppm for HCl. In NaCl, the IE% decreased after 250 ppm, implying that 250 ppm is the optimum concentration. For the potentiodynamic polarization test, the HMPE inhibitor, both in 0.5 M HCl and 0.6 M NaCl, was found to be a mixed-type inhibitor, with the highest IE% being 92% and 84%, respectively. In the EIS test, the charge transfers resistance (Rct) increases after the addition of an HMPE inhibitor, implying an increase in efficiency. The highest IE% for 0.5 M HCl and 0.6 M NaCl were 76% and 90%, respectively.

The last objective is to investigate the adsorption behaviour and surface interactions of the HMPE on mild steel in order to determine the mechanism of corrosion inhibitors. The HMPE inhibitor follows the Langmuir adsorption isotherm model for both 0.5 M HCl and 0.6 M NaCl. The adsorption of the HMPE inhibitor for 0.5 M HCl and 0.6 M NaCl on the mild steel surface is also mixed-type, meaning it involves both physisorption and chemisorption, where the HMPE molecules form a protective layer on the mild steel surface using both weak Van der Waals forces and strong chemical bonds.

## 5.2 Recommendation

For further study of HMPE as a corrosion inhibitor, different types of metals other than mild steel, such as copper, aluminium, alloys, and stainless steel, can be tested to broaden its potential applications. The HMPE performance can also be evaluated in different environments, including alkaline conditions and seawater, to reflect real industrial situations. To improve the quality of HMPE, green extraction methods such as water–ethanol, ultrasound, or microwave-assisted techniques can be used. Also, important active compounds such as mangiferin and gallic acid can be isolated and studied to understand their role in corrosion inhibition. In addition, more parameters, such as the effects of pH, temperature, and long-term exposure, should be investigated to optimize the HMPE's formulation. Computational chemistry methods such as Density Functional Theory (DFT) and molecular dynamics simulations can be used to explain the adsorption behaviour, electronic properties, and molecular-level interactions of HMPE on metal surfaces in corrosive environments. Additional analysis such as Raman and Atomic Force Microscopy (AFM) can be added to study more about the HMPE behaviour as corrosion inhibitor. Lastly, the combination of HMPE with surfactants or other eco-friendly co-inhibitors should be explored for possible synergistic effects. At the same time, long-term durability tests, cost–benefit as well as scalability studies should be done to confirm its practical, economical, and sustainable use in real industrial applications.

# REFERENCES


Abdelshafeek, K. A., Abdallah, W. E., Elsayed, W. M., Eladawy, H. A., & El-Shamy, A. M. (2022). Vicia faba peel extracts bearing fatty acids moieties as a cost-effective and green corrosion inhibitor for mild steel in marine water: computational and electrochemical studies. *Scientific Reports, 12(1).* https://doi.org/10.1038/s41598-022-24793-3

Al-Baghdadi, S., Gaaz, T. S., Al-Adili, A., Al-Amiery, A. A., & Takriff, M. S. (2021). Experimental studies on corrosion inhibition performance of acetylthiophene thiosemicarbazone for mild steel in HCl complemented with DFT investigation. *International Journal of Low-Carbon Technologies, 16(1)*, 181-188.

Al-Ghouti, M. A., & Da'ana, D. A. (2020). Guidelines for the use and interpretation of adsorption isotherm models: A review. *Journal of Hazardous Materials*, 393, 122383. https://doi.org/10.1016/j.jhazmat.2020.122383

Ali, M. R., Yong, M. J., Gyawali, R., Mosaddik, A., Ryu, Y. C., & Cho, S. K. (2012). Mango (Mangifera indica L.) peel extracts inhibit proliferation of HeLa human cervical carcinoma cell via induction of apoptosis. *Journal of the Korean Society for Applied Biological Chemistry*, *55*(3), 397–405. https://doi.org/10.1007/s13765-012-1024-x

Alimohammadi, M., Ghaderi, M., Ramazani SA, A., & Mahdavian, M. (2023). Falcaria vulgaris leaves extract as an eco-friendly corrosion inhibitor for mild steel in hydrochloric acid media. *Scientific Reports*, 13(1), 3737.

Aljamali, N. M., Mohsin, N. M. B., & AliH, N. (2019). Review on corrosion and rust inhibition of machines in chemical engineering field. *International Journal of Thermodynamics and Chemical Kinetics, 5(1)*, 1-9.

Aljibori, H. S., Alamiery, A., Gaaz, T. S., & Al-Azzawi, W. K. (2024). Exploring corrosion protection for mild steel in HCl solution: An experimental and theoretical analysis of an antipyrine derivative as an anticorrosion agent. *Carbon Neutralization, 3(1)*, 74-93.

Alonso, J. M., Fabre, B., Trilling, A. K., Scheres, L., Franssen, M. C., & Zuilhof, H. (2015). Covalent attachment of 1-alkenes to oxidized platinum surfaces. Langmuir, *31(9)*, 2714-2721.

Alrefaee, S. H., Rhee, K. Y., Verma, C., Quraishi, M., & Ebenso, E. E. (2021). Challenges and advantages of using plant extract as inhibitors in modern

corrosion inhibition systems: Recent advancements. *Journal of Molecular Liquids*, *321*, 114666. https://doi.org/10.1016/j.molliq.2020.114666

Alvarez, L. X., Troconis de Rincón, O., Escribano, J., & Rincon Troconis, B. C. (2023). Organic compounds as corrosion inhibitors for reinforced concrete: a review. *Corrosion Reviews*, 0. https://doi.org/10.1515/corrrev-2023-001

Amoko, J. S., Akinyele, O. F., Oyeneyin, O. E., & Olayanju, D. (2021). Corrosion Inhibitive Potentials Of (E)-5-((4-Benzoylphenyl)Diazenyl)-2-Hydroxybenzoic Acid On Mild Steel Surface In 0.5 M HCl- Experimental And DFT Calculations. *Journal of the Turkish Chemical Society, Section A: Chemistry, 8(1)*, 343–362. https://doi.org/10.18596/JOTCSA.821488

ASTM G 31 – 72, Standard Practice for Laboratory Immersion Corrosion Testing of Metals, vol 72(2012).

ASTM G 59 – 97, Standard Test Method for Conducting Potentiodynamic Polarization Resistance Measurements, (2020)

Bala, A., MsheliA, R. B., Muhammad, J. Y., & Adam, M. (2022). Production and determination of properties of ethanol from mango and orange peels. *International Journal of Energy Studies, 7(2)*, 83–97. https://doi.org/10.58559/ijes.1147674

Berradja, A. (2019). Electrochemical Techniques for Corrosion and Tribocorrosion Monitoring: Fundamentals of Electrolytic Corrosion. *Corrosion Inhibitors*. https://doi.org/10.5772/intechopen.85392

Bouiti, K., aldeen Al-sharabi, H., Bensemlali, M., Bouhlal, F., Abidi, B., Labjar, N., & El Hajjaji, S. (2022). Effect of temperature on corrosion inhibition by ethanolic extract of Eriobotrya Japonica seeds in chloride medium 1M. *The European Physical Journal Applied Physics,* 97, 67.

Božović, S., Gvozdanović, T., Kraš, A., Grudić, V., Kurajica, S., & Martinez, S. (2020). Rust layer growth and modification by a tannin-based mixture for lowering steel corrosion rates in neutral saline solution. *Corrosion engineering, science and technology, 55(5)*, 372-380.

Brycki, B. E., Kowalczyk, I. H., Szulc, A., Kaczerewska, O., & Pakiet, M. (2018). Organic Corrosion Inhibitors. *Corrosion Inhibitors, Principles and Recent Applications*. https://doi.org/10.5772/intechopen.72943

Chaiwarit, T., Kantrong, N., Sommano, S. R., Rachtanapun, P., Junmahasathien, T., Kumpugdee-Vollrath, M., & Jantrawut, P. (2021). Extraction of tropical fruit

peels and development of HPMC film containing the extracts as an active antibacterial packaging material. *Molecules, 26(8)*, 2265. https://doi.org/10.3390/molecules26082265

Chigondo, M., & Chigondo, F. (2016). Recent Natural Corrosion Inhibitors for Mild Steel: An Overview. *Journal of Chemistry*, *2016*, 1–7. https://doi.org/10.1155/2016/6208937

Danaee, I., Rameshkumar, S., RashvandAvei, M., & Vijayan, M. (2020). Electrochemical and Quantum Chemical Studies on Corrosion Inhibition Performance of 2,2'-(2-Hydroxyethylimino)bis[N-(alphaalpha-dimethylphenethyl)-N-methylacetamide] on Mild Steel Corrosion in 1M HCl Solution. *Materials Research-ibero-american Journal of Materials*, 23(2). https://doi.org/10.1590/1980-5373-mr-2018-0610

Daniel, S. (2023). Characterization of carbon dots. *Elsevier eBooks,* 43–58. https://doi.org/10.1016/b978-0-323-98350-1.00015-3

Dariva, C. G., & Galio, A. F. (2014). Corrosion Inhibitors – Principles, Mechanisms and Applications. *In InTech eBooks*. https://doi.org/10.5772/57255

Dehghani, A., & Ramezanzadeh, B. (2022). Rosemary extract inhibitive behavior against mild steel corrosion in tempered 1 M HCl media. *Industrial Crops and Products, 193*, 116183. https://doi.org/10.1016/j.indcrop.2022.116183

Dehghani, A., Bahlakeh, G., Ramezanzadeh, B., & Ramezanzadeh, M. (2020). Potential role of a novel green eco-friendly inhibitor in corrosion inhibition of mild steel in HCl solution: Detailed macro/micro-scale experimental and computational explorations. *Construction and Building Materials*, *245*, 118464. https://doi.org/10.1016/j.conbuildmat.2020.118464

Devikala, S., Kamaraj, P., Arthanareeswari, M., & Patel, M. B. (2019). Green corrosion inhibition of mild steel by aqueous Allium sativum extract in 3.5% NaCl. *Materials Today: Proceedings*, *14*, 580–589. https://doi.org/10.1016/j.matpr.2019.04.182

Di Gianfrancesco, A. (2017). Technologies for chemical analyses, microstructural and inspection investigations. *Materials for Ultra-Supercritical and Advanced Ultra-Supercritical Power Plants*, 197–245. https://doi.org/10.1016/b978-0-08-100552-1.00008-7

Dryden, M. D. M., & Wheeler, A. R. (2015). DStat: A Versatile, Open-Source Potentiostat for Electroanalysis and Integration. *PLOS ONE*, *10*(10), e0140349. https://doi.org/10.1371/journal.pone.0140349

Engelhard, M. H., Droubay, T. C., & Du, Y. (2017). X-Ray Photoelectron Spectroscopy Applications. *Elsevier eBooks*, 716–724. https://doi.org/10.1016/b978-0-12-409547-2.12102-x

Evangeliene, S. S., Smart, D. R., Saravanan, V., & Ramachandran, M. (2023). An overview High performance of stress corrosion cracking behavior for aeronautic applications. *Journal on Materials and Its Characterization, 2(2)*, 9–19. https://doi.org/10.46632/jmc/2/2/2

Faiz, M., Zahari, A., Awang, K., & Hussin, H. (2020). Corrosion inhibition on mild steel in 1 M HCl solution by*Cryptocarya nigra*extracts and three of its constituents (alkaloids). *RSC Advances*, *10*(11), 6547–6562. https://doi.org/10.1039/c9ra05654h

Fidrusli, A., Suryanto, & Mahmood, M. (2018). Ginger extract as green corrosion inhibitor of mild steel in hydrochloric acid solution. *IOP Conference Series: Materials Science and Engineering*, *290*, 012087. https://doi.org/10.1088/1757-899x/290/1/012087

Garcia-Mendoza, M. P., Paula, J. T., Paviani, L. C., Cabral, F. A., & Martinez-Correa, H. A. (2015). Extracts from mango peel by-product obtained by supercritical CO2 and pressurized solvent processes. *LWT, 62(1),* 131–137. https://doi.org/10.1016/j.lwt.2015.01.026

Garg, R., Garg, R., & Eddy, N. (2024). The Role of Corrosion Inhibitors. Advances in Chemical and Materials Engineering Book Series, 100–129. https://doi.org/10.4018/979-8-3693-3088-3.ch005

Gayakwad, N., Patil, V., & Rao, B. M. (2022). The effect of Rhoeo discolor plant leaves extract on mild steel of corrosion inhibition in acid media. *Materials Today: Proceedings*, *49*, 536–541. https://doi.org/10.1016/j.matpr.2021.03.671

Gerard, O., Ramesh, K., & Subramaniam, R. (2021). A review on plant extracts as natural additives in coating applications. *Progress in Organic Coatings, 151*, 106091. https://doi.org/10.1016/j.porgcoat.2020.106091

Haldhar, R., Prasad, D., Mandal, N., Benhiba, F., Bahadur, I., & Dagdag, O. (2021). Anticorrosive properties of a green and sustainable inhibitor from leaves extract of Cannabis sativa plant: Experimental and theoretical approach. *Colloids and*

*Surfaces A: Physicochemical and Engineering Aspects*, *614*, 126211. https://doi.org/10.1016/j.colsurfa.2021.126211

Harsimran, S., Santosh, K., & Rakesh, K. (2021). Overview of Corrosion and its Control: A Critical Review. *Proceedings on Engineering Sciences*, *3*(1), 13–24. https://doi.org/10.24874/pes03.01.002

Hernández, H. H., Reynoso, A. M. R., González, J. C. T., Morán, C. O. G., Hernández, J. G. M., Ruiz, A. M., ... & Cruz, R. O. (2020). Electrochemical impedance spectroscopy (EIS): A review study of basic aspects of the corrosion mechanism applied to steels. *Electrochemical Impedance Spectroscopy*, 137-144.

Hossain, N., Asaduzzaman Chowdhury, M., & Kchaou, M. (2020). An overview of green corrosion inhibitors for sustainable and environment friendly industrial development. *Journal of Adhesion Science and Technology*, *35*(7), 673–690. https://doi.org/10.1080/01694243.2020.1816793

Hossain, N., Chowdhury, M. A., Rana, M., Hassan, M., & Islam, S. (2022). Terminalia arjuna leaves extract as green corrosion inhibitor for mild steel in HCl solution. *Results in Engineering*, 14, 100438.

Hossain, N., Islam, M. A., & Chowdhury, M. A. (2023). Advances of plant-extracted inhibitors in metal corrosion reduction–future prospects and challenges. *Results in Chemistry*, 5, 100883.

Ibrahimi, B. E., Nardeli, J. V., & Guo, L. (2021). An Overview of Corrosion. *ACS Symposium Series*, 1–19. https://doi.org/10.1021/bk-2021-1403.ch001

Ifmaily, I. (2019). Pengaruh Ekstrak Kulit Buah Mangga Harum Manis (Mangifera indica L) terhadap Tekanan Darah pada Tikus Putih Jantan Hipertensi. *Jurnal Farmasi Sains Dan Terapan, 6(2)*, 103–108. https://doi.org/10.33508/jfst.v6i2.2240

Ituen, E., Akaranta, O., & James, A. (2017). Evaluation of performance of corrosion inhibitors using adsorption isotherm models: an overview. *Chem. Sci. Int. J*, *18*(1), 1-34.

Jakha, K. H., Goyal, C., Dhyani, P., Rai, D. C., Saharan, B. S., Dhull, S. B., & Duhan, J. S. (2024). Characterization of Langra mango peel powder and assessment of its prebiotic and antioxidant potential. *Journal of Food Biochemistry*, 2024, 1–17. https://doi.org/10.1155/2024/9026617

Jano, A., Kokalari, E., Lame, A., & Hoxha, V. (2021). Comparison of corrosion protection efficiency of two kinds of amino acids. *Proceedings of the World*

*Congress on Mechanical, Chemical, and Material Engineering.* https://doi.org/10.11159/iccpe21.109

Javid, S., Bhat, A., & Bashir, M. (2024). Bioactive compounds and antioxidant activity of mango peel (Mangifera indica L.) produced by different methods of extraction and solvents. *International Journal of Advanced Biochemistry Research, 8(1),* 283–286. https://doi.org/10.33545/26174693.2024.v8.i1d.460

Jimoh, I., & Usman, B. (2021). Corrosion Inhibition Potential of Ethanol Extract of Acacia nilotica Leaves on Mild Steel in an Acidic Medium. *Portugaliae Electrochimica Acta, 39(2)*, 105–128. https://doi.org/10.4152/pea.202102105

Kalam, S., Abu-Khamsin, S. A., Kamal, M., & Patil, S. (2021). Surfactant Adsorption Isotherms: A Review. ACS Omega, 6(48), 32342–32348. https://doi.org/10.1021/acsomega.1c04661

Kamachi Mudali, U., Jayaraj, J., Raman, R. S., & Raj, B. (2019). Corrosion. *Non-Destructive Evaluation of Corrosion and Corrosion-Assisted Cracking*, 56–74. https://doi.org/10.1002/9781118987735.ch2

Karattu Veedu, K., Peringattu Kalarikkal, T., Jayakumar, N., & Gopalan, N. K. (2019). Anticorrosive Performance of *Mangifera indica* L. Leaf Extract-Based Hybrid Coating on Steel. *ACS Omega*, *4*(6), 10176–10184. https://doi.org/10.1021/acsomega.9b00632

Keshavamurthy, R., Ramesh, C., Pradeep Kumar, G., & Tambrallimath, V. (2021). Experimental investigation of tribocorrosion. *Tribocorrosion*, 17–42. https://doi.org/10.1016/b978-0-12-818916-0.00001-8

Khasanova, A. R. (2022). Corrosion cracking under main pipelines stress. *Journal of Physics: Conference Series, 2176(1)*, 012051. https://doi.org/10.1088/1742-6596/2176/1/012051

Kučuk, N., Primožič, M., Kotnik, P., Knez, Ž., & Leitgeb, M. (2024). Mango Peels as an Industrial By-Product: A Sustainable Source of Compounds with Antioxidant, Enzymatic, and Antimicrobial Activity. *Foods, 13(4),* 553. https://doi.org/10.3390/foods13040553

Kumar, H., & Yadav, V. (2020). Musa acuminata (Green corrosion inhibitor) as anti-pit and anti-cracking agent for mild steel in 5M hydrochloric acid solution. Chemical Data Collections, 29, 100500. https://doi.org/10.1016/j.cdc.2020.100500

Kumar, S. (2006). Spectroscopy of organic compounds. *Cosmic rays,* 10(4).

Lamghafri, S., Daoudi, W., El Aatiaoui, A., Dagdag, O., Kim, H., Berisha, A., ... & Lamhamdi, A. (2024). Efficiency of alcohol and ester-imidazole in preventing mild steel corrosion: An integrated approach combining experimental and computational studies. *Journal of Molecular Structure, 1306,* 137924.

Li, W., Brown, B., Young, D., & Nešić, S. (2014). Investigation of pseudo-passivation of mild steel in $CO_2$ corrosion. *Corrosion, 70(3),* 294-302.

Loto, R. T. (2018). Surface coverage and corrosion inhibition effect of Rosmarinus officinalis and zinc oxide on the electrochemical performance of low carbon steel in dilute acid solutions. *Results in Physics*, *8*, 172–179. https://doi.org/10.1016/j.rinp.2017.12.003

Mamand, D. M., Azeez, Y. H., & Qadr, H. M. (2023). Monte Carlo and DFT calculations on the corrosion inhibition efficiency of some benzimide molecules. *Mongolian Journal Of Chemistry, 24(50),* 1-10.

Marcillo-Parra, V., Anaguano, M., Molina, M. G., Tupuna-Yerovi, D. S., & Ruales, J. (2021). Characterization and quantification of bioactive compounds and antioxidant activity in three different varieties of mango (Mangifera indica L.) peel from the Ecuadorian region using HPLC-UV/VIS and UPLC-PDA. *NFS Journal,* 23, 1–7. https://doi.org/10.1016/j.nfs.2021.02.001

Marsoul, A., Ijjaali, M., Elhajjaji, F., Taleb, M., Salim, R., & Boukir, A. (2020). Phytochemical screening, total phenolic and flavonoid methanolic extract of pomegranate bark (Punica granatum L): Evaluation of the inhibitory effect in acidic medium 1 M HCl. *Materials Today: Proceedings,* 27, 3193–3198. https://doi.org/10.1016/j.matpr.2020.04.202

McCafferty, E. (2011). Introduction to Corrosion Science.

Miralrio, A., & Espinoza Vázquez, A. (2020). Plant Extracts as Green Corrosion Inhibitors for Different Metal Surfaces and Corrosive Media: A Review. *Processes*, *8*(8), 942. https://doi.org/10.3390/pr8080942

Mohamed, A., Visco, D. P., & Bastidas, D. M. (2021). Significance of π–Electrons in the Design of Corrosion Inhibitors for Carbon Steel in Simulated Concrete Pore Solution. *Corrosion, 77(9),* 976–990. https://doi.org/10.5006/3844

Monticelli, C. (2018). Corrosion Inhibitors. *Encyclopedia of Interfacial Chemistry*, 164–171. https://doi.org/10.1016/b978-0-12-409547-2.13443-2

Njoku, C. N., Ikeuba, A. I., Anorondu, C. C., Shammah, I. C., Yakubu, E., Elendu, B. N., Enechukwu, C. S., Uduma, I. O., & Uzor, P. C. (2024). A review of the extraction and application of eco-friendly biomass for corrosion protection of metals. *Results in Chemistry, 7, 101286.* https://doi.org/10.1016/j.rechem.2023.101286

Ogunleye, O., Arinkoola, A., Eletta, O., Agbede, O., Osho, Y., Morakinyo, A., & Hamed, J. (2020). Green corrosion inhibition and adsorption characteristics of Luffa cylindrica leaf extract on mild steel in hydrochloric acid environment. *Heliyon*, *6*(1), e03205. https://doi.org/10.1016/j.heliyon.2020.e03205

Olajire, A. A. (2017). Corrosion inhibition of offshore oil and gas production facilities using organic compound inhibitors - A review. *Journal of Molecular Liquids,* 248, 775–808. https://doi.org/10.1016/j.molliq.2017.10.097

Omotosho, O. A., Okeniyi, J. O., Loto, C. A., Popoola, A. P. I., Obi, C. E., Sonoiki, O. O. O., Oni, A. B., Alabi, A. S., & Olarewaju, A. E. (2016). Performance of Terminalia catappa on mild steel corrosion in HCl medium. *AIP Conference Proceedings*. https://doi.org/10.1063/1.4959423

Omran, B. A., & Abdel-Salam, M. O. (2020). Basic Corrosion Fundamentals, Aspects and Currently Applied Strategies for Corrosion Mitigation (pp. 1–45). *Springer, Cham.* https://doi.org/10.1007/978-3-030-49532-9_1

Pardede, T. K., & Sofyan, N. (2023). Potential use of natural dyes extracted from Melastoma malabathricum L. seeds as corrosion inhibitors on low carbon steel: A review. *AIP Conference Proceedings.* https://doi.org/10.1063/5.0115202

Parhizkar, N., Shahrabi, T., & Ramezanzadeh, B. (2017). A new approach for enhancement of the corrosion protection properties and interfacial adhesion bonds between the epoxy coating and steel substrate through surface treatment by covalently modified amino functionalized graphene oxide film. *Corrosion Science*, 123, 55–75. https://doi.org/10.1016/j.corsci.2017.04.011

Patle, T. K., Shrivas, K., Kurrey, R., Upadhyay, S., Jangde, R., & Chauhan, R. (2020). Phytochemical screening and determination of phenolics and flavonoids in Dillenia pentagyna using UV–vis and FTIR spectroscopy. *Spectrochimica Acta Part A: Molecular and Biomolecular Spectroscopy*, *242*, 118717. https://doi.org/10.1016/j.saa.2020.118717

Pinto, V., Pinto, G. M., Kateel, L. D., & Thomas, A. (2023). Green Approach to Corrosion Inhibition of Mild Steel in Hydrochloric Acidusing Extractfromthe

Pericarp of the fruit Tamarindus indica (Tamarind). *Biointerface Research in Applied Chemistry, 13(6)*, 544-553.

Popoola, L. T. (2019). Organic green corrosion inhibitors (OGCIs): a critical review. *Corrosion Reviews, 37(2),* 71–102. https://doi.org/10.1515/corrrev-2018-0058

Radin Sukimi, N. A., Yahya, S., Alias, N. Z., Shamsudin, S. R., Ahmad, Z., & Din Yati, M. S. (2023). Corrosion inhibition efficiency of steel by mango peel extract in hydrochloric acid at different temperature. *Scientific Research Journal*, 20, 75-96.

Rao, D., & Nayak, A. (2019). Corrosion behaviour of mild steel. *International Journal of Research in Engineering and Science (IJRES) ISSN*, *7*(1), 35-41.

Rehioui, M., Abbout, S., Benzidia, B., Hammouch, H., Erramli, H., Daoud, N. A., Badrane, N., & Hajjaji, N. (2021). Corrosion inhibiting effect of a green formulation based on Opuntia Dillenii seed oil for iron in acid rain solution. *Heliyon, 7(4),* e06674. https://doi.org/10.1016/j.heliyon.2021.e06674

Reza, N. A., Akhmal, N. H., Fadil, N. A., & Taib, M. F. M. (2021). A Review on Plants and Biomass Wastes as Organic Green Corrosion Inhibitors for Mild Steel in Acidic Environment. *Metals*, *11*(7), 1062. https://doi.org/10.3390/met11071062

Riaz, T., Hayat, Z., Akram, K., Saleem, K., Rehman, H. U., Azam, M., Tariq, Z., Rehman, S. U., Meraj, A., Farooq, U., & Shafi, A. (2023). Optimization of gallic acid-enriched ultrasonic-assisted extraction from mango peels. *Open Chemistry, 21(1).* https://doi.org/10.1515/chem-2023-0116

Rocha, J. C. D., Gomes, J. A. D. C. P., & D'Elia, E. (2014). Aqueous extracts of mango and orange peel as green inhibitors for carbon steel in hydrochloric acid solution. *Materials Research*, *17*(6), 1581–1587. https://doi.org/10.1590/1516-1439.285014

Rosli, N. A., Yusuf, S. M., Sauki, A., & Razali, W. M. F. a. W. (2019). Musa Sapientum (Banana) Peels as Green Corrosion Inhibitor for Mild Steel. *Key Engineering Materials,* 797, 230–239. https://doi.org/10.4028/www.scientific.net/kem.797.230

Salleh, S. Z., Yusoff, A. H., Zakaria, S. K., Taib, M. a. A., Abu Seman, A., Masri, M. N., Mohamad, M., Mamat, S., Ahmad Sobri, S., Ali, A., & Teo, P. T. (2021). Plant extracts as green corrosion inhibitor for ferrous metal alloys: A review. *Journal of Cleaner Production*, *304*, 127030. https://doi.org/10.1016/j.jclepro.2021.127030

Sani, M. A., Abbas, H., Jaafar, M. N., Bahagia, M., & Ghaffar, A. (2018). Morphological characterisation of Harumanis mango (Mangifera indica Linn.) in Malaysia. *Horticulture*, 2, 4.

Shalavadi, M. H. (2019). High-performance liquid chromatography analysis of gallic acid and kaempferol in chloroform and ethanol extract of Cassia hirsuta seeds. *International Journal of Green Pharmacy (IJGP), 13(3).*

Shyamvarnan, B., Shanmugapriya, S., Arockia Selvi, J., Kamaraj, P., & Mohankumar, R. (2021). Corrosion inhibition effect of Elettaria cardamomum extract on mild steel in 3.5% NaCl medium. *Materials Today: Proceedings*, *40*, S192–S197. https://doi.org/10.1016/j.matpr.2020.09.085

Sliem, M. H., Basiony, N. E., Zaki, E. G., Sharaf, M. A., & Abdullah, A. M. (2020). Corrosion Inhibition of Mild Steel in Sulfuric Acid by a Newly Synthesized Schiff Base: An Electrochemical, DFT, and Monte Carlo Simulation Study. *Electroanalysis, 32(12),* 3145–3158. https://doi.org/10.1002/elan.202060461

Stango, S. a. X., & Vijayalakshmi, U. (2018). Studies on corrosion inhibitory effect and adsorption behavior of waste materials on mild steel in acidic medium. *Journal of Asian Ceramic Societies, 6(1),* 20–29. https://doi.org/10.1080/21870764.2018.1439608

Taghavikish, M., Dutta, N., & Roy Choudhury, N. (2017). Emerging Corrosion Inhibitors for Interfacial Coating. *Coatings*, *7*(12), 217. https://doi.org/10.3390/coatings7120217

Tait, W. S. (2018). Electrochemical Corrosion Basics. *Handbook of Environmental Degradation of Materials*, 97–115. https://doi.org/10.1016/b978-0-323-52472-8.00005-8

Tait, W. W. (2018). Electrochemical Corrosion Basics. In Elsevier eBooks (pp. 97–115). https://doi.org/10.1016/b978-0-323-52472-8.00005-8

Thangarasu, V., & Anand, R. (2019). Comparative evaluation of corrosion behavior of Aegle Marmelos Correa diesel, biodiesel, and their blends on aluminum and mild steel metals. *Advanced Biofuels*, 443–471. https://doi.org/10.1016/b978-0-08-102791-2.00017-9

Thanh, L. T. M., Vu, N. S. H., Binh, P. M. Q., Dao, V. A., Thu, V. T. H., Hiến, P. V., Panaitescu, C., & Nam, N. Đ. (2020). Combined experimental and computational studies on corrosion inhibition of Houttuynia cordata leaf extract

for steel in HCl medium. *Journal of Molecular Liquids*, 315, 113787. https://doi.org/10.1016/j.molliq.2020.113787

Thomas, A., Prajila, M., Shainy, K., & Joseph, A. (2020). A green approach to corrosion inhibition of mild steel in hydrochloric acid using fruit rind extract of Garcinia indica (Binda). *Journal of Molecular Liquids*, 312, 113369. https://doi.org/10.1016/j.molliq.2020.113369

Uda, M. N. A., Gopinath, S. C. B., Hashim, U., Hakimi, A., Afnan Uda, M. N., Anuar, A., Bakar, M. a. A., Sulaiman, M. K., & Parmin, N. A. (2020). Harumanis Mango: Perspectives in Disease Management and Advancement using Interdigitated Electrodes (IDE) Nano-Biosensor. *IOP Conference Series: Materials Science and Engineering*, *864*(1), 012180. https://doi.org/10.1088/1757-899x/864/1/012180

Umeozokwere, A. O., Mbabuike, I. U., Oreko, B. U., & Ezemuo, D. T. (2016). Corrosion rates and its impact on mild steel in some selected environments. *Journal of Scientific and Engineering Research, 3(1),* 34-43.

Verified Market Research. (2021, August 17). *Inorganic Corrosion Inhibitors Market Size, Opportunities & Forecast*. https://www.verifiedmarketresearch.com/product/inorganic-corrosion-inhibitors-market/

Verma, C. (2022). Forms of corrosion (pp. 11–20). https://doi.org/10.1016/b978-0-323-90589-3.00015-x

Verma, C., Ebenso, E. E., Bahadur, I., & Quraishi, M. (2018). An overview on plant extracts as environmental sustainable and green corrosion inhibitors for metals and alloys in aggressive corrosive media. *Journal of Molecular Liquids*, *266*, 577–590. https://doi.org/10.1016/j.molliq.2018.06.110

Verma, C., Ebenso, E. E., Quraishi, M., & Hussain, C. M. (2021). Recent developments in sustainable corrosion inhibitors: design, performance and industrial scale applications. *Materials Advances, 2(12)*, 3806–3850. https://doi.org/10.1039/d0ma00681e

Vorobyova, V. I., Skiba, M. I., Shakun, A. S., & Nahirniak, S. V. (2019). Relationship between the inhibition and antioxidant properties of the plant and biomass wastes extracts-A Review. *International Journal of Corrosion and Scale Inhibition, 8(2),* 150-178.

Vorobyova, V., & Skiba, M. (2021). Peach pomace extract as novel cost-effective and high-performance green inhibitor for mild steel corrosion in NaCl solution: experimental and theoretical research. Waste and Biomass Valorization, 12, 4623-4641.

Vorobyova, V., Skiba, M., & Gnatko, E. (2023). Agri-food wastes extract as sustainable-green inhibitors corrosion of steel in sodium chloride solution: aclose look at the mechanism of inhibiting action. *South African Journal of Chemical Engineering, 43(1)*, 273-295.

Wang, F., Ma, T., Zhang, S., Tan, B., Guo, L., Du, H., Wang, X., Han, X., & Liu, R. (2024). Corrosion inhibition performance and mechanism of nitrogen-containing organic compounds on copper in an alkaline slurry. *Journal of Molecular Liquids.* https://doi.org/10.1016/j.molliq.2024.124207

Wei, H., Heidarshenas, B., Zhou, L., Hussain, G., Li, Q., & Ostrikov, K. K. (2020). Green inhibitors for steel corrosion in acidic environment: state of art. *Materials Today Sustainability*, *10*, 100044. https://doi.org/10.1016/j.mtsust.2020.100044

Yadav, M. K., Gope, L., & Sarkar, T. K. (2016). Synthesized amino acid compounds as eco-friendly corrosion inhibitors for mild steel in hydrochloric acid solution: electrochemical and quantum studies. *Research on Chemical Intermediates, 42(3),* 2641–2660. https://doi.org/10.1007/s11164-015-2172-5

Yang, J., Wang, L., Blawert, C., Lamaka, S. V., Feiler, C., Zheludkevich, M. L., & Li, W. (2024). Cathodic inhibition mechanism of magnesium alloys by using iron-complex inhibitor. *Transactions of Nonferrous Metals Society of China, 34(5)*, 1496–1506. https://doi.org/10.1016/s1003-6326(24)66486-1

Zadeh, S. akramian. (2023). Erosion-corrosion. *IntechOpen.* https://doi.org/10.5772/intechopen.109106

Zhao, W., Li, F., Lv, X., Chang, J., Shen, S., Dai, P., Xia, Y., & Cao, Z. (2023). Research progress of organic corrosion inhibitors in metal corrosion protection. *Crystals, 13(9),* 1329. https://doi.org/10.3390/cryst13091329

# APPENDICES

# APPENDIX 1

## The HPLC chromatogram for Mangiferin

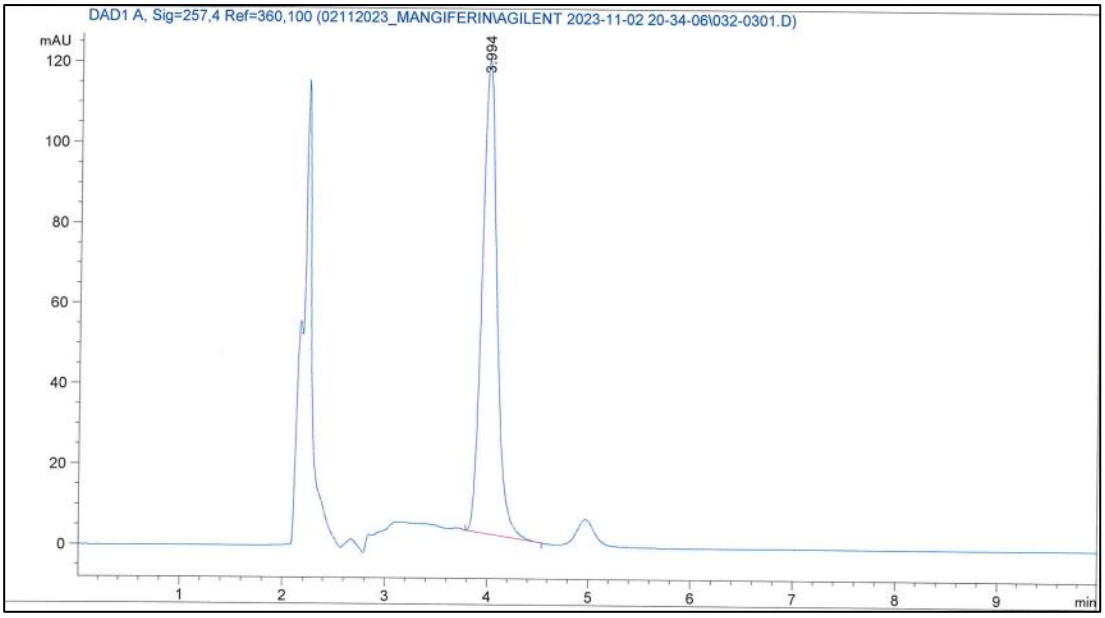

# AUTHOR'S PROFILE

Nur Aina binti Radin Sukimi obtained her Bachelor of Science in Chemistry (Hons.) in 2022 from Universiti Teknologi MARA, Arau, Perlis. She is currently pursuing a Master's degree in Chemistry, with a research focus on corrosion science. Her ongoing study explores the potential of *Harumanis* mango peel extracts as a green corrosion inhibitor.

**LIST OF PUBLICATION:**

**JOURNAL**

**Nur Aina Radin Sukimi**, Solhan Yahya, Nurul Zawani Alias, Shaiful Rizam Shamsudin, Zuliahani Ahmad, Mohd Subhi Din Yati; Corrosion Inhibition Efficiency Of Steel By Mango Peel Extract In Hydrochloric Acid At Different Temperature, Scientific Research Journal 20, 2023, 75 – 96. [indexed MyCite]

**Nur Aina Radin Sukimi**, Solhan Yahya, Nurul Zawani Alias, Razif Muhammed Nordin, Shaiful Rizam Shamsudin, and Mohd Subhi Din Yati; Exploring the Potential of Mango Peel Waste as Green Corrosion Inhibitor for Mild Steel in Chloride Solution, *Malaysian Journal of Chemistry*, 2025, Vol. 27(3), 100-109 [indexed SCOPUS]

Solhan Yahya, Zuliahani Ahmad, Nor Hafizah Che Ismail, Nurul Izzati Rosli, Nurul Hayani Ramlan, **Nur Aina Radin Sukimi,** Soybean and Glycine as Potential Corrosion Inhibitors for Steel in Hydrochloric Acid: Electrochemical and

Morphological Studies, *Scientific Research Journal*, Vol 21, No 1 (2024) 43-65. [indexed MyCite]

**PROCEEDING**

**Nur Aina Radin Sukimi**, Solhan Yahya, Nurul Zawani Alias, Zuliahani Ahmad, Shaiful Rizam Shamsudin, Mohd. Subhi Din Yati, HM-CorrBreak: An Alternative New Material for Corrosion Inhibitors Formulation from Harumanis Peel, *The 11th International Innovation, Invention and Design Competition 2022 (INDES 2022),* 14-25 Nov 2022, Unit Penerbitan UiTM Perak, 233-237.e-ISSN 2756-8733 [Proceeding]

Nur Syauqina Afiqah Mohd Sukri, Nurain Atiqah Ahmad Zapwan, Solhan Yahya, **Nur Aina Radin Sukimi**, Dzulkifli Osman; Corrosion Inhibition of Aluminum Alloy by Mango Leaf Extract in Different Acid, *1st International Science, Engineering and Technology Colloquium 2024 (ISETC 2024),* Faculty of Applied Sciences, Universiti Teknologi MARA, Perak Branch Tapah Campus, Perak, 45-46978-629-97630-2-4 [Proceeding]

Nurain Atiqah Ahmad Zapwan, Nur Syauqina Afiqah Mohd Sukri, Solhan Yahya, **Nur Aina Radin Sukimi**, Nurul Zawani Alias Aqueous Extracts Of Mango Leaf As Green Corrosion Inhibitors For Steel In Different Acid Solution, *1st International Science, Engineering and Technology Colloquium 2024 (ISETC 2024),* Faculty of Applied Sciences, Universiti Teknologi MARA, Perak Branch Tapah Campus, Perak, 10-12.978-629-97630-2-4 [Proceeding]